UNIVERSITY COLLEGE LONDON

Semi-Empirical Modelling of Separating Dispersed Pipe Flows

by

Nikola Evripidou

Submitted to the Department of Chemical Engineering in partial fulfilment of the requirements for the degree of

Doctor of Philosophy in Chemical Engineering

at University College London

December, 2023

I, Nikola Evripidou, confirm that the work presented in my thesis is my own. Where information has been derived from other sources, I confirm that this has been indicated in the thesis.

December 2023

London, United Kindgom

Abstract

This thesis introduces a one-dimensional semi-empirical model predicting flow pattern transitions in separating dispersed liquid-liquid horizontal pipe flows. Based on the mechanisms of drop settling, drop-interface coalescence, and drop-drop coalescence, the model captures the evolution of distinct layers and the drop growth in oil-in-water and water-in-oil systems. Model validation uses experimental data for oil-in-water dispersions from a pilot scale two-phase flow facility. The separation dynamics were influenced by drop settling and coalescence rates. Oil-in-water dispersions separated faster than water-in-oil dispersions, higher mixture velocities increased the separation length, while smaller drops led to dense-packed layer depletion and longer separation lengths.

A comparative analysis of two coalescence models, the *asymmetric film drainage model* (Henschke et al. 2002) and the i*nterfacial mobility film drainage model* (Jeelani and Hartland 1994), is carried out. Parameter estimates for the *asymmetric film drainage model* exhibit sufficient precision and good agreement with experimental measurements. In contrast, the *interfacial mobility film drainage model* exhibits dependency on mixture velocity, with substantial discrepancies between model predictions and experimental data when parameter estimates obtained at lower mixture velocity are used for higher mixture velocities. Consequently, the *asymmetric film drainage model* emerges as the preferred choice.

Parameter estimation, parametric sensitivity analysis (PSA) and model-based design of experiments (MBDoE) are carried out to acquire precise parameter estimates and propose optimal experimental conditions, thereby enhancing the accuracy of the model. These studies utilize experimental data from Pereyra et al. (2013). PSA reveals regions of high sensitivity of the model outputs to uncertain parameters, which correspond to favourable sampling locations. Manipulating mixture velocity, dispersed phase fraction, and layer heights at the inlet, influences these sensitive regions. Clustered measurements around highly sensitive regions enhance the information content they provide. MBDoE demonstrates that A-, D-, or E-optimal experimental design criteria improve the expected parameter precision.

Impact Statement

The work presented in this thesis addresses a critical issue in the engineering sector, specifically focusing on pipe flows of two immiscible liquids. These are a common occurrence in diverse industrial settlings such as chemical, pharmaceutical, and nuclear plants, and in the oil and gas industry. These industries collectively constitute substantial portions of the global economy, with revenues in the trillions and employing millions of individuals worldwide. The impact of this research is highlighted by the support of Chevron Corporation, a major player in the oil and gas industry. Importantly, however, the applications of this research extend beyond this sector encompassing all chemical and process industries involving immiscible liquids.

Dispersions often form in liquid-liquid flows and can separate downstream. This thesis investigates the complex separation dynamics of unstable dispersions in pipes, offering valuable insights into the flow pattern transitions observed. A key contribution of this thesis is the development of a semi-empirical model for predicting the evolution of flow patterns and the separation length in dispersed pipe flows. The model provides rapid predictions for systems with sparse experimental data, which is often the case in industry, offering an efficient alternative to computationally and time intensive CFD models. The aim is to fill the gap in the available data that is

crucial for the effective design and sustainable operation of industrial facilities.

Using the model, the thesis explores different case studies to understand the separation dynamics of dispersed flows in horizontal pipes. This investigation provides important insights into how the inlet and flow conditions, the nature of the dispersed phase, and the initial drop size influence flow pattern development, potentially resulting in two distinct types of separation: coalescence-controlled and settling-controlled.

Nevertheless, the implementation of the model in industry faces challenges, as its accuracy depends on the precision of certain fitted parameters. However, estimating the values of these parameters poses difficulties due to the scarcity of essential measurements required for parameter estimation from industrially acquired data. Consequently, there is a need to rely on pilot-scale experiments. Nonetheless, these experiments present challenges due to the restricted length of the test section, demanding careful design to ensure that measurements contain sufficient information for precise parameter estimation.

To address space constraints of pilot-scale experiments and make the model readily available, the thesis employs a comprehensive approach, integrating parameter estimation, parametric sensitivity analysis (PSA), and

model-based design of experiments (MBDoE) techniques for acquiring precise parameter estimates hence improving the accuracy of the model. Essentially a framework is introduced for estimating model parameters, evaluating their relative impact on model predictions through PSA, and providing guidance on optimal experimental conditions to use in future experiments to obtain precise parameter estimates. Leveraging PSA and MBDoE streamlines the experimental design process, optimising data collection efficiency and eliminating the need for iterative trial-and-error approaches. This contributes to significant savings in time and resources, ultimately serving as a valuable guide for future experimental work.

UCL Research Paper Declaration Forms

referencing the doctoral candidate's own published work(s)

Please use this form to declare if parts of your thesis are already available in another format, e.g. if data, text, or figures:

- *have been uploaded to a preprint server*
- *are in submission to a peer-reviewed publication*
- *have been published in a peer-reviewed publication, e.g. journal, textbook.*

This form should be completed as many times as necessary. For instance, if you have seven thesis chapters, two of which containing material that has already been published, you would complete this form twice.

1. For a research manuscript that has already been published (if not yet published, please skip to section 2)

a) **What is the title of the manuscript?**

A mechanistic model for the prediction of flow pattern transitions during separation of liquid-liquid pipe flows

b) **Please include a link to or doi for the work**

https://doi.org/10.1016/j.ijmultiphaseflow.2022.104172

c) **Where was the work published?**

International Journal of Multiphase Flow, Volume 155

d) **Who published the work?** (e.g. OUP)

Elsevier

e) **When was the work published?**

2022

f) **List the manuscript's authors in the order they appear on the publication**

Nikola Evripidou, Carlos Avila, Panagiota Angeli

g) **Was the work peer reviewed?**

Yes

h) **Have you retained the copyright?**

No

i) **Was an earlier form of the manuscript uploaded to a preprint server?** (e.g. medRxiv). If 'Yes', please give a link or doi)

No

If 'No', please seek permission from the relevant publisher and check the box next to the below statement:

☒

*I acknowledge permission of the publisher named under **1d** to include in this thesis portions of the publication named as included in **1c**.*

2. **For a research manuscript prepared for publication but that has not yet been published** (if already published, please skip to section 3)

   a) **What is the current title of the manuscript?**

   N/A

   b) **Has the manuscript been uploaded to a preprint server?** (e.g. medRxiv; if 'Yes', please give a link or doi)

   N/A

   c) **Where is the work intended to be published?** (e.g. journal names)

   N/A

   d) **List the manuscript's authors in the intended authorship order**

   N/A

   e) **Stage of publication** (e.g. in submission)

   N/A

3. **For multi-authored work, please give a statement of contribution covering all authors** (if single-author, please skip to section 4)

   Nikola Evripidou: Conceptualization, Methodology, Software, Writing – Original Draft preparation.
   Carlos Avila: Supervision.
   Panagiota Angeli: Supervision, Writing – Review and Editing.

4. **In which chapter(s) of your thesis can this material be found?**

   Chapters 2 and 3.

5. **e-Signatures confirming that the information above is accurate** (this form should be co-signed by the supervisor / senior author unless this is not appropriate, e.g. if the paper was a single-author work)

   Candidate

   Date:

   18/12/2023

   Supervisor / Senior Author (where appropriate)

   Date:

   18/12/2023

UCL Research Paper Declaration Form

referencing the doctoral candidate's own published work(s)

Please use this form to declare if parts of your thesis are already available in another format, e.g. if data, text, or figures:

- *have been uploaded to a preprint server*
- *are in submission to a peer-reviewed publication*
- *have been published in a peer-reviewed publication, e.g. journal, textbook.*

This form should be completed as many times as necessary. For instance, if you have seven thesis chapters, two of which containing material that has already been published, you would complete this form twice.

1. **For a research manuscript that has already been published** (if not yet published, please skip to section 2)

a) **What is the title of the manuscript?**

Mechanistic modelling of separating dispersions in pipes using model-based design of experiments techniques

b) **Please include a link to or doi for the work**

https://doi.org/10.1016/j.ces.2023.119504

c) **Where was the work published?**

Chemical Engineering Science, Volume 284

d) **Who published the work?** (e.g. OUP)

Elsevier

e) **When was the work published?**

2023

f) **List the manuscript's authors in the order they appear on the publication**

Nikola Evripidou, Federico Galvanin, Panagiota Angeli

g) **Was the work peer reviewed?**

Yes

h) **Have you retained the copyright?**

No

i) **Was an earlier form of the manuscript uploaded to a preprint server?** (e.g. medRxiv). If 'Yes', please give a link or doi)

No

If 'No', please seek permission from the relevant publisher and check the box next to the below statement:

☒

*I acknowledge permission of the publisher named under **1d** to include in this thesis portions of the publication named as included in **1c**.*

2. **For a research manuscript prepared for publication but that has not yet been published** (if already published, please skip to section 3)

   a) **What is the current title of the manuscript?**

   N/A

   b) **Has the manuscript been uploaded to a preprint server?** (e.g. medRxiv; if 'Yes', please give a link or doi)

   N/A

   c) **Where is the work intended to be published?** (e.g. journal names)

   N/A

   d) **List the manuscript's authors in the intended authorship order**

   N/A

   e) **Stage of publication** (e.g. in submission)

   N/A

3. **For multi-authored work, please give a statement of contribution covering all authors** (if single-author, please skip to section 4)

   Nikola Evripidou: Conceptualization, Methodology, Software, Writing – Original Draft preparation.
   Federico Galvanin: Supervision, Writing – Review and Editing.
   Panagiota Angeli: Supervision, Writing – Review and Editing.

4. **In which chapter(s) of your thesis can this material be found?**

   Chapters 2, 4, and 5.

5. **e-Signatures confirming that the information above is accurate** (this form should be co-signed by the supervisor / senior author unless this is not appropriate, e.g. if the paper was a single-author work)

   Candidate

   Date:

   18/12/2023

   Supervisor / Senior Author (where appropriate)

   Date:

   18/12/2023

UCL Research Paper Declaration Form

referencing the doctoral candidate's own published work(s)

Please use this form to declare if parts of your thesis are already available in another format, e.g. if data, text, or figures:

- *have been uploaded to a preprint server*
- *are in submission to a peer-reviewed publication*
- *have been published in a peer-reviewed publication, e.g. journal, textbook.*

This form should be completed as many times as necessary. For instance, if you have seven thesis chapters, two of which containing material that has already been published, you would complete this form twice.

1. For a research manuscript that has already been published (if not yet published, please skip to section 2)

a) **What is the title of the manuscript?**

Effect of coalescence models on the prediction of the separation of dispersed oil-water pipe flows.

b) **Please include a link to or doi for the work**

https://doi.org/10.1016/B978-0-443-15274-0.50176-1

c) **Where was the work published?**

Computer Aided Chemical Engineering, Volume 52

d) **Who published the work?** (e.g. OUP)

Elsevier

e) **When was the work published?**

2023

f) **List the manuscript's authors in the order they appear on the publication**

Nikola Evripidou, Federico Galvanin, Panagiota Angeli

g) **Was the work peer reviewed?**

Yes

h) **Have you retained the copyright?**

No

i) **Was an earlier form of the manuscript uploaded to a preprint server?** (e.g. medRxiv). If 'Yes', please give a link or doi)

No

If 'No', please seek permission from the relevant publisher and check the box next to the below statement:

☒

*I acknowledge permission of the publisher named under **1d** to include in this thesis portions of the publication named as included in **1c**.*

2. **For a research manuscript prepared for publication but that has not yet been published** (if already published, please skip to section 3)

   a) **What is the current title of the manuscript?**

   N/A

   b) **Has the manuscript been uploaded to a preprint server?** (e.g. medRxiv; if 'Yes', please give a link or doi)

   N/A

   c) **Where is the work intended to be published?** (e.g. journal names)

   N/A

   d) **List the manuscript's authors in the intended authorship order**

   N/A

   e) **Stage of publication** (e.g. in submission)

   N/A

3. **For multi-authored work, please give a statement of contribution covering all authors** (if single-author, please skip to section 4)

   Nikola Evripidou: Conceptualization, Methodology, Software, Writing – Original Draft preparation.
   Federico Galvanin: Supervision, Writing – Review and Editing.
   Panagiota Angeli: Supervision, Writing – Review and Editing.

4. **In which chapter(s) of your thesis can this material be found?**

   Chapter 4.

5. **e-Signatures confirming that the information above is accurate** (this form should be co-signed by the supervisor / senior author unless this is not appropriate, e.g. if the paper was a single-author work)

   Candidate

   Date:

   18/12/2023

   Supervisor / Senior Author (where appropriate)

   Date:

   18/12/2023

Acknowledgements

I extend my deepest gratitude to my supervisor Prof. Panagiota Angeli for her invaluable advice, patient guidance, and profound influence in shaping me as a researcher. I am sincerely grateful for the numerous opportunities she provided to showcase my work and for her exceptional support throughout these years. Special appreciation goes to Dr. Federico Galvanin for introducing me to systems-based approaches and for his guidance and support during my exploration of this field. I am also grateful to Chevron Corporation for sponsoring this project, especially Dr. Carlos Avila and Dr. Haijing Gao for their insightful comments and suggestions, which enriched the depth of my work. I would like to thank all the members of the Advanced Multiphase Systems (ThAMeS) group for their collaborative attitude. Last but not least, I would like to thank my family for their love, support, and unshakeable confidence in me, sustaining me through every endeavour, big or small.

Contents

Table of Contents

List of Tables

List of Figures

List of Symbols

Latin

A	Cross-sectional area (m^2)
Ar	Archimedes number (-)
C	Collision frequency (Chesters 1991) (s^{-1} m^{-3})
C_{CT}	Collision frequency (Coulaloglou and Tavlarides 1977) (s^{-1})
C_h	Hindered settling coefficient (-)
CI	Confidence interval
C_{w}	Modified friction coefficient (-)
C_1, C_2	Coefficients obtained on the basis of continuity (-)
d_j, d_m	Drop diameters of colliding drops (m)
d_{p}	Drop diameter (m)
$d_{\mathrm{p,I}}$	Drop diameter at the interface (m)
$d_{\mathrm{p,0}}$	Drop diameter at the pipe inlet (m)
F	Force due to gravity (N)

$F_{collision}$	Collision force (N)
g	Gravitational acceleration (m s^{-2})
H	Hamaker coefficient (N m)
h	Thickness (m)
h_f	Interfacial film thickness (m)
$h_{f,0}$	Initial film thickness (m)
$\widetilde{h_P}$	Drop-packing height
ID	Internal diameter of the pipe (m)
K_{HR}	Hadamard-Rybczynski factor (-)
k	Collision coefficient (-)
La	Modified Laplace number (-)
m	Interface mobility parameter (-)
N	Number of measured responses (-)
N_θ	Number of parameters (-)
n	Number of drops per unit volume (m^{-3})
n_ϕ	Number of design variables (-)

Re_∞	Reynolds number of a single drop moving vertically in an infinite medium (-)
r_p	Drop radius (m)
r_f	Drop-interface film radius (m)
$r_\mathrm{F,C}$	Drop-drop contact radius (m)
$r_\mathrm{F,I}$	Drop-interface contact radius (m)
r_V^*	Dimensionless asymmetry coefficient (-)
r_α	Channel contour radius (m)
sf	Scaling factor
t	Time (s)
t_{ch}	Characteristic drainage time (s)
$t_{collision}$	Collision time (s)
t_i	*t*-value for the *i*-th model parameter
t_{ref}	Reference *t*-value
u_M	Mixture velocity (m s^{-1})
u_s	Settling velocity (m s^{-1})

V	Relative velocity of colliding drops (m s^{-1})
V_{Re}	Reynolds film thinning velocity (m s^{-1})
$v_{\theta,i}$	Estimated variance for the *i*-th model parameter
x	Displacement in the axial direction of the flow downstream of the inlet (m)
$\bar{x}$	Length of depletion of the settling layer (m)
$\bar{\bar{x}}$	Length of depletion of the dense-packed layer (m)
y	Vertical displacement from the bottom of the pipe (m)
y_{C}	Settling curve (m)
y_{D}	Coalescence curve (m)
y_{P}	Dense-packed layer curve (m)
y_i	*i*-th predicted response

Greek

γ	Interfacial tension (N m^{-1})
$\dot{\gamma}$	Shear rate (s^{-1})
δ_r	Critical film thickness for rupture (m)

ε	Finite small perturbation in parameter *i*
ε_r	Turbulence-energy dissipation rate per unit mass (W kg^{-1})
θ_i	*i*-th model parameter
λ	Flotation parameter (-)
μ	Viscosity (Pa s)
ν	Kinematic viscosity (m^2 s^{-1})
ξ	Flotation parameter (-)
ρ	Density (kg m^{-3})
σ	Standard deviation
τ_{C}	Drop-drop coalescence time (s)
τ_{I}	Drop-interface coalescence time (s)
$\tau_{\mathrm{I},0}$	Initial drop-interface coalescence time of a full dispersion (s)
φ	Dispersed-phase fraction (-)
$\bar{\varphi}_{\mathrm{P}}$	Average holdup in the dense-packed layer
χ_i^2	Chi-square statistic for the i-th model parameter

χ^2_{ref}	Reference Chi-square
ψ	Scalar quantity
$\hat{\psi}$	Parameter obtained on the basis of continuity (-)

Superscripts & Subscripts

$+$	Dimensionless variable
0	Initial
C	Continuous phase
D	Initially dispersed phase
I	Interface
M	Mixture
P	Dense-packed layer
p	Drop
$pipe$	Pipe
S	Settling
sep	Separation

Vectors & Matrices [dimension]

$\mathbf{D}$	Matrix of eigenvalues $[N_\theta \times N_\theta]$
$\mathbf{H_\theta}$	Fisher information matrix $[N_\theta \times N_\theta]$
$\mathbf{Q}$	Sensitivity matrix $[N_\theta \times N_\theta]$
$\mathbf{V_\theta}$	Variance-covariance matrix of model parameters $[N_\theta \times N_\theta]$
$\mathbf{v_\theta}$	Matrix of eigenvectors $[N_\theta \times N_\theta]$
$\mathbf{\Sigma_y}$	Variance-covariance matrix of measurement errors $[N_\theta \times N_\theta]$
$\boldsymbol{\phi}$	Design vector $[n_\phi]$
$\boldsymbol{\phi_{opt}}$	Optimal design vector $[n_\phi]$

Chapter 1

1. Introduction

1.1. Motivation

Pipe flows of two immiscible liquids are common in the engineering sector and are often encountered in chemical and nuclear plants, and in the oil and gas industry (Danielson 2012). Dispersions can be formed as part of the process or in equipment such as choke valves and bends. These dispersions may be unstable and separate further downstream. The tendency to separate can be exploited to design in-line separators, which are often favourable to other separators as they are simple, small, and lightweight with low operating cost (Zhong et al. 2013). In the oil and gas industry, they can be employed to increase oil recovery, hence have the potential to extend the operational lifetime of older oil fields by making extraction economically viable (Skjefstad and Stanko 2019).

Unstable dispersions of two immiscible liquids can also undergo gravity-controlled separation while flowing through horizontal pipes (Voulgaropoulos and Angeli 2017) at relatively high velocities compared to horizontal pipe separators. In cases where dispersions are important for enhancing mass transfer, minimising pipe erosion (Wang and Zhang 2016) or frictional losses during transportation of crude oil (Pilehvari et al. 1988), the tendency of liquid-liquid mixtures to separate can be detrimental.

Separation is always observed, unless the dispersions are stabilised by surfactants or by flow-induced mixing at high flow velocities. The separation process is rather complex and depends on several factors including the properties of the fluids, the size distribution of the drops present, the mixture velocity, and the pipe geometry.

As the dispersions settle giving rise to distinct layers along the pipe, different flow patterns emerge. Accurate characterization of the flow pattern transitions in unstable dispersed flows is vital for the design and operation of industrial facilities. Despite the surge of research dedicated to liquid-liquid flows in the recent decades, only a few studies investigate flow pattern transitions. The available information, is often limited to measurements of the phase holdup and the pressure gradient of the mixtures (Oddie and Pearson 2004), as the opaque fluids or test sections and the difficult thermodynamic conditions restrict the implementation of several sampling techniques.

Computational fluid dynamics (CFD) models, although an attractive alternative to experiments, are time-intensive. Thus, semi-empirical models, which are simplified mathematical models with fitted parameters and are based on the underlying physical mechanisms governing a process, present an attractive alternative for predicting the evolution of flow patterns and the separation length in dispersions, offering rapid insights into systems where experimental data is sparse and CFD

simulations prohibitively computationally demanding.

1.2. Objectives

Recent works have addressed problems related to flow assurance applications, including phase inversion (Hu 2006; Ioannou 2006; Ngan 2011), interfacial coalescence characteristics (Barral 2014), and the separation of dispersions (Voulgaropoulos 2017), all through detailed experimental measurements conducted within the pilot-scale facilities at the Department of Chemical Engineering, University College London.

In contrast, the current work primarily adopts a computational approach, building on existing models for the separation of dispersions in batch vessels and horizontal-pipe separators. The main objective is to develop a semi-empirical model that accurately predicts the separation process and the flow pattern transitions occurring during the separation of oil/water dispersions. This will be achieved through the following steps:

1. Development of a semi-empirical model predicting the evolution of characteristic layers and the growth in drop size in separating dispersed liquid-liquid pipe flows,
2. Refinement of the model through the investigation of different coalescence models.

3. Establishment of a framework utilising model-based design of experiments for the precise estimation of model parameters by guiding future experiments.

1.3. Outline

The thesis is structured into six chapters. This chapter provides a brief introduction to the topic, while Chapter 2 presents a thorough literature review. The objective is to outline the fundamental theory necessary for understanding and predicting phenomena observed in dispersed pipe flows, to present existing models while identifying their limitations, and to introduce model-based design of experiments techniques for parameter precision that can be used in the refinement of semi-empirical models. Chapter 2 starts with a discussion on multiphase flows and the flow patterns observed in oil/water pipe flows, including experimental observations of previous works. The dynamics of dispersion separation are then discussed, along with the theory behind the coalescence process and a description of relevant experimental findings in the literature. Subsequently, dispersion separation modelling is discussed, encompassing a brief description of computational fluid dynamics (CFD) modelling of pipe flows and mathematical modelling of batch and in-line separators. The chapter concludes with a discussion on techniques for the statistical validation of mathematical models and the application of MBDoE for precise parameter estimation.

Chapter 3 introduces a semi-empirical model for predicting the separation of dispersed liquid-liquid flows in horizontal pipes. This includes the evolution of characteristic layer thicknesses and drop sizes, applied to both oil-in-water and water-in-oil flows. The model accounts for the coalescence of drops with continuous layers of their homophase and with other drops. Chapter 4 compares two coalescence models from the literature when implemented into the model outlined in Chapter 3. Chapter 5 presents a methodology that guides future experiments for precisely estimating model parameters using techniques such as parameter estimation, PSA, and MBDoE. Finally, Chapter 6 summarises the main conclusions and provides recommendations for future work.

Chapter 2

2. Review of literature

2.1. Multiphase flows

Multiphase flows consist of multiple immiscible phases, which are either gases, liquids, or solids, and are characterised by the presence of an interface between these phases. These flows are crucial to industrial processes and are often encountered in chemical and nuclear plants, and in the oil and gas industry (Danielson 2012). Despite their significant, widespread practical importance, multiphase flows are inherently complex, hence remain the subject of extensive research (Ibarra-Hernandez 2017; Hosseinzadeh et al. 2018; Voulgaropoulos et al. 2019).

2.2. Liquid-liquid flows in horizontal pipes

Multiphase flows that involve only two phases include gas-liquid, gas-solid, liquid-liquid, and liquid-solid flows. Among these, immiscible liquid-liquid flows specifically refer to the coexistence of two immiscible liquids, typically an aqueous and an organic phase. Amundsen (2011) conducted a comprehensive literature review focusing on horizontal liquid-liquid flows, identifying and documenting a total of 63 studies between 1959 and 2009, underscoring the substantial depth of research in this area.

2.2.1. Flow patterns

When a liquid-liquid mixture is introduced into a pipe, the two fluids naturally organise themselves into different spatial configurations, known as “flow regimes” or “flow patterns”. The resulting flow pattern depends on specific parameters including the fluid fractions and velocities, the fluid properties (i.e. density, viscosity, and interfacial tension), and the geometry of the pipe (Angeli and Hewitt 2000a; Brauner 2003). Understanding the flow pattern is essential for designing and operating process facilities, as the flow regime significantly affects critical factors like pressure drop and phase separation. However, classifying these flow patterns can be subjective and varies among researchers. The literature shows a wide array of approaches to flow pattern classification, with researchers employing different techniques, names, and definitions to identify the flow patterns. The properties of specific liquids, the geometry of the test section used as well as the way the flow is initialised can also affect the transition boundaries between different flow patterns.

In general, horizontal liquid-liquid pipe flows, can be classified into four main flow regimes, as shown in Figure 2.1: (1) stratified flow (ST), (2) dual-continuous flow (DC), (3) dispersed flow (o/w or w/o), and (4) core-annular flow (CAF). A detailed discussion of the flow patterns encountered in these flows can be found in a review by Ibarra et al. (2014).

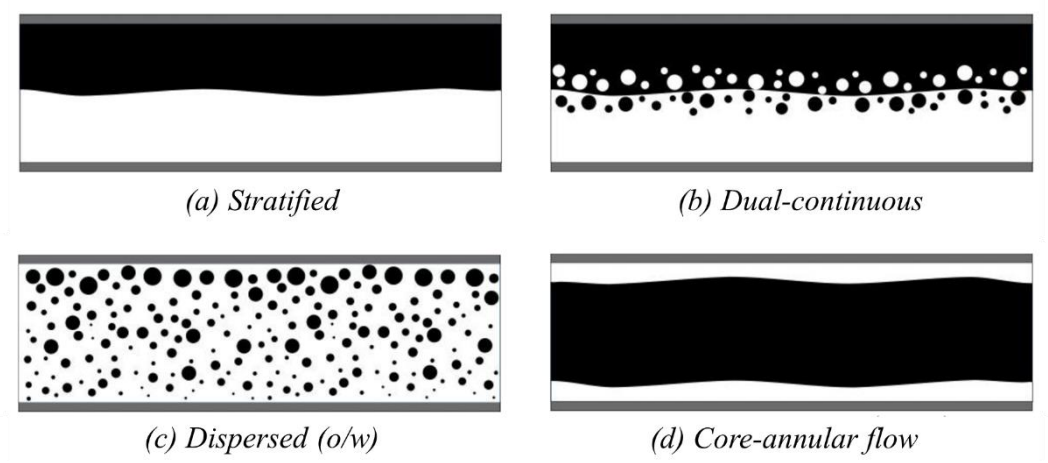

Figure 2.1. Diagrams of the main flow patterns observed in liquid-liquid horizontal pipe flows. The oil phase is represented in black, while the water phase is represented in white (adapted from Voulgaropoulos 2017).

Stratified flows (see Figure 2.1(a)) occur when two immiscible fluids with different densities flow parallel to each other separated by an interface. The gravitational force plays a crucial role in stratified flow, with the more dense fluid found at the bottom of the pipe. Interfacial waves of small amplitude may exist. This flow pattern has been studied extensively in the literature, with research focusing mainly on the investigation of the height of the interface and its curvature, both analytically (Brauner et al. 1998) and numerically (Ng et al. 2002). Transitions from stratified to dual-continuous flow can occur when interfacial waves form and grow in size, leading to ligament break-up and the formation of drops that become entrained in the other phase.

The dual-continuous configuration (see Figure 2.1(b)) is a two-phase flow regime where both phases retain their continuity, but there are drops of one phase dispersed into the other. The mixing zone between the two liquids can vary in nature and may be significant in size. Within this flow pattern several sub-categories emerge depending on the density of the drops and their location. Several studies have investigated the dual-continuous configuration, with Trallero et al. (1997), Lovick and Angeli (2004a), and Rodriguez and Oliemans (2006) exploring its onset boundaries, pressure drop, and interface shape. Research has also explored drop size distributions (Lovick and Angeli 2004b), revealing that larger drops tend to be found near the interface. At sufficiently high velocities, interfacial waves intensify, leading to the complete breakdown of one of the continuous phases into entrained drops and the flow transitions to the dispersed flow regime.

Dispersed flow (see Figure 2.1(c)) is a configuration in which one of the two immiscible liquids is dispersed within the other phase, which forms the continuous medium. Depending on the continuous phase, these patterns are classified as either oil-in-water (o/w) or water-in-oil (w/o) dispersions. This flow configuration is of great importance in the petrochemical industry. Water-in-oil dispersions can be exploited to minimise pipe erosion during transfer of crude oil (Wang and Zhang, 2016). On the other hand, oil-in-water dispersions can be utilised to reduce pressure losses during

transportation of high viscosity oils (Pilehvari et al. 1988). This can be achieved in flows of low dispersed phase fraction and relatively high mixture velocities.

Core-annular flow (see Figure 2.1(d)) refers to the flow of a high-viscosity liquid at the core of a horizontal pipe surrounded by an annular layer of a low-viscosity liquid. Similarly to o/w dispersions, this flow configuration provides an attractive means for transportation of viscous oils, achieving lower pressure losses (Brauner 2003) as the low viscosity aqueous phase wets the walls of the pipe while the oil has the tendency to occupy the centre of the pipe. The energy saving capabilities of CAF and the factors affecting the energy savings achieved through CAF are discussed in a review by Xie et al. (2023). Oliemans (1986) conducted fundamental work demonstrating the hydrodynamic stability of CAF. Building upon Oliemans' work, Omms and Poesio (2003) explored the characteristics of the interfacial waves of the annulus theoretically and their relation to pattern stability. In laboratory scale experiments of liquid-liquid flows, stable CAF is rare. It is only observed in pipes of small diameters, within a restricted range of mixture velocities (Al-Wahaibi and Angeli 2007) and highly viscous oils (>0.5 Pa s) Oliemans (1986), where the viscous effects are sufficient to counteract both buoyancy and shear forces.

2.3. Dispersion separation dynamics

In horizontal liquid-liquid flows, differences in properties like density and viscosity between the two fluids are common. Even relatively small differences in density are usually sufficient to induce separation and stratification of the liquids due to gravity. The tendency to separate can be exploited to design in-line separators, which are often favourable to other separators as they are simple, small, and lightweight with low operating costs (Zhong et al. 2013). In the oil and gas industry, they can be employed to increase oil recovery, hence have the potential to extend the operational lifetime of older oil fields by making extraction economically viable (Skjefstad and Stanko 2019). On the other hand, in cases where dispersions are important for enhancing mass transfer, minimising pipe erosion (Wang and Zhang 2016) or frictional losses during transportation of crude oil (Pilehvari et al. 1988), the tendency of liquid-liquid mixtures to separate can be detrimental.

Separation is always observed, unless the dispersions are stabilised by surfactants or by flow-induced mixing at high mixture velocities. The separation process is rather complex and depends on several factors including the properties of the fluids, the size distribution of the drops present, the mixture velocity, and the pipe diameter and inclination.

Several authors have studied the separation of dispersions experimentally and in different set-ups, including batch and steady-state settlers, and pipe flows. Ryon et al. (1960) was the first to experimentally investigate the separation of liquid-liquid dispersions, while Barnea and Mizrahi (1975) noted the existence of a dense-packed zone. Later, Hartland and Jeelani (1988) explained the batch separation in terms of the physical processes occurring. According to them, dispersions in batch and steady-state settlers consist of settling and dense-packed layers. The drops grow in size due to drop-drop coalescence, they accumulate into a dense-packed zone near the liquid-liquid interface, and finally coalesce with their homophase. They also noted that the rate of settling depends on the drop size and hold-up of the dispersed phase, while the interfacial coalescence rate is a function of the drop size at the coalescing interface and the thickness of the dense-packed zone.

The information available in flow pattern transitions in multiphase flows is often limited to measurements of the phase holdup and the pressure gradient of the mixtures (Oddie and Pearson 2004), as the opaque fluids or test sections and the difficult thermodynamic conditions restrict the implementation of several sampling techniques.

Laboratory experiments typically utilize model oils to observe and identify different flow configurations at steady state (Trallero et al. 1997; Angeli and Hewitt 2000a; Elseth 2001; Simmons and Azzopardi 2001; Lovick and

Angeli 2004a; Voulgaropoulos and Angeli 2017; Voulgaropoulos et al. 2019). Drop size measurements in unstable dispersions during flow are more challenging and only a few researchers have conducted them (Angeli and Hewitt 2000b; Simmons et al. 2000; Maaß et al. 2011; Morgan et al. 2013; Yang 2014).

Few authors explored the evolution of dispersions in horizontal pipes. El-Hamouz and Stewart (1996) investigated changes in the drop size distribution with pipe length, conducting measurements at distances of approximately 10 and 28 pipe diameters downstream from the inlet. They generated dispersions using a static mixer at a mixture velocity of $1\ \mathrm{m\ s^{-1}}$, observing a transition towards flatter size distributions as the dispersions evolved, with a higher likelihood of encountering larger drops and a 43% increase in the arithmetic mean drop diameter d_{10}.

Schümann et al. (2016) examined dispersions at low velocities and documented positive drop growth rates across a wide range of phase fractions for three distinct oils with different viscosities. Larger drop sizes were observed in the direction of buoyancy of the dispersed phase, while a reduction in the drop size was consistently recorded near the pipe wall due to high shear in that region that enhances break-up. Drop size also increased with higher input volume fractions of the dispersed phase and lower mixture velocities.

Voulgaropoulos (2017) studied spatially evolving dispersions in horizontal pipes under varying conditions, including four different oil fractions ranging from 15% to 60% and mixture velocities of approximately $0.5\ \mathrm{m\ s^{-1}}$ and $1\ \mathrm{m\ s^{-1}}$. Partial oil-in-water dispersions were generated at the inlet of the test section using a multi-nozzle mixer. Measurements were conducted at three distinct axial locations, measuring the dispersed phase volume fraction and the drop size. The formation of a continuous oil layer near the top of the pipe and an increase in the drop size with pipe length were recorded. Larger drop sizes were also observed at lower mixture velocities and larger dispersed phase fractions.

Pérez (2005) and Voulgaropoulos et al. (2019) used static mixers to generate dispersions of different dispersed phase fractions φ_0, which were then fed to a horizontal pipe. Both authors observed significant stratification downstream of the inlet at low mixture velocities u_M (see Figure 2.2). Conan et al. (2007) and Voulgaropoulos et al. (2016) employed different multi-nozzle inlet configurations to generate dispersions at low velocities and reported similar findings to those shown in Figure 2.2.

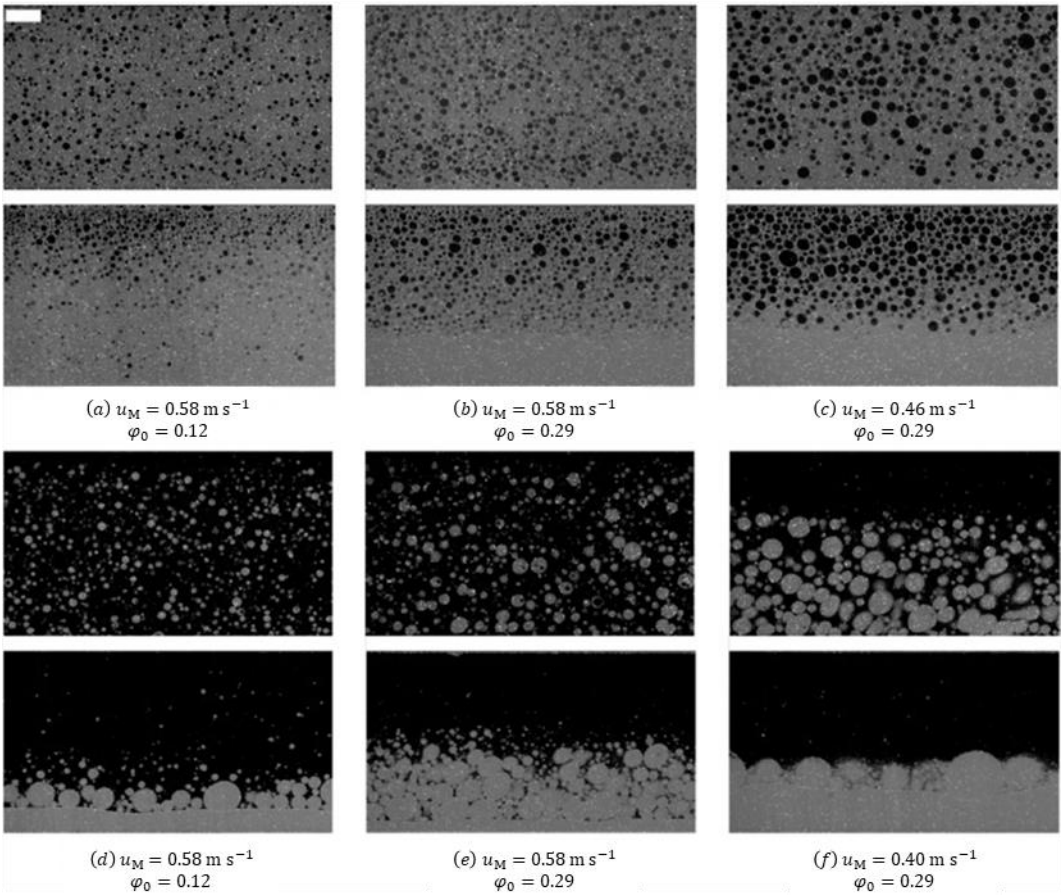

Figure 2.2. Planar Laser-Induced Fluorescence images acquired for a few typical flow conditions investigated at 15 pipe diameters (top) and 135 pipe diameters (bottom) downstream of the static mixer. The scale bar is 5 mm long. (a)–(c) correspond to cases of water-continuous dispersions, while (d)–(f) correspond to cases of oil-continuous (adapted from Voulgaropoulos et al. 2019).

Dispersions, despite their thermodynamic instability, can maintain kinetic stability even for long time duration. In general, dispersions tend to be more stable when the dispersed droplets are small in size. Hartland and Jeelani

(1988) state that the separation of dispersions is driven by two main mechanisms:

- Drop coalescence, i.e. the merging of two drops to form one larger drop or the incorporation of a drop into a continuous layer of the same liquid.
- Drop settling (flotation or sedimentation), i.e. the settling of droplets through the continuous medium due to gravity in the direction of buoyancy of the dispersed phase.

2.3.1. Coalescence mechanism

As two bodies of the same liquid approach, they come into contact at a single location. Eventually they merge, forming one large volume. This process is called coalescence. The process of coalescence can be split into the following categories as shown in Figure 2.3:

1. two droplets coalescing in a gas medium,
2. two droplets coalescing in an immiscible liquid phase,
3. a single droplet in a gas medium coalescing with a bulk liquid phase, and
4. a single droplet in an immiscible liquid medium coalescing with a bulk liquid phase.

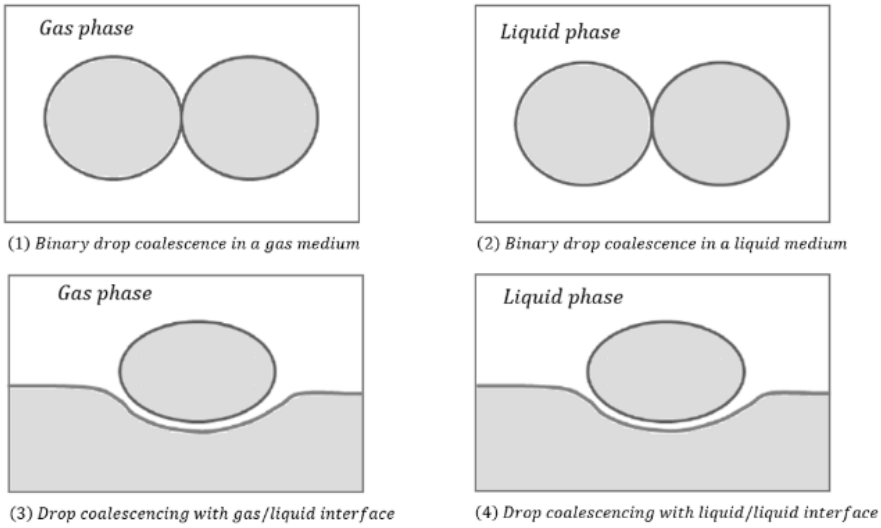

Figure 2.3: Types of drop coalescence.

Due to the large density difference between gases and liquids, coalescence taking place in an gas medium (i.e. cases 1 and 3 in Figure 2.3) differs substantially from coalescence in a liquid medium (i.e. cases 2 and 4 in Figure 2.3). In this work, only coalescence occurring in a liquid phase will be considered.

In cases 2 and 4 the coalescence dynamics are considered to be identical. In these scenarios, most authors (Barnea and Mizrahi 1975; Tobin et al. 1990; Chesters 1991; Palermo 1991; Rommel et al. 1992; Lobo et al. 1993; Tsouris and Tavlarides 1994; Bazhelkov et al. 2000; Klaseboer et al. 2000; Fang et al. 2001; Saboni et al. 2002) agree that the process of coalescence occurs in a sequence of events as shown in Figure 2.4 and involves the following steps:

1. the droplet approaches the liquid-liquid interface under a driving force;
2. the thin film trapped between the two coalescing volumes starts to drain as the coalescing bodies approach each other;
3. as the film becomes sufficiently thin (approximately 1000 Å, as noted by Chen in 1985), the film ruptures and the neck starts to grow.

Eventually, the drop either merges completely with the bulk liquid or creates a daughter droplet along the interface. The process described is influenced by several variables, including the drop size, the interfacial tension of the liquids involved, their density and viscosity ratios, the presence of surfactants, and external factors like temperature and mechanical vibrations (Charles and Mason, 1960).

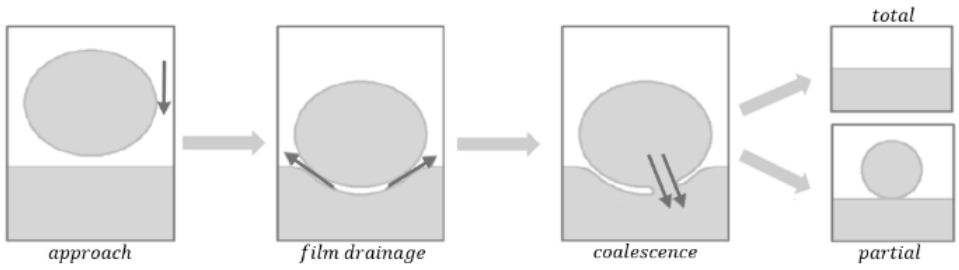

Figure 2.4: Stages of the process of drop coalescence.

The subsequent sections provide a concise overview of the three key steps of coalescence. Comprehensive reviews on coalescence have been written by Chesters (1991), Palermo (1991), Rommel et al. (1992), and Danov (2004), Kavehpour (2015).

2.3.1.1. Drop approach and collision

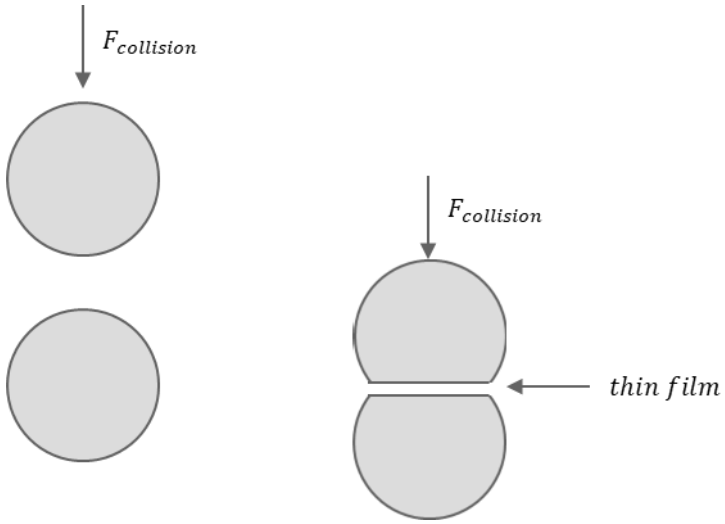

Figure 2.5: Two approaching drops (left) colliding (right). F being the collision force acting on the upper drop, while the lower drops is stationary (adapted from Lobo et al. 1993).

Drop collision, as illustrated in Figure 2.5, is primarily characterised by the collision frequency. The collision frequency refers to the rate of collisions within a specific volume per unit time and is predominantly influenced by the concentration of the dispersed phase and the level of turbulence within the continuous medium. In the case of two spherical drops of equal size following the same basic continuous-phase flow, Chesters (1991) provides equation 2.1 for the collision frequency C.

$$C = kvd_p{}^2\, n^2 \qquad 2.1$$

In the equation above, v is the characteristic velocity between the two drops, d_p is the drop diameter, and n is the number of drops per unit volume. Correlations for the characteristic velocity v and the coefficient k for three key flow types are given in Table 1.1.

Table 1.1: Particle collision rates in various flow regimes.

Flow type	v	k	Reference
Viscous simple shear	$\dot{\gamma} d_p$	2/3	Smoluchowski (1917)
Fine-scale turbulence	$\left(\frac{\varepsilon_r}{\nu}\right)^{1/2} d_p$	$\left(\frac{2\pi}{15}\right)^{1/2}$	Saffman and Turner (1956)
Inertial-subrange turbulence	$\left(\varepsilon_r d_p\right)^{1/3}$	$\left(\frac{8\pi}{3}\right)^{1/2}$	Kuboi et al. (1972)

Here, $\dot{\gamma}$ represents the shear rate, ε_r the energy dissipation in the system, and ν the kinematic viscosity.

Coulaloglou and Tavlarides (1977) propose equation 2.2 for the collision frequency C_{CT} of drops with sizes d_m and d_j

$$C_{CT}(d_m, d_j) = k_1 \frac{\varepsilon_r^{1/3}}{1+\varphi} \left(d_m + d_j\right)^2 \left(d_m^{2/3} + d_j^{2/3}\right)^{1/2}, \qquad 2.2$$

where φ represents the dispersed-phase volume fraction. Equation 2.2 appears to challenge the intuitive belief that a more concentrated dispersed phase is associated with a higher collision frequency.

Several authors (Van der Zande 2000; Henschke et al. 2002) propose that the collision frequency within the dense-packed zone is approximately equal to one, given that the drops are constantly in contact with each other. In such cases, the process of coalescence is primarily limited by the film drainage time.

In order for two drops to coalesce upon collision, it is essential that both the force of the collision and its duration are sufficiently high. If two drops come into contact without the required force, they will rebound before the film that separates them drains. According to Chesters (1991), the forces controlling particle collisions depend on whether the particle Reynolds number Re_p is significantly smaller or larger than one. In laminar flows, collisions tend to be primarily governed by viscous forces. In turbulent flows, collisions are governed by viscous forces if the particles involved are significantly smaller than the length scale of the smallest eddies (i.e. smaller than the Kolmogorov length scale), while collisions are governed by inertial forces if the particles are much larger than this length scale.

In viscous collisions, the collision force $F_{collision}$ is given by a Stokes-type expression

$$F_{collision} \approx \pi \mu_C r_p (\dot{\gamma} r_p) \qquad 2.3$$

where r_p is the drop radius. The typical collision duration $t_{collision}$ (i.e. the time two drops spend in close proximity) is expected to be

$$t_{collision} \approx \frac{r_p}{\dot{\gamma} r_p} \approx (\dot{\gamma})^{-1}. \qquad 2.4$$

In inertial collisions, the collision force $F_{collision}$ and the collision time $t_{collision}$ are given by equations 2.5 and 2.6 respectively (Chesters 1991).

$$F_{collision} \approx \rho_C v^2 d_p^2 \approx \rho_C d_p^2 \left(\varepsilon_r d_p\right)^{\frac{2}{3}} \qquad 2.5$$

$$t_{collision} \approx \frac{d_p}{v} \approx \left(\frac{d_p^2}{\varepsilon_r}\right)^{1/3} \qquad 2.6$$

In the dense-packed layer, where drops are frequently in contact, the approach and collision steps are rarely the limiting factors of the coalescence mechanism. Instead, the interfacial film drainage becomes the limiting step (Henschke et al. 2002). Consequently, modelling the time

required for the interfacial film to drain completely (referred to as the “drop rest time” or “drainage time”) is crucial to effectively model the coalescence mechanism in dense packed layers.

2.3.1.2. Drop rest time

The drop rest or drainage time, as defined by Charles and Mason (1960), represents the time interval between the arrival of the drop at the interface and the moment of the film rupture. The study of this rest time is of great importance as it represents a large fraction of the total coalescence time.

When a drop approaches the interface, liquid becomes trapped and a thin film is formed between the two coalescing bodies. Due to the narrowness of the channel formed between the drop and the bulk liquid, the film requires a long time to drain, hence drop-resting phenomena are often observed. While the drop rests on the interface, its body force deforms the interface. This leads to the deviation of the drop shape from its ideal spherical form. These deformations greatly influence the coalescence dynamics. Three forces control this deformation of the drop: the dynamic pressure, the fluid viscosity, and the surface tension (Hinze 1955).

Several researchers studied the rest time of droplets on the interface and observed variations in the times recorded, even under identical conditions. This phenomenon was attributed to several possible reasons, including drop

size variations, the presence of surfactants, interface impurities, temperature fluctuations, and mechanical instability. With a sufficiently large sample size, however, a distribution curve emerged. MacKay and Mason (1963) showed an increased rest time with increasing drop sizes. Hodgson and Lee (1969) and Chen et al. (1998) validated these findings, while Dreher et al. (1999) showed that the coalescence time is almost linearly dependent on the drop size.

Reynolds (1886) first attempted to model the drainage time through a simplistic approach by considering two parallel plane disks being squeezed together and proposed equation 2.7, which gives the velocity at which the interfacial film thins, V_{Re}.

$$V_{Re} = \frac{2h_f^3 F_{collision}}{3\pi\mu_C r_f^4} \qquad 2.7$$

In equation 2.7, h_f is the film thickness, $F_{collision}$ is the interaction force between the two planes, and r_f is the film radius. More recent and more complex models describe the evolution of the film drainage in greater detail (see Figure 2.6).

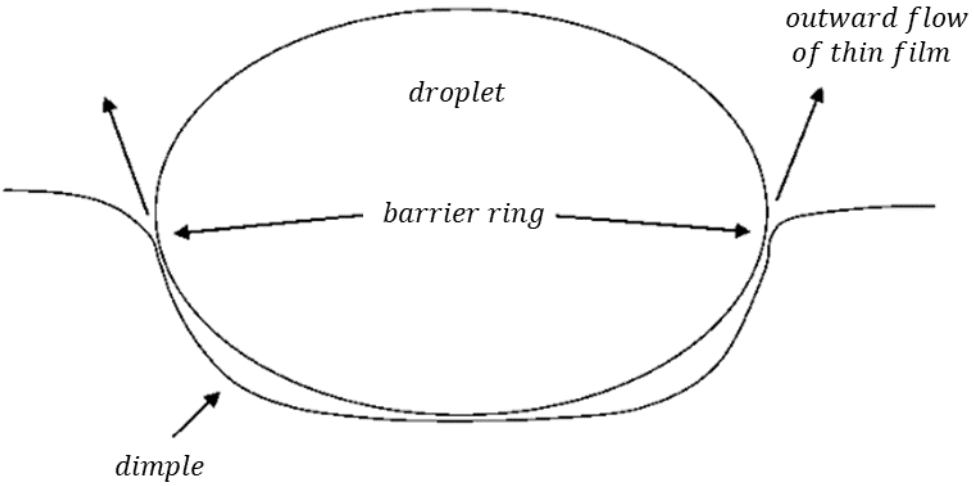

Figure 2.6: Drainage of the interfacial continuous film between a drop and its homophase (adapted from Rommel et al. 1992).

According to Rommel et al. (1992), interfacial film drainage is always accompanied by a non-uniformity in the film thickness, known as dimpling. Figure 2.6 illustrates the presence of a barrier ring at the ends of the draining film. The barrier ring hinders the drainage of the film between the two coalescing bodies, before the film reaches the critical thickness at which rupture occurs and coalescence occurs. This phenomenon is primarily attributed to the Marangoni effect. Palermo (1991) further provides a step-by-step description of the film flow process. Nevertheless, these descriptions remain largely qualitatively and phenomenological due to the intricate nature of the system. Only Rommel et al. (1992) list some empirical or semi-empirical models from the literature. The thinning of the liquid film then progresses until it reaches a critical thickness, at which point the film

becomes unstable, and thermal or mechanical stresses can result in film rupture. (Palermo, 1991)

The mobility of the interface between the droplet and the thin film is also very important for the determination of the drainage time. Three different types of interfaces are typically identified in the literature:

- Immobile interfaces.
- Partially mobile interfaces
- Mobile interfaces

Palermo (1991) characterises an interface as immobile when no tangential velocity is observed. This definition does not inherently influence the deformation of the interface or the motion of the drop itself. From a more practical standpoint, Chesters (1991) suggests that the assumption of immobile interfaces holds true when the dispersed phase has a very high viscosity, approaching the behaviour of solid particles, or when sufficient concentration of surfactants is present at the interface. The latter condition appears to be applicable to nearly all water/crude oil emulsions, where natural surfactants (such as, asphaltenes and resins) are typically abundant (Frising et al. 2006). Klaseboer et al. (2000) confirmed that the existence of surfactants in the continuous phase is a sufficient condition for employing the immobile interface approximation.

Drainage between deformable immobile interfaces

In cases where the immobile interface approximation applies, the approach velocity $-dh/dt$ is determined by equation 2.8:

$$-\frac{dh_f}{dt} = \frac{2h_f^3 F_{collision}}{3\pi\mu_C r_f^4} \qquad 2.8$$

According to Chesters (1991) $F_{collision} \cong \pi r_f^2 (2\gamma/r_p)$. This equation allows the elimination of the film radius r_f, hence equation 2.8 becomes:

$$-\frac{dh_f}{dt} \cong \frac{8\pi\gamma^2 h_f^3}{3\mu_C r_p^2 F_{collision}} \qquad 2.9$$

where γ is the interfacial tension and r_p the drop radius.

If F is constant, equation 2.9 integrates to

$$\frac{1}{h_f^2} - \frac{1}{h_{f,0}^2} \cong \frac{16\pi\gamma^2}{3\mu_C r_p{}^2 F_{collision}} t \qquad 2.10$$

where $h_{f,0}$ is the initial film thickness.

Drainage between deformable partially-mobile interfaces

The approximation of immobile interface applies primarily to systems with exceptionally high dispersed-phase viscosities or those that include a surfactant. In numerous pure liquid-liquid systems, the drainage process is

mainly influenced by the motion of the film surface. Chesters (1991) referred to this condition as partial mobility, reserving the term full mobility for systems where the interface is essentially shear-stress free. In the case of partially-mobile interfaces, the film thinning rate is given by (Chesters 1991)

$$-\frac{dh_f}{dt} \cong \frac{2(2\pi\gamma/r_p)^{3/2}}{\pi\mu_{\mathrm{D}}\sqrt{F_{collision}}} h_f^2. \qquad 2.11$$

At constant $F_{collision}$, integration of equation 2.11 gives

$$\frac{1}{h_f} - \frac{1}{h_{f,0}} \cong \frac{2(2\pi\gamma/r_p)^{3/2}}{\pi\mu_{\mathrm{D}}\sqrt{F_{collision}}} t \qquad 2.12$$

Drainage between deformable fully mobile interfaces

When the dispersed phase viscosity is sufficiently low, drainage is no longer controlled by the dispersed phase as in partially-mobile interfaces, but by the resistance of the film to deformation and/or acceleration. The prevalence of forces related to the film resistance to deformation characterises viscous control, while the prevalence of forces related to the film resistance to acceleration corresponds to inertia control. (Chesters 1991)

When viscous forces dominate the rate of film thinning becomes

$$-\frac{dh_f}{dt} = \frac{2\gamma h_f}{3\mu_C r_p}. \quad 2.13$$

Upon integration, equation 2.13 becomes

$$h_f = h_{f,0} e^{-t/t_{ch}}, \quad 2.14$$

where

$$t_{ch} = \frac{3\mu_C r_p}{2\gamma}. \quad 2.15$$

When inertial forces dominate, equation 2.14 is still valid, however the characteristic time becomes

$$t_{ch} = \frac{\rho_C V {r_p}^2}{8\gamma}, \quad 2.16$$

where V is the relative velocity of the colliding droplets. Nevertheless, determining simple and readily applicable criteria in the literature for determining the interfacial mobility of a system remains challenging.

2.3.1.3. Film rupture

When the film drains to a thickness of approximately 0.1 μm, the van der Waals forces become significant and rupture occurs, as noted by Chen (1985). Film rupture occurs almost instantaneously in comparison to drop collision and film drainage, which is why it has attracted relatively little

attention from researchers. Nevertheless, research on film rupture is rapidly growing (Mohamed-Kassim and Longmire 2004; Aarts and Lekkerkerker 2008; Eri and Okumura 2010; De Malmazet et al. 2015).

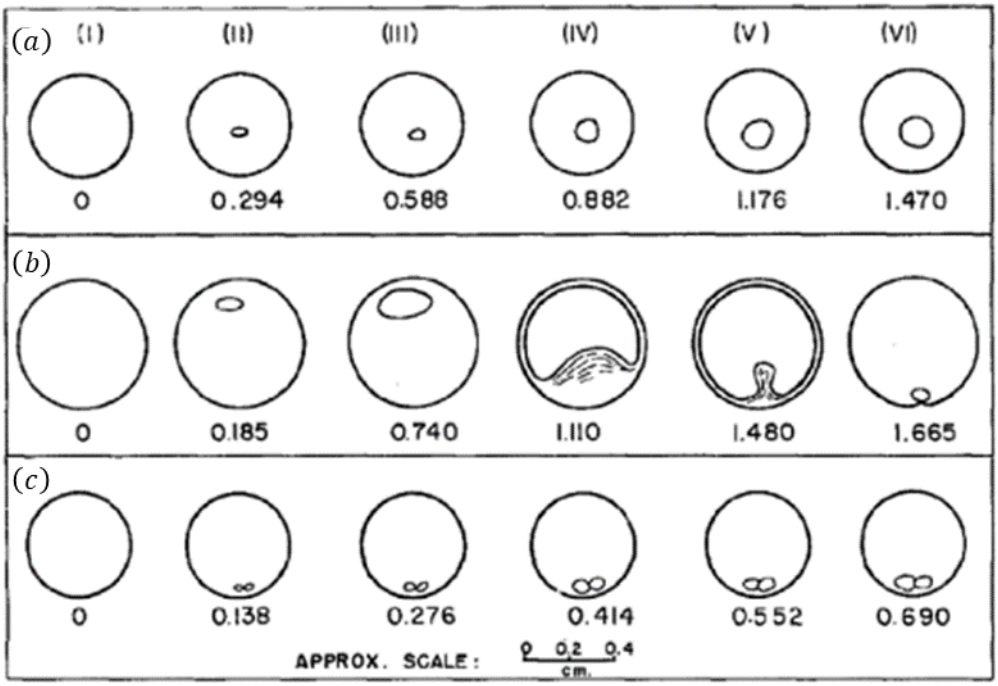

Figure 2.7: Different types of film rupture: (a) central rupture, (b) off-central rupture, (c) double rupture (adapted from Charles and Mason 1960).

Rupture is identified with the first observable hole in the film, and typically occurs at its thinnest location, which can be either at the centre or off-centre. Existing literature identifies three main types of rupture: central rupture, off-centre rupture, and double rupture (Charles and Mason 1960; Neitzel and Dell'Aversana 2002). Off-centre rupture was more frequently observed in

experiments than central rupture, while double rupture was the least frequent of all. In the cases of central rupture, the hole maintained its circular shape upon expansion. In the cases of the off-centre rupture, a retarded film segment was observed. This eventually detached from the film and formed a single droplet (see Figure 2.7(b)). In the rare cases of double rupture, the film breaks at two points simultaneously resulting to two holes. The two holes eventually merged into one when they expanded sufficiently.

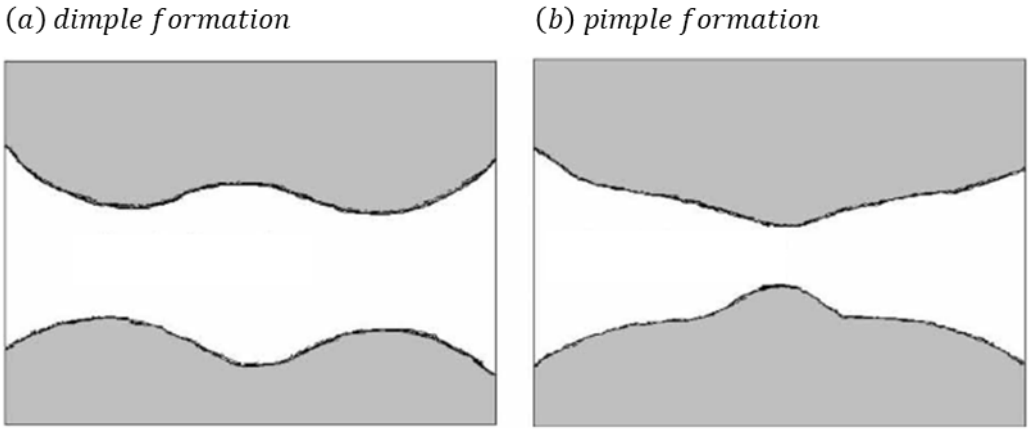

Figure 2.8: Rupture of the interfacial film by formation of a dimple (left) or a pimple (right) (adapted from Frising et al. 2006).

According to Chesters (1991), when the film thickness exceeds the range of intermolecular interactions, these forces can be sufficiently represented by the approximation of an interfacial tension. In situations involving thin films, however, Chesters (1991) notes that a tangential force also exists, which alters the drainage mechanics. Yeo et al. (2003) performed a parametric study on the drainage dynamics and identified three distinct

regimes of drainage and possible rupture depending on the relative magnitudes of the drop approach velocity and the van der Waals interactions:

1. Nose rupture: When the drops collide at low approach velocities and strong van der Waals interactions, the film protrudes at the centre of the drop, forming a so-called pimple and rupture occurs in the nose region (see Figure 2.8).
2. Interface immobilisation: When the drops collide at high approach velocities and weak van der Waals interactions, under the action of weak negative disjoining pressure forces, a dimple forms, gradually flattening into an almost parallel film. This leads to the immobilisation and flattening of the film, with no film rupture being observed.
3. Rim rupture: At moderate approach velocities and van der Waals interactions, a dimple forms that subsequently ruptures along the curvature of the rim of the dimple (see Figure 2.8).

Most authors in the literature predominantly focus on dimple formation and nose rupture.

2.4. Dispersion separation modelling

As the dispersions settle, distinct layers form along the pipe and different flow patterns emerge. Accurate characterization of the flow pattern transitions in unstable dispersed flows is vital for the design and operation of industrial facilities.

Due to the intricate nature of dispersed pipe flows and the challenges in acquiring direct measurements in industry, models play a vital role in the prediction and understanding of their behaviour. Models offer invaluable insights, particularly for systems where experimental data is scarce. Such knowledge is critical for optimising the design and operation of industrial facilities, as well as for predicting the behaviour of the dispersed system under different operating conditions or when different fluids are used. Despite these crucial aspects, there has been limited focus on the development of accurate models for predicting the evolution of patterns of liquid-liquid flows in pipes and the separation length of dispersions.

2.4.1. CFD modelling

Computational fluid dynamics (CFD) approaches can provide phase distribution with high resolution. Thus far, few CFD studies have been reported on predicting the flow pattern and phase distribution in horizontal oil-water flows (Walvekar et al. 2009; El-Batsh et al. 2012; Pouraria et al. 2016, Voulgaropoulos et al. 2019, Chen et al. 2022). The prediction of the flow patterns and the phase fraction profiles at low mixture velocities where the effect of gravity becomes significant and transitions take place is even more complex.

2.4.2. Semi-empirical modelling

Semi-empirical models for dispersed flows focus exclusively on the primary separation mechanisms while also incorporating fitted parameters specific to each liquid-liquid system. They have the advantage of providing fast predictions, but their performance relies heavily on the precise estimation of their parameters. Nevertheless, they are often preferred by industry to complex CFD simulations due to their low computational time and their ability to provide predictions quickly for extrapolation and scale-up.

Previously a few authors attempted to model the separation of dispersions in batch settlers using semi-emprical models (Hartland and Jeelani 1988; Jeelani and Hartland 1998; Henschke et al 2002). Later works attempted to extend the batch models to one-dimensional flows in horizontal pipe separators (Pereyra et al. 2013; Othman et al. 2018) by changing the time scale to a length scale using the average mixture velocity and accounting for the change in geometry.

2.4.2.1. Batch separator

Several semi-empirical models have been developed for dispersion separation in batch settlers. Assuming an oil-in-water dispersion in a batch settler, separation begins with the formation of a pure water layer at the bottom of the settler as the oil drops begin to float upwards. Eventually, several drops reach the coalescing interface and accumulate into a dense-

packed zone. Interfacial coalescence of drops with the pure oil layer results in an increase in the oil layer thickness.

Frising et al. (2006) published a comprehensive review of the models available in literature for the prediction of the separation behaviour of batch liquid-liquid dispersions. The authors noted that these models can be broadly classified into two types: settling-based models and coalescence-based models. Settling-based models were mostly developed by Hartland and Jeelani and their colleagues (Jeelani and Hartland 1986a,b; Jeelani and Hartland 1988; Jeelani et al. 1990; Jeelani and Hartland 1993; Bhardwaj and Hartland 1994; Mason et al. 1995; Panoussopoulos et al. 1997; Balmelli et al 2000; Jeelani et al. 2005a,b; Jeelani et al. 1999), and assume that the separation process involves two main mechanisms, namely drop-settling and interfacial coalescence. On the other hand, coalescence-based models focus on very small ($< 100\ \mu m$), non-deformable drops, and consider drop-drop coalescence as the primary separation mechanism (Lobo et al. 1993). Other models, such as those developed by Henschke et al. (2002) and Noïk et al. (2013), comprehensively include all three separation mechanisms (i.e. settling, drop-drop coalescence, and drop-interface coalescence).

2.4.2.2. In-line separator

Pereyra et al. (2013) extended the batch model by Henschke et al. (2002) to one-dimensional horizontal pipe separators, by considering the change in geometry and by utilizing the average mixture velocity to convert the time

scale to a length scale. Similarly to the majority of batch separation models, the rate of drop-settling was considered to surpass the coalescence rate, leading to the formation and growth of a dense-packed zone.

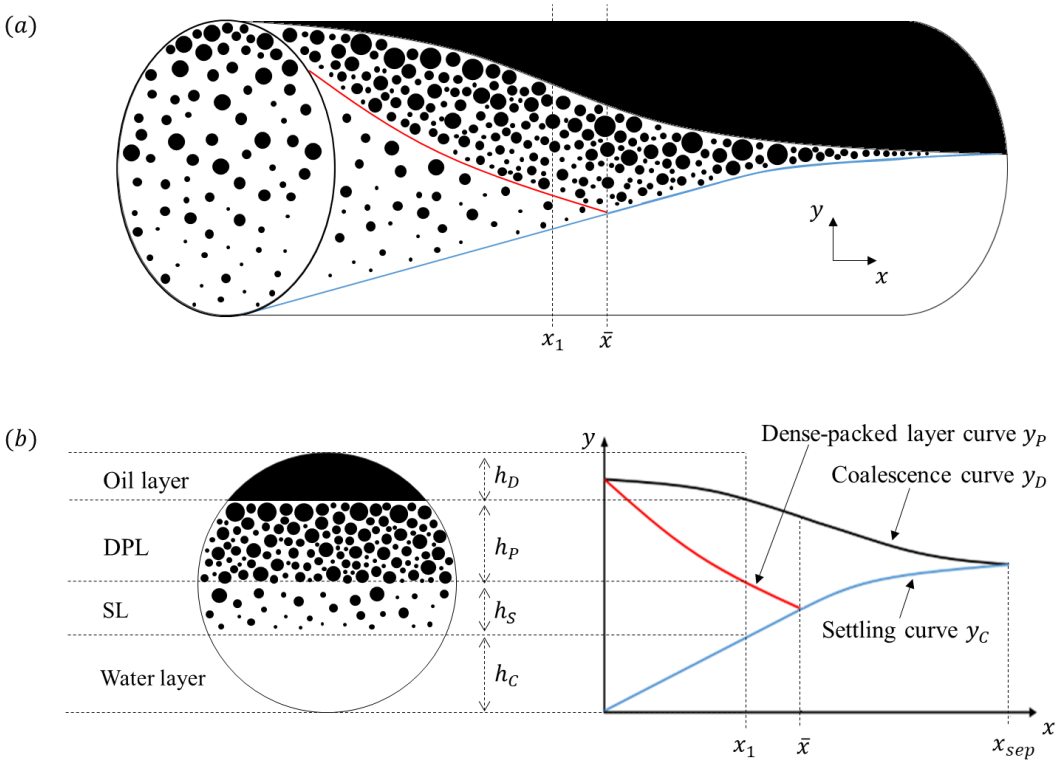

Figure 2.9. (a) A schematic illustrating dispersion separation in a horizontal pipe separator, (b) graph showing the layer evolution in the pipe separator and a schematic of the pipe cross section that shows the distinct layers at x=x₁. The oil phase is represented in black, while the water phase is represented in white. (Evripidou et al. 2023a)

According to this model, in the case of a fully dispersed oil-in-water flow in a horizontal pipe separator, separation process begins as the less dense oil

drops begin to float upwards, forming a pure water layer at the bottom of the pipe (Figure 2.9). As the drops continue to float, the thickness of the pure water layer gradually increases. Eventually, some drops reach the top of the pipe where they accumulate into a dense-packed zone. Within the dense-packed zone, the drops remain in contact with each other for a sufficient duration, facilitating their coalescence. This process continues until a thin film of pure oil eventually develops at the top of the pipe. Coalescence of drops with the liquid film results in an increase in the thickness of the pure oil layer. This process continues until complete separation is achieved (see $x = x_{sep}$ in Figure 2.9).

Voulgaropoulos (2017) applied this model to pipe flows, where the mixture velocities are typically orders of magnitude larger than those observed in horizontal pipe separators. He reported cases where the dense-packed layer depletes, highlighting a major limitation of current models, which are only valid for certain flow configurations and flow pattern transitions, and cannot be applied to all pipef flows.

2.5. Statistical verification of models

All models should be validated, as the use of unvalidated models can result in highly inaccurate conclusions. The ability of a model to accurately represent a physical system must be evaluated by comparing its predictions against observed experimental data. Semi-empirical models, including

those discussed in Section 2.4.2 and those to be developed here, incorporate adjustable parameters with physical significance. Precise parameter estimates can be challenging to obtain as the system may be affected by identifiability issues (Galvanin et al. 2013). Identifiability refers to the ability to estimate the true values of the model parameters given an infinite volume of data (Lavielle and Aarons, 2016). Therefore, it is crucial to assess the feasibility of determining the values of the parameters and their highest attainable precision, while also subjecting both the estimates and the model to statistical validation.

Batch separation models, such as those developed by Jeelani and Hartland (1994) and Henschke et al. (2002), incorporate coalescence parameters that are determined experimentally. Henschke et al. (2002) determined the values of the coalescence parameter for different liquid-liquid systems through batch-settling experiments, conducting a large number of measurements of the heights of the settling and the coalescence curves over time until complete separation was achieved.

In multiphase flows, it is usually impossible to fit the parameters using industrially acquired data due to the scarcity of essential measurements required for parameter estimation, particularly measurements that entail the necessary level of detail, in many industrial settings. Additionally, limitations posed by the opaque test-sections and fluids, which restrict visual

observations and hinder the use of several sampling methods, further exacerbate the difficulty. Instead, the necessary information can be obtained in pilot-scale laboratory experiments (Pereyra et al. 2013; Voulgaropoulos et al. 2019). Pilot-scale facilities, however, are often small in length and diameter; hence, the experiments must be carefully designed to ensure that the measurements provide sufficient information for parameter estimation.

When conducting experiments to measure the layer heights during the separation of dispersions in pipes, it becomes unfeasible to perform measurements until complete separation occurs. This limitation arises from the need for excessively long pipes, surpassing the typical lengths available in laboratories. Pereyra et al. (2013) conducted measurements of the layer heights spanning only 6 m from the pipe inlet and noted that due to the limited length of the pilot-scale facilities, experimental data never demonstrate complete separation. In a specific case study, Pereyra et al. (2013) estimated the predicted length of the separator to be more than twice the length of the experimental facility. Similarly, Voulgaropoulos et al. (2017) explored six case studies involving the separation of dispersions in pipes within a pilot-scale flow facility and obtained predicted separation lengths that were as large as 15 times the length of the sampled section. Consequently, more sophisticated approaches are needed to precisely estimate the fitted parameters in the separation of dispersions in pipes and in-line separators.

Several computational methods are available for parameter estimation. These methods either utilise existing experimental measurements or entail model-based experimental design to maximise the collection of information available for parameter estimation. Parametric sensitivity analysis (PSA) is a convenient tool that is utilised during experimental design, to understand the effect of parameters on the model responses (Saltelli et al. 2009). PSA helps to identify parametrically sensitive regions in a pipe, which are favourable sampling locations. A pipe region is said to be parametrically sensitive when a small variation in some of the uncertain model parameters leads to significant variations in one or more of the model outputs. Additionally, model-based design of experiments (MBDoE) methods can be used to ensure that the designed experiment will maximize the information produced by the measurements.

Various MBDoE techniques have been suggested in the literature to design experiments that aim to improve the statistical precision of parameter estimates (Quaglio et al. 2018; Huang et al. 2023). Franceschini and Macchietto (2008) present a comprehensive review of MBDoE for parameter precision including several applications of the techniques across various fields.

According to Franceschini and Macchietto (2008) MBDoE is characterised by:

1. the use of the equations of the model, including any constraints, and the current parameter estimates to predict the “information content” of an upcoming experiment, by evaluating of a suitable objective function, and
2. the application of an optimisation framework to solve the resulting numerical problem.

Drawing from the work of Espie and Macchietto (1989), Zullo (1991), and Asprey and Macchietto (2000), Franceschini and Macchietto (2008) defined a procedure for developing and statistically verifying dynamic process models. This process comprises of up to three steps:

1. Preliminary analysis studying the issues of identifiability and distinguishability (i.e. the ability to differentiate between different models), with the aim of either making an initial selection between competing models or analysing a single model prior to data collection.
2. Design of optimal experiments to differentiate between competing models that were selected in the first step.
3. Design of optimal experiments to enhance the precision of the parameter estimates for the model chosen in the second step.

According to the authors, in certain cases it is justified to skip certain stages. For instance, in the case where there is only one candidate model, it may

be appropriate to skip the first two steps and only perform a MBDoE for parameter precision. Given that the available information at each stage is frequently limited, incomplete, or imprecise, the statistical validation process for a model is inherently iterative, involving multiple iterations both within and between the steps outlined above.

Three primary approaches exist in iterative MBDoE: sequential, parallel, and parallel/sequential. In a sequential approach, the aim is to improve the nominal values of the parameters through an iterative process that alternates between experiment design and parameter identification. Every subsequent experiment being designed uses the parameter estimates acquired in the previous parameter estimation step as the initial parameter values. This iterative process continues until statistically adequate parameter estimates are obtained. Sequential MBDoE stands out as the most prevalent strategy (Hosten and Emig 1975; DiStefano 1981; Kalogerakis and Luus 1983, 1984; Wu 1985; Ford et al. 1985, 1989; Pinto et al. 1990; Walter and Pronzato 1997; Bernaerts et al. 2002).

Galvanin et al. (2007) suggested that several experiments can be conducted either sequentially or in parallel, based on the experimental set-up available. This led to the development of parallel and mixed parallel/sequential strategies. In a parallel approach, multiple optimal experiments are simultaneously designed, with each experiment using the

same initial parameter values. The designed experiments are then conducted in the laboratory. Subsequently, the parameters are estimated using all the data acquired from the experiments designed in parallel, and their statistical significance is assessed. If after the parameter estimation, it is proven that the n_{exp}^{P} parallel experiments provide inadequate information for parameter estimation, the process is repeated using the new estimates as the nominal parameter values, leading to a parallel/sequential approach.

Conventional MBDoE methods for parameter precision are based on the solution of an optimization problem where the objective function to maximize is a metric of expected information. The expected information for the estimation of the model parameters is evaluated through the Fisher Information Matrix (FIM) (Pukelsheim 1993). The FIM is a measure of the sensitivity of the model responses to a variation in the values of the model parameters (Walter and Pronzato 1997). Typically, the experimental design metric being maximized is a scalar quantity (e.g. the trace) of the *expected* FIM (Walter and Pronzato 1997) which is the inverse of the variance-covariance matrix of model parameters. Popular experimental design metrics are the so-called alphabetical criteria (Pukelsheim 1993) including FIM determinant (D-optimal criterion), trace (A-optimal criterion), minimum eigenvalue (E-optimal criterion), or ratio between maximum and minimum FIM eigenvalues (modified E-optimal). Once the experiment is performed, data are collected and the measurements are used in the parameter

estimation problem to compute the observed FIM and characterise the variance of model parameters.

2.6. Conclusions

Existing semi-empirical models for separating dispersions in pipes are essentially extensions of batch separation models. They operate under the assumption of coalescence-controlled separation, where the rate of drop-settling was considered to exceed the coalescence rate, resulting in the formation and growth of a dense-packed zone. However, Voulgaropoulos (2017) reported cases in which the dense-packed layer depletes, underscoring a significant limitation of current models. These models are only applicable to specific flow configurations and flow pattern transitions, rendering them unsuitable for certain pipe flows.

The objective of this work is to develop a semi-empirical model capable of predicting the development of flow patterns and the separation of unstable liquid-liquid dispersed pipe flows. The aim is to predict all potential flow pattern transitions during dispersion separation in pipes, particularly in pipe locations where only a dilute dispersed layer is present. This scenario is common in dispersed systems with high mixture velocities or small drops, which are not captured by previous models. The applicability of the model will be tested for both oil-in-water and water-in-oil dispersions.

The role of coalescence models in the separation will be explored through a comparative study. This analysis seeks to understand their impact on

model predictions and identify the most suitable model for application in pipe flows.

Finally, the literature review has highlighted a significant challenge in fitting adjustable parameters within semi-empirical models for the separation of dispersions in pipes. This challenge arises from limitations in the pipe test section of experimental facilities, which impose constraints on the sampling length, making it impossible to conduct measurements up to the point of complete separation. To overcome this, a combination of techniques, including parameter estimation, parametric sensitivity analysis, and model-based design of experiments, will be employed. The objective is to propose optimal experimental conditions for obtaining precise parameter estimates, thus enhancing the accuracy of the forthcoming model. The ultimate aim is to establish a framework for identifying optimal experimental conditions when utilising semi-empirical models to analyse the separation of dispersed flows in pipes. This approach can be applied to determine optimal configurations for existing setups and to develop new experimental protocols from inception, with the goal of ensuring that the acquired measurements contain sufficient information for the precise estimation of parameters.

Chapter 3

3. Semi-empirical modelling[1]

In this chapter, a semi-empirical model is developed that predicts the flow pattern development and separation of unstable liquid-liquid dispersed pipe flows. New approaches are proposed to predict all possible flow pattern transitions occurring during flow separation, which are not captured in existing models. The model is based on the horizontal pipe separator approach described in Pereyra et al. (2013), which, however, was valid only for systems where a dense-packed layer is formed. In what follows, all flow pattern transitions that may arise during separation of dispersions are identified. The development of the model is then described, placing emphasis on the pipe locations where only a dilute dispersed layer is present, which is often the case in dispersed systems at high mixture velocities or with small drops present, and which are not predicted by previous models. Lastly, the applicability of the model to flows of both oil-in-water and water-in-oil dispersions is demonstrated. The model accounts for the main mechanisms that occur during pipe flow and provides information on the evolution of dispersed flows in systems where sampling is not feasible.

[1] The work presented in this chapter has been published in the International Journal of Multiphase Flow (Evripidou et al. 2022).

3.1. Semi-empirical model

The separation of liquid-liquid dispersions is driven by three main mechanisms: drop settling (flotation or sedimentation), drop-drop coalescence, and drop-interface coalescence. Separation can give rise to four distinct layers: a pure layer of the continuous phase, a settling layer (a dilute dispersion where drop settling occurs), a dense-packed layer (a densely packed dispersion where drop-drop coalescence occurs), and a pure layer of the initially dispersed phase. Throughout this paper, the four layers are denoted by the subscripts C, S, P, and D respectively.

Figure 3.1 shows schematics of different flow profiles that can arise from fully or partially dispersed flows at the pipe inlet and the flow patterns observed along the pipe in each case. The flow profiles are plots that show the progression of the characteristic layers along the pipe. On the x-axis, they have the axial displacement from the pipe inlet and on the y-axis the height from the bottom of the pipe.

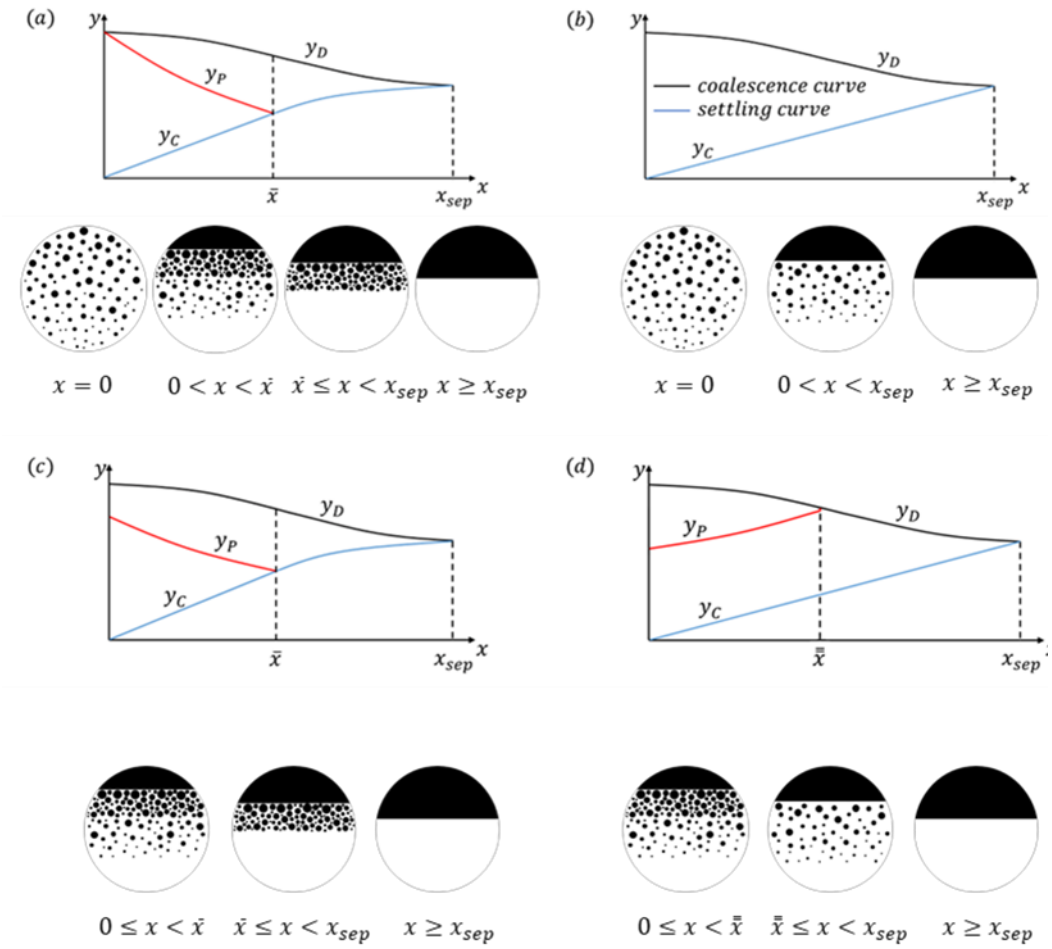

Figure 3.1. Schematics of flow profiles showing the evolution of the characteristic layers and the flow patterns along the pipe for dispersed liquid-liquid systems with different inlet conditions.

The *settling (flotation/sedimentation) curve* is given by y_C, and in an oil-in-water dispersion, it corresponds to the height of the water layer from the bottom of the pipe. The *coalescence curve*, denoted by y_D, gives the location of the pure oil interface. The thickness, h, of each of the characteristic layers is dependent on drop settling rate, as well as the drop-drop and drop-interface coalescence rates. If the rate of drop settling is faster than the rate of drop-interface coalescence, accumulation of drops

into a dense-packed zone is observed at the oil-water interface (cf. Figure 3.1 (a)). Within the dense-packed zone, the drops are in close proximity and the contact time often exceeds the coalescence time leading to drop-drop coalescence and an increase in the average drop size along the pipe. Coalescence of the oil drops with the bulk oil phase also occurs and results in an increase of the oil layer thickness with pipe length.

Depletion of the settling layer is possible as the flow evolves, as shown in Figure 3.1(a) and Figure 3.1(c) at $x = \bar{x}$. Alternatively, if the rate of drop settling is smaller than the rate of drop-interface coalescence, the dense-packed zone is depleted. This is the case in Figure 3.1(d) at $x = \bar{\bar{x}}$. At lengths greater than $\bar{\bar{x}}$ (i.e. for $x > \bar{\bar{x}}$), the settling layer is in direct contact with the pure oil layer and the rate of drop settling (and availability of drops at the interface) limits the rate of coalescence. If the flow is initially fully dispersed, but the drop settling rate is less than the drop-interface coalescence rate, the rate of drop settling will control the rate of coalescence throughout the pipe, and a dense-packed zone will never form (cf. Figure 3.1(b)). The length required to reach complete separation of the two immiscible liquids ($x = x_{sep}$) can be determined from the intersection point of the *coalescence curve* and the *settling curve*.

The model developed here predicts the changes in thickness of the various layers and the mean drop diameter along the pipe, giving the complete flow profile up to the point of complete phase separation. The model assumes a

constant velocity, equal to the mixture velocity u_{M}, across all layers along the spanwise direction, thus neglecting velocity profiles and exchange of momentum between the layers. This is a reasonable assumption for liquid-liquid systems where experiments showed that the slip is very small, especially in the dispersed regions (Lovick and Angeli 2004b). The surface tension is assumed to be constant throughout, while the mixture is assumed to be monodispersed. Drop break-up is not considered. Although in reality there is no apparent interface between the two dispersed layers, settling and dense-packed, for modelling purposes, it was assumed that these are two distinct layers. The dispersed-phase fraction within each layer is taken as constant with height and a step-change in the fraction is assumed at the interface between the two layers.

Below the various parts of the model are described in detail.

3.1.1. Settling curve

The primary separation mechanism acting on a dispersed liquid-liquid mixture is density-driven settling. In the presence of a settling layer, the *settling curve*, y_{C}, changes solely due to the vertical displacement of drops. In an oil-in-water dispersion, the *settling curve* corresponds to the height of the pure water layer from the bottom of the pipe and can be predicted in terms of pure water layer thickness by

$$\frac{dh_{\mathrm{c}}}{dx} = \frac{u_{\mathrm{s}}}{u_{\mathrm{M}}}. \qquad 3.1$$

Assuming a continuous phase of viscosity μ_{C} and density ρ_{C}, and a dispersed phase of viscosity μ_{D} and density ρ_{D}, the vertical (sedimentation/flotation) velocity u_{s} of drops of size d_{p}, within a settling layer with dispersed-phase fraction φ_{S} can be obtained using

$$u_{\mathrm{s}} = C_h \frac{3\lambda\varphi_{\mathrm{S}}\mu_{\mathrm{C}}}{C_{\mathrm{w}}\xi(1-\varphi_{\mathrm{S}})\rho_{\mathrm{C}}d_{\mathrm{p}}}\left[\left(1 + Ar\frac{C_{\mathrm{w}}\xi(1-\varphi_{\mathrm{S}})^3}{54\lambda^2\varphi_{\mathrm{S}}^2}\right)^{0.5} - 1\right]. \qquad 3.2$$

Equation 3.2 is based on an empirical model developed by Pilhofer and Mewes (1979) from drop settling experiments in batch vessels, but has been modified by Evripidou et al. (2019) who introduced a fitted hindered settling parameter, $\mathrm{C_h}$, to better capture delay in settling due to the flow. This correlation was developed for a monodispersed system taking as the average drop diameter the Sauter mean diameter in the settling layer.

In equation 3.2 the two settling parameters are equal to

$$\lambda = \frac{1-\varphi_{\mathrm{S}}}{2\varphi_{\mathrm{S}}K_{\mathrm{HR}}}\exp\left(\frac{2.5\varphi_{\mathrm{S}}}{1-0.61\varphi_{\mathrm{S}}}\right) \qquad 3.3$$

and

$$\xi = 5K_{\mathrm{HR}}^{-\frac{3}{2}}\left(\frac{\varphi_{\mathrm{S}}}{1-\varphi_{\mathrm{S}}}\right)^{0.45}. \qquad 3.4$$

Other dimensionless numbers include the Archimedes number, *Ar*, which is given by

$$Ar = \frac{\rho_{\mathrm{C}} \Delta\rho g d_{\mathrm{p}}^3}{\mu_{\mathrm{C}}^2} \tag{3.5}$$

where g is the gravitational constant, the Hadamard-Rybczynski factor, K_{HR}, given by

$$K_{\mathrm{HR}} = \frac{3(\mu_{\mathrm{C}} + \mu_{\mathrm{D}})}{2\mu_{\mathrm{C}} + 3\mu_{\mathrm{D}}}, \tag{3.6}$$

and a modified friction coefficient, C_{W} , given by

$$C_{\mathrm{w}} = \frac{Ar}{6Re_{\infty}^2} - \frac{3}{K_{\mathrm{HR}} Re_{\infty}}. \tag{3.7}$$

The Re_{∞} is the Reynolds number of a single drop moving vertically in an infinite medium. According to Ishii and Zuber (1979)

$$Re_{\infty} = 9.72\left[(1 + 0.01Ar)^{\frac{4}{7}} - \bar{1}\right]. \tag{3.8}$$

In the absence of a settling layer (i.e. for $x > \bar{x}$ in Figure 3.1(a) and Figure 3.1(c)), the thickness of the continuous phase layer can be obtained by

$$h_{\mathrm{C}} = ID - h_{\mathrm{P}} - h_{\mathrm{D}}, \tag{3.9}$$

where ID denotes the internal diameter of the pipe.

3.1.2. Coalescence curve

Accumulation of drops near the top of the pipe due to drop settling results in coalescence. Eventually a continuous oil layer of thickness h_{D} is formed. The increase in h_{D} with pipe length is captured by the *coalescence curve*, y_{D}, and is determined by the volume rate of coalescence of drops with the oil interface. Assuming a monodispersed mixture at the interface, where all drops have the same diameter $d_{\mathrm{p,I}}$, Pereyra (2011) showed that the evolution of the oil layer thickness along a horizontal pipe is given by

$$\frac{\mathrm{d}h_{\mathrm{D}}}{\mathrm{d}x} = \frac{2\varphi_{\mathrm{I}}\mathrm{d}_{\mathrm{p,I}}}{3\tau_{\mathrm{I}}u_{\mathrm{M}}}, \qquad 3.10$$

where τ_{I} is the drop-interface coalescence time. In the presence of a dense-packed layer, we set the oil fraction at the interface, φ_{I}, to 0.9 which is a reasonable value for maximum packing for a polydispersed mixture (Farr and Groot 2009; Dorr et al. 2013). In the absence of a dense-packed layer (i.e. Figure 3.1(b) and Figure 3.1(d) for $x > \bar{\bar{x}}$), such that the settling layer is in direct contact with the pure oil layer, we suggest that φ_{I} is determined by the relative rates of drop settling and drop-interface coalescence. Assuming monodispersed layers, the average drop diameter at the interface $d_{\mathrm{p,I}}$ is taken to be equal to the Sauter mean diameter in the respective dispersed layer (dense-packed or settling).

3.1.3. Drop size evolution

Drop-drop coalescence can only occur if the contact time between two

drops exceeds the drop-drop coalescence time, τ_{C}. The relative motion of the drops with respect to each other is negligible within the dense-packed layer and along the coalescing interface, thus drop-drop coalescence is always considered in these locations. Following the assumption that all layers are monodispersed, at every axial location the drops found along the interface or within a dense-packed layer, have the same size $d_{\mathrm{p,I}}$. Jeelani and Hartland (1998) suggested the following expression for the prediction of drop size evolution as a function of drop-drop coalescence time τ_C:

$$\frac{d\left(d_{\mathrm{p,I}}\right)}{dx} = \frac{d_{\mathrm{p,I}}}{6\tau_{\mathrm{C}} u_{\mathrm{M}}}. \qquad 3.11$$

Computation of the Reynolds numbers of the settling layer for the case studies considered here showed that the settling layer falls into the transition to turbulent flow regime, and drop-drop coalescence within the settling layer is not considered further in this work.

3.1.4. Coalescence time

Coalescence models for the calculation of coalescence rates or times in separating dispersions in batch vessels have been proposed by Jeelani and Hartland (1994) and Henschke et al. (2002). The coalescence models will be investigated in detail in Chapter 4. Meanwhile, the coalescence correlations developed by Henschke et al. (2002), as presented in Pereyra et al. (2013), have been incorporated here into the model.

Henschke et al. (2002) assumed film drainage during coalescence and concluded that the drop-drop and drop-interface coalescence times can be obtained by

$$\tau_{\mathrm{C}} = \frac{(6\pi)^{7/6}\mu_{\mathrm{C}} r_{\alpha}^{7/3}}{4\gamma^{5/6} H^{1/6} r_{\mathrm{F,C}} r_V^*} \qquad 3.12$$

and

$$\tau_{\mathrm{I}} = \frac{(6\pi)^{7/6}\mu_{\mathrm{C}} r_{\alpha}^{7/3}}{4\gamma^{5/6} H^{1/6} r_{\mathrm{F,I}} r_V^*} \qquad 3.13$$

respectively. In equations 3.12 and 3.13, γ is the interfacial tension between the two phases. r_V^* is the asymmetry parameter describing the asymmetry of the film between adjacent drops. It can be obtained from experimental settling curves and is characteristic for the system used. The Hamaker coefficient H is set to 10^{-20} N m, as proposed by Henschke et al. (2002) for any system. The drop-drop contact area radius $r_{\mathrm{F,C}}$ is calculated by

$$r_{\mathrm{F,C}} = 0.3025 d_{\mathrm{p}} \sqrt{1 - \frac{4.7}{La + 4.7}}, \qquad 3.14$$

the drop-interface contact area radius $r_{\mathrm{F,I}}$ can be related to the drop-drop contact area radius using equation

$$r_{\mathrm{F,I}} = \sqrt{3} r_{\mathrm{F,C}} \qquad 3.15$$

and the radius of the channel contour formed when three drops approach, r_a, is given by

$$r_{\alpha} = 0.5 d_{\mathrm{p}} \left(1 - \sqrt{1 - \frac{4.7}{La + 4.7}} \right). \qquad 3.16$$

La is a modified Laplace number and is given by

$$La = \left(\frac{|\rho_{\mathrm{C}} - \rho_{\mathrm{D}}| g}{\gamma} \right)^{0.6} \tilde{h}_{\mathrm{P}}{}^{0.2} d_{\mathrm{p}}. \qquad 3.17$$

La accounts for the close packing of drops and represents the ratio between the hydrostatic pressure and the interfacial tension. The hydrostatic pressure is a result of the drop-packing height below the draining film, $\tilde{h}_{\mathrm{P}}$. Consequently, $\tilde{h}_{\mathrm{P}}$ equals to the thickness of the dense-packed zone if one is present. In the absence of a dense-packed zone, the settling layer is in direct contact with the pure oil layer. In that case, we suggest that $\tilde{h}_{\mathrm{P}}$ is taken to be equal to the drop size at the interface $d_{\mathrm{p,I}}$.

3.1.5. Settling layer dispersed-phase fraction

In initially fully dispersed flows, the dispersed-phase volume fraction of the settling layer φ_{S} is equal to the oil volume fraction at the inlet, φ_0. However, in cases where the flow is partially separated at the inlet, such as the cases shown in Figure 3.1(c) and Figure 3.1(d), φ_{S} can differ to φ_0. In that instance, φ_{S} can be obtained from a mass balance on the pipe cross section

$$\varphi_{\mathrm{S}} = \frac{A_{\mathrm{pipe}} \varphi_0 - A_{\mathrm{D,0}} - A_{\mathrm{P,0}} \varphi_{\mathrm{P,0}}}{A_{\mathrm{S,0}}}, \qquad 3.18$$

where A is the cross-sectional area, while the subscript 0 denotes quantities at the pipe inlet.

3.1.6. Dense-packed layer thickness and dispersed-phase fraction

Assuming that all four characteristic layers are present at a given axial location from the inlet, we calculate the change in the thickness of the dense-packed layer by performing a mass balance on the pipe cross-sectional area. The cross-sectional area of the dense-packed layer is given by

$$A_{\mathrm{P}} = \frac{A_{\mathrm{pipe}}(\varphi_0 - \varphi_{\mathrm{S}}) - A_{\mathrm{D}}(1 - \varphi_{\mathrm{S}}) + A_{\mathrm{C}}\varphi_{\mathrm{S}}}{\varphi_{\mathrm{P}} - \varphi_{\mathrm{S}}} \qquad 3.19$$

where φ_{P} is the average dispersed-phase fraction in the dense-packed layer. In the presence of a settling layer the average hold-up of the dense-packed layer is taken equal to

$$\varphi_{\mathrm{P}} = \frac{\varphi_{\mathrm{S}} + \varphi_{\mathrm{I}}}{2} \qquad 3.20$$

as suggested by Henschke et al. (2002). In equation 3.20 $\varphi_{\mathrm{I}} = 0.9$. If depletion of the settling layer occurs, equation 3.19 simplifies to

$$A_{\mathrm{P}} = \frac{A_{\mathrm{pipe}}\varphi_0 - A_{\mathrm{D}}}{\overline{\varphi}_{\mathrm{P}}}. \qquad 3.21$$

In this case, the average holdup in the dense-packed zone is given by $\overline{\varphi}_{\mathrm{P}}$.

In the absence of a settling layer, we allowed $\bar{\varphi}_{\mathrm{P}}$ to increase from its previous value. According to Henschke et al. (2002), since the *settling curve* is continuous at $x = \bar{x}$ (cf. Figure 3.1(a) and Figure 3.1(c)), the holdup φ_{P} in the region $x \geq \bar{x}$ can be calculated by the following exponentially increasing expression:

$$\bar{\varphi}_{\mathrm{P}} = \varphi_{\mathrm{I}} - exp\left(-C_1 \frac{x}{u_{\mathrm{M}}} - C_2\right). \tag{3.22}$$

C_1 and C_2 are coefficients determined based on continuity ensuring that at $x = \bar{x}$, $\varphi_{\mathrm{P}} = \bar{\varphi}_{\mathrm{P}}|_{\bar{x}}$. The two coefficients are given by

$$C_1 = \frac{\bar{\varphi}_{\mathrm{P}}|_{\bar{x}}{}^2 \psi}{(A_{\mathrm{pipe}}\varphi_0 - A_{\mathrm{D}})(\varphi_{\mathrm{I}} - \bar{\varphi}_{\mathrm{P}}|_{\bar{x}})}. \tag{3.23}$$

and

$$C_2 = -C_1 \frac{\bar{x}}{u_{\mathrm{M}}} - \ln(\varphi_{\mathrm{I}} - \bar{\varphi}_{\mathrm{P}}|_{\bar{x}}). \tag{3.24}$$

where, according to Pereyra et al. (2013),

$$\hat{\psi} = \left[\frac{\partial A_{\mathrm{P}}}{\partial h_{\mathrm{P}}}\left(u_{\mathrm{s}} + u_{\mathrm{M}} \frac{\mathrm{d}h_{\mathrm{D}}}{\mathrm{d}x}\right) - \frac{u_{\mathrm{M}}}{\bar{\varphi}_{\mathrm{P}}|_{\bar{x}}} \frac{\partial A_{\mathrm{D}}}{\partial h_{\mathrm{D}}} \frac{\partial h_{\mathrm{D}}}{\partial x} - u_{\mathrm{M}} \frac{\partial A_{\mathrm{P}}}{\partial h_{\mathrm{D}}} \frac{\partial h_{\mathrm{D}}}{\partial x}\right]_{x=\bar{x}}. \tag{3.25}$$

If at any axial location, the calculated thickness of the dense-packed layer is smaller than the estimated drop size within the layer (i.e. if $h_{\mathrm{P}} < d_p$), we suggest that depletion of the dense-packed layer occurs and equation 3.19 reduces to

$$A_{\mathrm{P}} = 0. \tag{3.26}$$

This transition is shown at the location $x = \bar{\bar{x}}$ in Figure 3.1(d). At that point, the settling layer comes into contact with the pure oil layer and the dense-packed layer is replaced by a monolayer of drops.

3.1.7. Settling layer/Oil layer interface

The oil fraction at the coalescing interface φ_{I}, is very high in the presence of a dense-packed layer. In this paper, we set that to 0.9. In the absence of the dense-packed layer, where the settling layer is in direct contact with the pure oil layer, φ_{I} is determined by the relative rates of settling and drop-interface coalescence and can be estimate by

$$\varphi_{\mathrm{I}} = \frac{A_{\mathrm{pipe}}\varphi_0 - A_{\mathrm{D}} - A_{\mathrm{S}}\varphi_{\mathrm{S}}}{A_{\mathrm{I}}}. \tag{3.27}$$

In this case, if φ_{I} reaches the average hold-up of the dense-packed layer φ_{P} as calculated in equation 3.20, we expect a dense-packed layer to form.

If the dense-packed layer does not form, once the thickness of the settling layer becomes smaller than the drop diameter, the oil fraction at the interface is the same as the oil fraction remaining in the dispersion

$$\varphi_{\mathrm{I}} = \frac{A_{\mathrm{pipe}}\varphi_0 - A_{\mathrm{D}}}{A_{\mathrm{S}}}. \tag{3.28}$$

3.1.8. Geometric equations

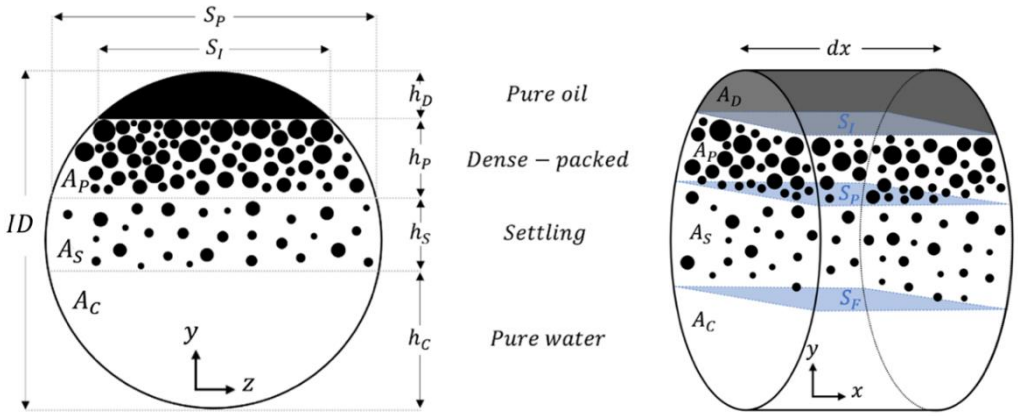

Figure 3.2. Schematic of a pipe with oil-in-water dispersed flow.

The cross-sectional area of the pure continuous water phase, as shown in Figure 3.2 is given by

$$A_{\mathrm{C}} = \frac{ID^2}{4}\left[\pi - \cos^{-1}(\omega_{\mathrm{C}}) + (\omega_{\mathrm{C}})\sqrt{1-\omega_{\mathrm{C}}^2}\right], \qquad 3.29$$

where $\omega_{\mathrm{C}} = \frac{2h_{\mathrm{C}}}{ID} - 1$.

The area of the pure oil layer is

$$A_{\mathrm{D}} = \frac{ID^2}{4}\left[\pi - \cos^{-1}(\omega_{\mathrm{D}}) + (\omega_{\mathrm{D}})\sqrt{1-\omega_{\mathrm{D}}^2}\right], \qquad 3.30$$

where $\omega_{\mathrm{D}} = \frac{2h_{\mathrm{D}}}{ID} - 1$, and its partial derivative is

$$\frac{\partial A_{\mathrm{D}}}{\partial h_{\mathrm{D}}} = 2\sqrt{h_{\mathrm{D}}(ID - h_{\mathrm{D}})}, \qquad 3.31$$

The area of the dense-packed zone can be calculated from

$$A_{\mathrm{P}} = \frac{ID^2}{4}\left[\pi - \cos^{-1}(\omega_{\mathrm{D}}) + (\omega_{\mathrm{D}})\sqrt{1-\omega_{\mathrm{D}}^2}\right] - A_{\mathrm{D}}, \qquad 3.32$$

where $\omega_{\mathrm{P}} = \frac{2h_{\mathrm{P}}}{ID} - 1$, and its partial derivative by

$$\frac{\partial A_{\mathrm{P}}}{\partial h_{\mathrm{P}}} = 2\sqrt{(h_{\mathrm{D}} + h_{\mathrm{P}})(ID - h_{\mathrm{P}} - h_{\mathrm{D}})}. \qquad 3.33$$

$\frac{\partial A_{\mathrm{P}}}{\partial h_{\mathrm{D}}}$ can be obtained from the difference of $\frac{\partial A_{\mathrm{P}}}{\partial h_{\mathrm{P}}}$ and $\frac{\partial A_{\mathrm{D}}}{\partial h_{\mathrm{D}}}$, as

$$\frac{\partial A_{\mathrm{P}}}{\partial h_{\mathrm{D}}} = \frac{\partial A_{\mathrm{P}}}{\partial h_{\mathrm{P}}} - \frac{\partial A_{\mathrm{D}}}{\partial h_{\mathrm{D}}}$$
$$= 2\sqrt{(h_{\mathrm{D}} + h_{\mathrm{P}})(ID - h_{\mathrm{P}} - h_{\mathrm{D}})} - 2\sqrt{h_{\mathrm{D}}(ID - h_{\mathrm{D}})}. \qquad 3.34$$

The area of the monolayer of drops along the coalescing interface can be calculated from

$$A_{\mathrm{I}} = \frac{ID^2}{4}\left[\pi - \cos^{-1}(\omega_{\mathrm{I}}) + (\omega_{\mathrm{I}})\sqrt{1-\omega_{\mathrm{I}}^2}\right] - A_{\mathrm{I}}, \qquad 3.35$$

where $\omega_{\mathrm{I}} = \frac{2d_{\mathrm{p}}}{ID} - 1$.

Finally, a mass balance on the cross-section gives the area of the settling layer as

$$A_{\mathrm{S}} = A_{pipe} - A_{\mathrm{D}} - A_{\mathrm{C}} - A_{\mathrm{P}}. \qquad 3.36$$

3.2. Model implementation

The equations presented above were solved numerically using gPROMS ModelBuilder along the pipe length. The input parameters required for the model include the fluid properties (densities, viscosities, and surface tension) and the pipe diameter. The drop size at the inlet and the initial thickness of each layer are also needed to initialize the simulation.

The conditions at which transitions between flow patterns occur can be specified to allow the code to transition between sets of equations. For an initial oil-in-water dispersed flow, the conditions for each transition were specified as follows:

Dense-packed layer formation (cf. Figure 3.1(a)). If a uniform settling layer is present at the pipe inlet, a dense-packed layer is assumed to form if the oil interface becomes concentrated. We assume that this occurs once $\varphi_{\mathrm{I}} = \varphi_{\mathrm{P}}$.

Depletion of the settling layer (cf. $x = \bar{x}$ in Figure 3.1(a) and Figure 3.1(c)), i.e. transition from stratified mixed flow with dispersed settling and dense-packed layers to stratified mixed flow with a dispersed dense-packed layer only occurs when the *settling curve* y_{C} meets the *dense-packed zone curve* y_{P} (i.e. if $y_{\mathrm{C}} = y_{\mathrm{P}}$). Since the equations in gPROMS were solved at discrete lengths along the pipe, if at any step the *settling curve* is calculated to be higher than the dense-packed layer interface (i.e. if $y_{\mathrm{C}} > y_{\mathrm{P}}$), depletion

of the settling layer is assumed.

Depletion of the dense-packed layer (cf. $x = \bar{\bar{x}}$ in Figure 3.1(d)), i.e. transition from stratified mixed flow with dispersed settling and dense-packed layers to stratified mixed flow with a dispersed settling layer is assumed to occur if the thickness of the dense-packed layer becomes smaller than the average drop diameter in the layer (i.e. $d_{\mathrm{p}} > h_{\mathrm{P}}$). At this particular pipe length, the dense-packed layer transforms into a single layer of drops of thickness d_{p}. The dense-packed layer thickness cannot further decrease as a result of drop-interface coalescence. Instead, as the drops continue to coalesce with their homophase, the dispersed phase fraction of drops at the interface, φ_{I}, decreases until the drops are no longer densely packed. This results in an apparent discontinuity in the dense-packed layer curve, y_{P}. However, this jump in the curve simply signifies this transition.

Transition to fully stratified flow (**cf. $x = x_{sep}$ in Figure 3.1)** occurs when the *settling curve* y_{C} meets the *coalescence curve* y_{D}. Hence, if at any step the *settling curve* is found higher than the *coalescence curve* (i.e. if $y_{\mathrm{C}} > y_{\mathrm{D}}$) stratification has been achieved.

3.3. Results

The experimental data used to assess the performance of the model were obtained in a two-phase liquid-liquid flow facility discussed in detail in

Voulgaropoulos et al. (2016). In the experiments, tap water and an oil (density 828 kg m^{-3}, viscosity 5.5 mPa s, surface tension 0.029 N m^{-1}) were used as test fluids. The test section was a transparent acrylic pipe with an internal diameter of $37\,\mathrm{mm}$ and overall length of around $8\,\mathrm{m}$. Partial dispersions of oil in water were generated at the inlet of the test section using a multi-nozzle mixer. High-speed imaging was employed at three locations along the spanwise dimension of the pipe to enable the identification of the flow patterns. A dual-conductance probe was implemented to measure the local volume fractions and the drop size distributions of the mixture along a vertical pipe diameter. Measurements were taken every $2\,\mathrm{mm}$, spanning the whole pipe diameter. The equations presented in the paper were solved for six cases with different inlet conditions shown in Table 3.1.

Table 3.1. Inlet conditions of experiments.

$u_{\mathrm{M}}\ (\mathrm{m\ s^{-1}})$	φ_0
0.52	0.30
	0.45
1.04	0.15
	0.30
	0.45
	0.60

The hindered settling parameter C_h was taken to be equal to 0.01 as proposed by Voulgaropoulos (2017), while the asymmetric dimple parameter r_V^* was taken to be equal to 0.007, a value that was obtained experimentally by Pereyra et al. (2013) for a similar system. The predicted dimensionless flow profiles are presented in Figures 3.3 and 3.4 together with experimental measurements to allow comparison. The dimensionless values of the layer heights and the pipe length were obtained using the internal diameter of the pipe. Dimensionless quantities are denoted with $^+$.

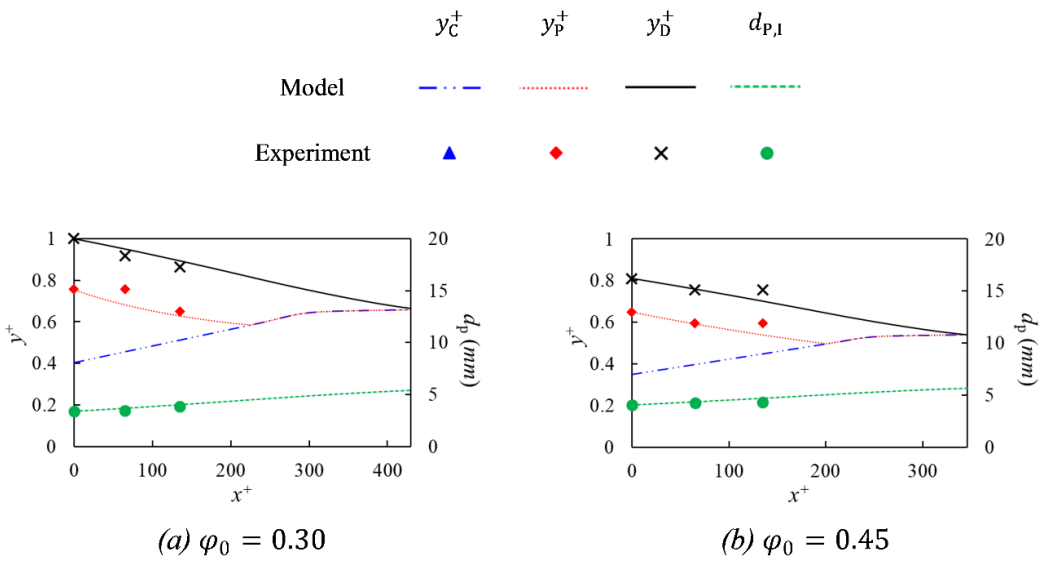

Figure 3.3. Predictions of the flow profile and the Sauter mean diameter for oil-in-water dispersions flowing at u_M = 0.52 m s^{-1}.

At the low mixture velocity, the drops initially float towards the top of the pipe causing the height of the water layer y_C^+, to increase linearly as expected by equation 3.1. Meanwhile, the height of the dense-packed layer y_P^+

decreases until it meets the *settling curve*. At this pipe length, the settling process is complete and all drops are found within the dense-packed layer. Coalescence between drops within the dense-packed layer results in an increase in the average drop diameter at the interface. Coalescence between the drops and the oil-water interface causes the oil layer to increase in thickness (interface decreases in height). Eventually complete separation occurs as the oil layer curve meets the water layer one. Little difference is observed in the length of complete separation between the two different oil fractions flowing at $0.52\ \mathrm{m\ s^{-1}}$. No correlation between the separation length and the oil fraction can be established, as the total separation length is dependent on several variables, including the mixture velocity, the thickness of the dispersed layer at the inlet, and the drop size.

At the high mixture velocity of $1.04\ \mathrm{m\ s^{-1}}$ the inlet is almost fully dispersed. In cases (a)-(c) in Figure 3.4 the dispersed layer consists of a single settling layer only, while both the dense-packed and the settling layers are present in case (d). At this velocity, the initial dispersions consist of smaller drops than to those present at the low mixture velocity. This results in a smaller settling velocity as shown by the smaller gradient of the *settling curve*; hence, the water layer height increases at a lower rate. In cases (a)-(c), the low settling rate limits the rate of separation, and a dense-packed layer does not form. In case (d) the rate of drop-interface coalescence is faster than the settling rate. This causes the dense-packed layer to decrease in thickness, until it eventually completely depletes and the settling layer

comes in direct contact with the pure oil layer. Settling and coalescence continue in a similar fashion until complete separation occurs. Longer separation lengths are predicted at $u_{\mathrm{M}} = 1.04\ \mathrm{m\ s^{-1}}$ as settling is the controlling separation mechanism.

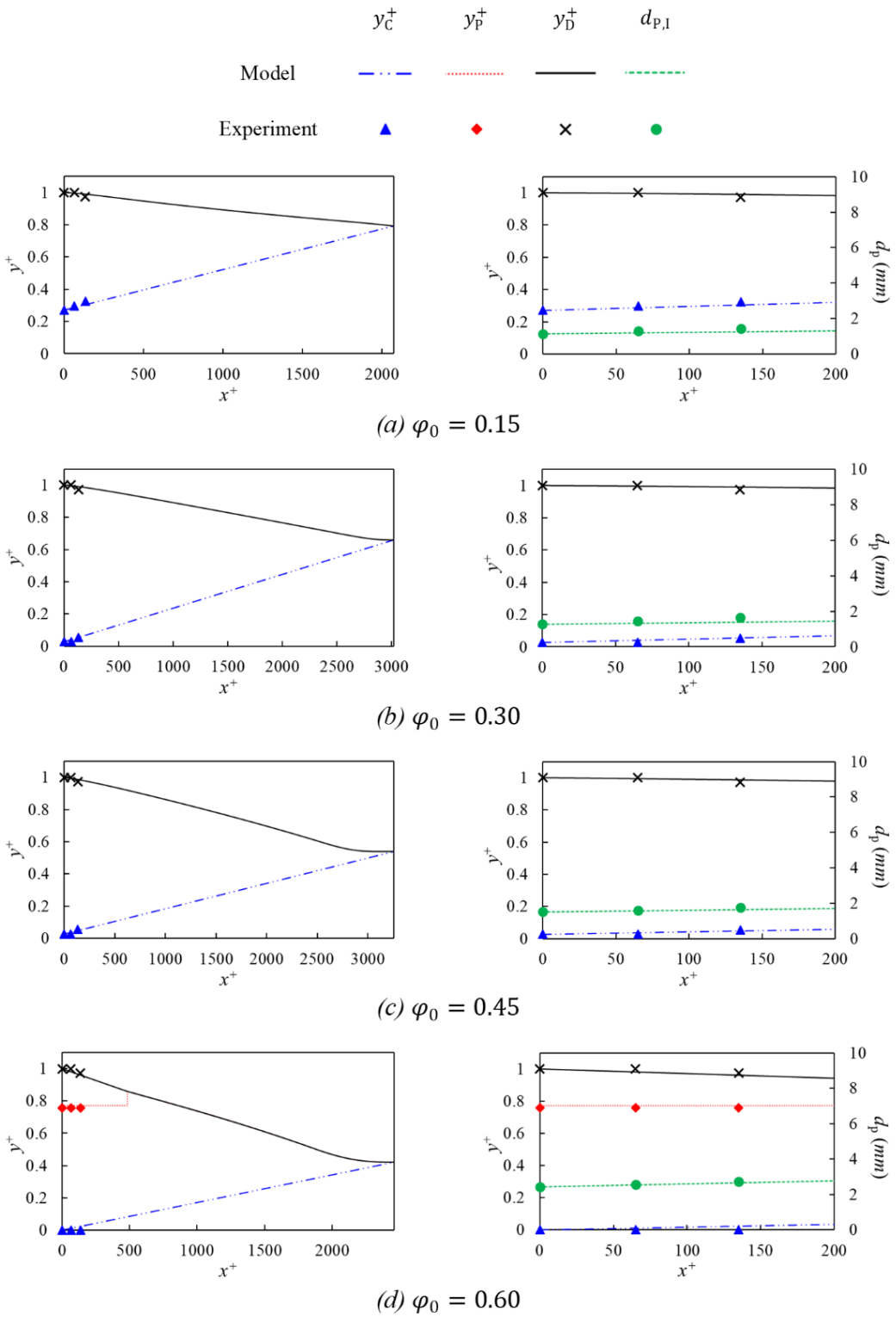

Figure 3.4. Predictions of the flow profile and the Sauter mean diameter for oil-in-water dispersions flowing at u_M = 1.04 m s^{-1}.

The results show that liquid-liquid mixtures at different flow conditions may approach separation in a different manner. These differences result from the relative rates of drop settling and drop-interface coalescence. A higher rate of settling than that of drop-interface coalescence results in the depletion of the settling layer, as seen in the flow profiles of the lower mixture velocity in Figure 3.3. On the contrary, higher rates of drop-interface coalescence than those of settling may cause the dense-packed layer to deplete if present at the inlet and the settling layer to persist up to the point of complete separation. This shift in the controlling mechanism is not a result of the change in the mixture velocity itself, but rather a consequence of the smaller drops generated at the inlet as a result of the higher mixture velocity.

The suggested model was also validated against experimental data from Pereyra et al. (2013) to assess its ability to predict the *settling curve*. The experimental data were obtained in a horizontal pipe separator of $0.1\ \mathrm{m}$ inner diameter and $6\ \mathrm{m}$ length, using tap water and mineral oil (density 857 kg m^{-3}, viscosity 13.6 mPa s, surface tension 0.029 N m^{-1}) as test fluids. The asymmetric dimple parameter r_V^* was taken as 0.007 as suggested by Pereyra et al. (2013). The initial drop diameter was assumed to be $250\ \mu\mathrm{m}$ and a hindered settling parameter C_h of 0.2 produced reasonable results. Oil-in-water dispersions with an oil fraction of 0.40 were studied at three different mixture velocities: $u_\mathrm{M} = 0.06\ \mathrm{m\ s^{-1}},\ 0.09\ \mathrm{m\ s^{-1}},$ and $0.13\ \mathrm{m\ s^{-1}}$. The results are presented in Figure 3.5.

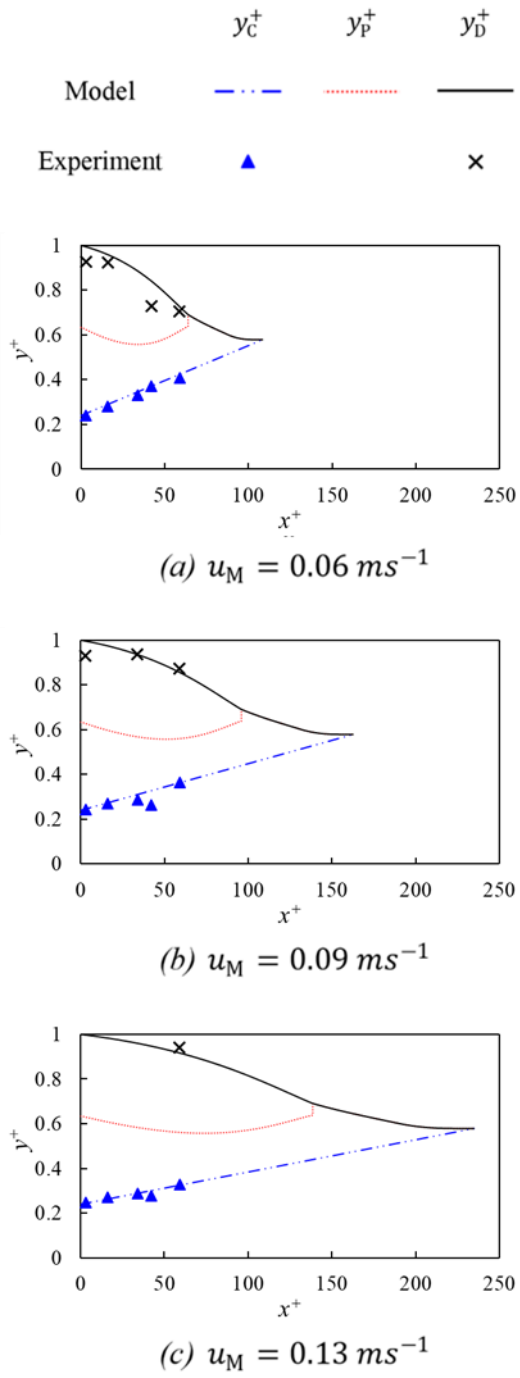

Figure 3.5. Predictions of the flow profiles for oil-in-water dispersions with φ_0 = 0.40 and comparison with experimental data obtained by Pereyra et al. (2013).

The model predicts the location of the *settling curve* y_C with reasonable accuracy when a hindered settling parameter of 0.2 is used. This suggests that the initial model by Pilhofer and Mewes (1979) which was developed for batch systems, overestimates the settling rate of separating dispersed pipe flows even at low mixture velocities. Comparison of the results in Figures 3.3 and 3.4 with the results in Figure 3.5 suggest a possible correlation between the mixture velocity and the hindered settling parameter. However, further studies are required to establish a relationship. The results also suggest that the current model can be used without accurate knowledge of the initial drop size, as long as there is enough data to fit C_h (i.e. measurements of y_C or y_P).

The characteristic layers evolve in a similar manner in the three cases, but there is a clear positive correlation between the mixture velocity and the separation length. Initially, the dispersions consist of settling and dense-packed layers. The dense-packed layers deplete first, while the settling layers persist up to the point of complete separation. The depletion of the dense-packed layer even at low mixture velocities suggests that this flow-pattern transition may be common in several set-ups in industry and highlights its significance.

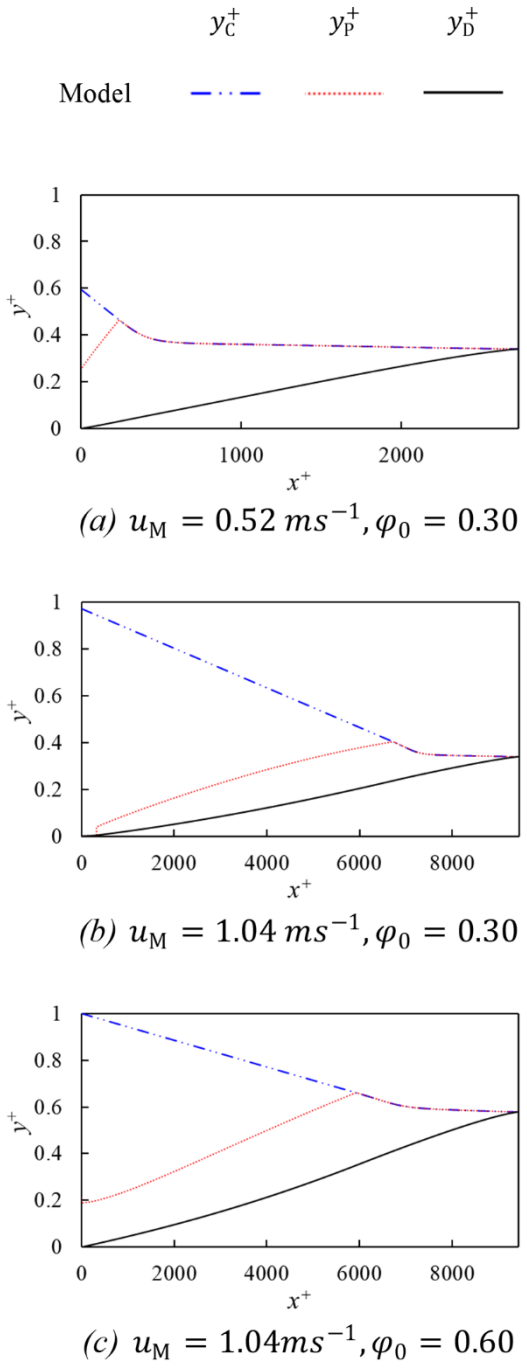

Figure 3.6. Prediction of the flow profiles for water-in-oil dispersions.

The applicability of the model to water-in-oil dispersions was investigated for three hypothetical cases. The average drop diameters and the initial thicknesses of the continuous phase, the dispersed phase, and the dense-

packed layer were taken to be the same as the corresponding oil-in-water cases studied above. Due to the lack of experimental data, the dimensionless asymmetry coefficient, r_V^*, was assumed to be the same as in the oil-in-water cases. Although this could be the case and such fluid combinations have been identified in the past, Henschke et al. (2002) argues that it cannot be concluded that this is always so, hence the results need to be treated with caution.

The results presented in Figure 3.6 show the predicted length required for separation to be significantly larger for water-in-oil dispersions than for oil-in-water ones. This is due to the lower coalescence rates predicted for the water-in-oil cases. In the case shown in Figure 3.6(a), the settling layer depletes at a similar axial length as the corresponding oil-in-water case (cf. Figure 3.3(a)), however the lower coalescence rates cause the dense-packed layer to persist for longer before complete separation occurs. Figure 3.6(b) shows the formation of a dense-packed layer from an almost fully dispersed inlet, in contrast to the corresponding oil-in-water case (cf. Figure 3.4(b)) where the dense-packed layer never forms. Finally, in the case in Figure 3.6(c) the dense-packed layer initially grows in thickness and persists up to the point of complete separation. This is again contrary to the corresponding oil-in-water case (cf. Figure 3.4(d)) where the dense-packed layer depletes first and the settling layer remains until separation occurs.

3.4. Conclusions

This chapter introduced a methodology for predicting the separation of dispersed liquid-liquid flows in horizontal pipes, relying on the physical mechanisms of drop settling, drop-interface coalescence, and drop-drop coalescence. The proposed model predicted the evolution of distinct layers up to the point of complete separation in both oil-in-water and water-in-oil systems. The model predictions of the layer thicknesses for initial oil-in-water dispersions demonstrated little deviation from experimental measurements. Drop growth due to drop-drop coalescence was also well captured.

The inlet and flow conditions were proven to control the type of separation, which can be either coalescence-controlled or settling-controlled, giving rise to different flow patterns and flow pattern transitions. The drop size was shown to influence the settling rate, with smaller drop sizes being more likely to lead to settling-controlled separation. Remarkably, accurate drop-size measurements at the inlet were deemed unnecessary, as the hindered settling parameter effectively compensated for any inaccuracies, yielding reasonable estimates for layer thicknesses. A potential relationship between mixture velocity and the hindered settling parameter was suggested, warranting further investigation. Furthermore, the investigation into oil-in-water dispersions revealed that the continuous phase influences the rate of coalescence. Lower coalescence rates were predicted for oil-continuous systems, increasing the likelihood of dense-packed layer

formation and persistence.

In this chapter, the investigation of various scenarios of dispersed flows in pipes highlighted the significance of coalescence phenomena in the separation process. The following chapter explores different coalescence models identified in the literature, aiming to understand their impact on model predictions and identify the most suitable model for application in pipe flows.

Chapter 4

4. Coalescence model identification[2]

In this chapter, two distinct coalescence models identified from the literature on the separation of liquid-liquid dispersions in batch vessels are introduced and integrated into the semi-empirical model outlined in Chapter 3. Each model depends on a fitted coalescence parameter; hence, a comparative study of the two coalescence models is performed through parameter estimation to identify the most appropriate model for integration into the semi-empirical model. The objective is to improve the accuracy of the semi-empirical model by identifying and incorporating the most suitable coalescence correlations available. In what follows, parameter estimation is performed using experimental data from the literature to identify the two uncertain coalescence parameters and assess their precision. The results are compared based on the Student's *t*-test and the χ^2 test. Expected flow profiles based on the parameter estimates are plotted and compared to experimental measurements. Given that these coalescence correlations were initially developed for batch vessels, a critical investigation into the dependency of the coalescence parameters on the mixture velocity is

[2] Part of this chapter has been published in Chemical Engineering Science (Evripidou et al. 2023a).

Similar findings to those outlined in this chapter have been published in the 52nd volume of Computer Aided Chemical Engineering (Evripidou et al. 2023b).

undertaken, exploring whether parameter estimates obtained at one mixture velocity are applicable to other mixture velocities.

4.1. Coalescence models

Two distinct models were identified in literature for the prediction of the coalescence times: the *asymmetric film drainage model* developed by Henschke et al. (2002) and the *interfacial mobility film drainage model* developed by Jeelani and Hartland (1994).

4.1.1. Asymmetric film drainage model (Henschke et al. 2002)

Henschke et al. (2002) developed coalescence correlations that capture both drop-drop and drop-interface coalescence phenomena. These correlations depend on the deformation of drops. The degree of deformation increases with packing below the drop considered hence is influenced by the thickness of the dense-packed layer.

The model discussed in Chapter 3 employs the *asymmetric film drainage* model for coalescence. A comprehensive description of this model can be found in Section 3.1.4. Additionally, a summary of the model is provided in Table 4.1.

Table 4.1. Correlations of the asymmetric film drainage model.

Asymmetric film drainage model	
Drop-interface coalescence time: $$\tau_{\mathrm{I}} = \frac{(6\pi)^{\frac{7}{6}}\mu_{\mathrm{C}}\, r_a^{\frac{7}{3}}}{4\gamma^{\frac{5}{6}}\,\mathrm{H}^{\frac{1}{6}}\, r_{\mathrm{F,I}} r_V^*}$$	4.1
Drop-drop coalescence time: $$\tau_C = \frac{(6\pi)^{\frac{7}{6}}\mu_{\mathrm{C}}\, r_a^{\frac{7}{3}}}{4\gamma^{\frac{5}{6}}\,\mathrm{H}^{\frac{1}{6}}\, r_{\mathrm{F,C}} r_V^*}$$	4.2
Drop-drop contact radius: $$r_{\mathrm{F,C}} \;=\; 0.3025 d_{\mathrm{p,I}} \sqrt{1 - \frac{4.7}{La + 4.7}}$$	4.3
Drop-interface contact radius: $$r_{\mathrm{F,I}} = \sqrt{3} r_{\mathrm{F,C}}$$	4.4
Channel contour radius: $$r_\alpha = 0.5 d_{\mathrm{p,I}} \left(1 - \sqrt{1 - \frac{4.7}{La + 4.7}} \right)$$	4.5
Modified Laplace number: $$La = \left(\frac{\lvert \rho_{\mathrm{C}} - \rho_{\mathrm{D}} \rvert g}{\sigma} \right)^{0.6} {h_{\mathrm{P}}}^{0.2} d_{\mathrm{p,I}}$$	4.6

4.1.2. Interfacial mobility film drainage model (Jeelani and Hartland 1994)

Jeelani and Hartland (1994) developed coalescence correlations based on the interfacial mobility of the two surfaces adjacent to the draining film. They later used these coalescence correlations in a semi-empirical model for separating dispersions in a batch vessel (Jeelani and Hartland 1998). Following their approach, the drop-interface coalescence time τ_{I} is given by

$$\tau_{\mathrm{I}} = \frac{\tau_{\mathrm{I},0} d_{\mathrm{p,I}}}{h_{\mathrm{P}}}. \qquad 4.7$$

where $\tau_{\mathrm{I},0}$ is the initial drop-interface coalescence time of a flow that is fully dispersed at the inlet and is equivalent to the coalescence time in the absence of a dense-packed layer, and $d_{\mathrm{p,I}}$ is the drop size at the coalescing interface.

By inserting equation 4.7, the coalescence curve equation 3.10 simplifies to

$$\frac{dh_{\mathrm{D}}}{dx} = \frac{2\varphi_{\mathrm{I}} h_{\mathrm{P}}}{3\tau_{\mathrm{I},0} u_{\mathrm{M}}}. \qquad 4.8$$

This coalescence model does not capture the increase in drop size. Instead, the above simplification makes the drop-interface coalescence time τ_{I} independent of the drop diameter at the interface $d_{\mathrm{P,I}}$.

The coalescence time in the absence of a dense-packed layer is estimated by

$$\tau_{\mathrm{I},0} = \frac{3\pi\mu_{\mathrm{C}} r_f^4}{4(1+2m)F\delta_r^2}. \qquad 4.9$$

In the equation above, m corresponds to the interface mobility, i.e. the sum of the mobilities due to induced circulation in the adjacent phases and the interfacial tension gradient (Jeelani and Hartland 1998) and is characteristic of each system. When $m = 0$ the velocity at the interfaces on both sides of the draining film is 0, and the surfaces are deemed immobile; when $m = 1.5$ the velocity at one of the interfaces is 0 while the velocity gradient at the other surface is 0. Under these conditions, film drainage, and thus the rate of coalescence, is extremely slow (Jeelani and Hartland 1994). Other values of m are also possible and correspond to different surface velocities and velocity gradients. Values of m larger than 1.5 correspond to more mobile interfaces.

In addition, r_f is the film radius given by

$$r_f = d_{\mathrm{p}}^2 \sqrt{\frac{|\rho_{\mathrm{C}} - \rho_{\mathrm{D}}|g}{12\gamma}}, \qquad 4.10$$

F is the gravitational force acting on the droplets

$$F = \frac{\pi d_p^3 |\rho_C - \rho_D| g}{6}, \qquad 4.11$$

and δ_r is the critical film thickness at which rupture is assumed to occur, and can be obtained from equation 4.12 as suggested by Vrij and Overbeek (1968),

$$\delta_r = 0.267 \left(\frac{\pi r_f^4 \mathrm{H}^2}{6\gamma F} \right)^{\frac{1}{7}}. \qquad 4.12$$

4.2. Methodology

4.2.1. Parameter estimation

Parameter estimation is the process of calculating the values of the unknown parameters of a model from physical measurements. This method was used here to estimate the coalescence parameters of each coalescence model: the dimensionless asymmetry coefficient r_V^* in the *asymmetric film drainage model* and the interface mobility m in the *interfacial mobility film drainage model*. Both parameters are specific to each system and must be determined experimentally. Each of the two parameters was estimated using the *Model Validation* entity in gPROMS ModelBuilder.

Model Validation in gPROMS is based on the Maximum Likelihood formulation. This is a linearization-based approach (Bard 1977), which aims to determine the optimal values for the uncertain parameters and the associated probability distribution that best fits the experimental measurements. Within *Model Validation,* gPROMS conducts a Student's *t*-test to assess the precision of the parameter estimates.

The *t*-value for the *i*-th model parameter is computed through equation 4.13.

$$t_i = \frac{\theta_i}{t(95\%, N - N_\theta)\sqrt{v_{\theta,i}}}, \qquad 4.13$$

where t_i is the 95% *t*-value of the *i*-th parameter, θ_i is the corresponding estimated value, and $v_{\theta,i}$ is its estimated variance (Bard 1977). $t(95\%, N - N_\theta)$ is the reference *t*-value with a 95% confidence level and $(N - N_\theta)$ degrees of freedom obtained from statistical tables, where N is the total number of measurements and N_θ is the number of uncertain parameters to be estimated. 95% *t*-values larger than the reference *t*-value tend to indicate precise parameter estimates (Draper and Smith 1998).

Finally, equation 4.14 gives the 95% confidence interval, *CI*. This interval represents the range within which the new parameter estimates would fall 95% of the time, when parameter estimation is repeated with new experimental data.

$$CI = t(95\%, N - N_\theta)\sqrt{v_{\theta,i}}. \quad 4.14$$

Finally, in *Model Validation*, gPROMS also performs a χ^2 test to calculate the χ^2 value, which serves as a statistical measure to assess the goodness of fit between a model and the experimental (observed) data. This value is calculated by summing the squared differences between the observed and expected values, and it is often used in hypothesis testing to determine whether a model adequately fits the data (Hines et al. 2008). A good fit between the model and experimental data is indicated when the calculated χ^2 value is lower than the critical χ^2 value, which is obtained from the χ^2-squared distribution table based on the chosen significance level and degrees of freedom for the hypothesis test.

4.3. Results and discussion

4.3.1. Experimental methods

Experimental data used in the parameter estimation were obtained from Voulgaropoulos et al. (2016), who conducted experiments within a two-phase liquid-liquid flow facility. A brief description of the experimental set-up is found in Section 3.3, while a comprehensive account is provided in Voulgaropoulos et al. (2016). The values of the parameters used in the model are summarised in Table 4.2.

Table 4.2. Model parameters

Parameter	Description	Value	Unit
ρ_{C}	Density of water	998	kg m^{-3}
ρ_{D}	Density of oil	857	kg m^{-3}
μ_{C}	Viscosity of water	0.00089	Pa s
μ_{D}	Viscosity of oil	0.0055	Pa s
γ	Interfacial tension	0.029	N m^{-1}
g	Gravitational acceleration	9.81	m s^{-2}
H	Hamaker coefficient	10^{-20}	N m
C_h	Settling parameter	0.1	Dimensionless

The experimental data available to be used in the parameter estimation include measurements of the height of the *dense-packed layer curve* y_{P}, the height of the *coalescence curve* y_{D}, and the drop-size in the dense-packed layer $d_{\mathrm{p,I}}$ at three axial locations ($x^+ = 0, 65, 135$). The variance of the experimental measurements of the layer heights was assumed to be constant, with a standard deviation σ of 0.001 m, while the variance of the experimental measurements of the drop size was assumed to be 10% of the measurement, i.e. 1/3 of the precision of the measurements stated by Voulgaropoulos (2017). Three cases with different oil fractions and/or mixture velocities were studied.

4.3.2. Parameter estimation

A series of parameter estimations were performed using the Model Validation entity in gPROMS ModelBuilder implementing the different coalescence correlations each time. The conditions of the three case studied are outlined in Table 4.3, together with the initial heights of the *settling curve* $y_{C,0}$, the *coalescence curve* $y_{\mathrm{D},0}$, and the average drop size at the inlet $d_{\mathrm{p},0.}$ The two cases at the lower mixture velocity were used in the parameter estimation, while the case at the higher mixture velocity was used for model validation. Since both models were developed for batch systems, this was done to investigate whether the coalescence parameter varies with the mixture velocity.

Table 4.3. Conditions of the experiments. (Voulgaropoulos et al. 2016)

Case	$u_{\mathrm{M}}\ (\mathrm{m\ s^{-1}})$	φ_0	$y_{\mathrm{C},0}\ (\mathrm{m})$	$y_{\mathrm{P},0}\ (\mathrm{m})$	$y_{\mathrm{D},0}\ (\mathrm{m})$	$d_{\mathrm{p},0}\ (\mathrm{mm})$
1	0.52	0.30	0.010	0.028	0.37	3.41
2	0.52	0.45	0.012	0.024	0.37	4.03
3	1.04	0.60	0	0.028	0.37	2.43

The *interfacial mobility film drainage model* predicts the evolution of the layer heights, but not the increase in drop-size at the interface. As a result, the parameter estimation for the interface mobility m relies solely on measurements of the *dense-packed layer curve* y_{P} and the *coalescence curve* y_{D}, and incorporating drop-size measurements is futile in the parameter estimation process.

Conversely, the *asymmetric film drainage model* predicts both layer height and drop size evolution. As a result the parameter estimation for the dimensionless asymmetry coefficient r_V^* could use any of the three measured variables (y_{P}, y_{D}, and $d_{\mathrm{P},0}$). In fact, the parameter estimation for r_V^* was executed twice: first using all three measured variables, and second using only measurements of the *dense-packed layer curve* y_{P} and the *coalescence curve* y_{D}. This approach was adopted to explore the complete

potential of the model, but also enable for an even comparison of the two models in scenarios where drop-size measurements are not available.

4.3.2.1. Student's *t*-test

Table 4.4 shows the results of the three parameter estimations, along with statistical measures derived from the *t*-test that are used to evaluate the accuracy and reliability of the model predictions. The table includes the measured variables that were used in the parameter estimation, the initial guesses of the parameter values, the lower and upper bounds for the parameters which were obtained from the literature, the final parameter estimates, the distance to the bounds of the respective 95% confidence interval, the 95% *t*-value corresponding to each parameter, and the reference 95% *t*-value for each parameter. If a parameter has a 95% *t*-value that is smaller than the reference *t*-value, it suggests that the available data is inadequate for estimating that particular parameter precisely.

Table 4.4. Parameter estimation initial guesses, results, and statistical measures based on the t-test.

Model parameter	Measured variables	Initial guess	Lower & upper bounds	Final value	95% Confidence interval	95% *t*-value
r_V^*	$y_\mathrm{P}, y_\mathrm{D}, d_{\mathrm{p},0}$	0.007	0.001-0.015	0.0080	0.0019	4.2
					Reference *t*-value (95%):	1.7
r_V^*	$y_\mathrm{P}, y_\mathrm{D}$	0.007	0.001-0.015	0.0087	0.0021	4.2
					Reference *t*-value (95%):	1.8
m	$y_\mathrm{P}, y_\mathrm{D}$	1	0-100	49	17	2.8
					Reference *t*-value (95%):	1.8

The dimensionless asymmetry coefficient r_V^* in the *asymmetric film drainage model* was estimated at 0.0080 when the drop size measurements were used in the parameter estimation in addition to the layer heights and at 0.0087 when only the layer heights were considered. The 95% *t*-values corresponding to r_V^* were computed as 4.2 in both cases, while the reference *t*-values in either case were found to be 1.7 and 1.8 respectively. In both cases, the 95% *t*-value for r_V^* was more than double the reference *t*-value, indicating that the parameter is estimated with sufficient precision.

Importantly, omitting drop-size measurements results in a parameter estimate deviating by less than 9% from the estimate obtained using all measurements.

Conversely, the interface mobility m within the *interfacial mobility film drainage model* was estimated to be 49, as shown in Table 4.4. The corresponding 95% *t*-value was calculated at 2.8, while the reference *t*-value was found to be 1.8. The 95% *t*-value is again larger than the reference *t*-value, indicating satisfactory precision in the parameter estimate. Nevertheless, the 95% *t*-value of the interface mobility parameter m is lower than the 95% *t*-values of the dimensionless asymmetry coefficient r_V^* suggesting that lower precision is associated with the parameter estimate for m. Despite repeating the parameter estimation process with different initial guesses and upper and lower bounds, the resulting parameter estimates remained nearly identical, showing deviations of less than 1%.

4.3.2.2. Chi-squared test

Tables 4.5, 4.6, and 4.7 show the χ^2 values computed from the residuals for the settling curve, y_{C}, the coalescence curve, y_{D}, and the drop size, $\mathrm{d}_{\mathrm{p,I}}$, where appropriate, across all cases using the parameter estimates from Table 4.4. Each table presents the χ^2 values obtained using the relevant parameter estimate in the respective model, for each case as well as the overall χ^2 values for all cases.

Table 4.5. χ^2 values for the three measured responses obtained using the asymmetric film drainage model with r_V^* = 0.0080.

Asymmetric film drainage model								
	Case 1		**Case 2**		**Case 3**		**Overall**	
	χ^2	χ^2-crit.	χ^2	χ^2-crit.	χ^2	χ^2-crit.	χ^2	χ^2-crit.
y_{P}	4.5	6.0	1.2	6.0	0.026	6.0	5.7	16
y_{D}	3.0	6.0	3.6	6.0	0.67	6.0	7.2	16
$d_{\mathrm{p,0}}$	0.40	6.0	0.57	6.0	0.0088	6.0	1.1	16
Total	7.9	16	5.3	16	0.79	16	14	39

An r_V^* estimate of 0.0080 implemented in the *asymmetric film drainage model* results in χ^2 values that are below the critical χ^2 values, as shown in Table 4.5. This holds true for the χ^2 values of all measured variables (namely *dense-packed layer curve* y_{P}, the *coalescence curve* y_{D}, and the average drop size in the dense-packed layer $d_{\mathrm{p,I}}$) for all cases. This indicates a strong agreement between the experimental measurements and the model predictions.

Table 4.6. χ^2 values for the three measured responses obtained using the asymmetric film drainage model with $r_V^* = 0.0087$.

	Asymmetric film drainage model							
	Case 1		**Case 2**		**Case 3**		**Overall**	
	χ^2	χ^2-crit.	χ^2	χ^2-crit.	χ^2	χ^2-crit.	χ^2	χ^2-crit.
y_{P}	1.8	6.0	4.7	6.0	0.88	6.0	5.7	16
y_{D}	1.8	6.0	4.7	6.0	0.88	6.0	7.4	16
Total	6.7	11	5.5	11	0.95	11	13	28

The χ^2 values consistently remain below the critical χ^2 values, even when the drop-size measurements are omitted from the parameter estimation, as shown in Table 4.6. Once again, this demonstrates good agreement between the experimental measurements and the model predictions, even when employing an r_V^* value of 0.0087.

Table 4.7. χ^2 values for the two measured responses obtained using the interfacial mobility film drainage model with m=49. (responses failing the t-test are indicated in boldface)

	Interfacial mobility film drainage model							
	Case 1		**Case 2**		**Case 3**		**Overall**	
	χ^2	χ^2-crit.	χ^2	χ^2-crit.	χ^2	χ^2-crit.	χ^2	χ^2-crit.
y_{P}	4.81	6.0	3.32	6.0	**7.24**	6.0	15.4	16
y_{D}	0.140	6.0	1.86	6.0	**12.5**	6.0	14.5	16
Total	4.95	11	5.18	11	**19.7**	11	**29.8**	28

Finally, Table 4.7 shows that the *interfacial mobility film drainage model* with an m value of 49 yields χ^2 values lower than the critical χ^2 values for both the *dense-packed layer curve* y_{P} and the *coalescence curve* y_{D} for case studies 1 and 2. However for case study 3, the χ^2 values are larger than the critical χ^2 values for both the *dense-packed layer curve* y_P and the *coalescence curve* y_{D} as shown in Table 4.7. The overall χ^2 value for all cases also exceeds the critical χ^2 value. These findings highlight a significant lack of agreement between the model predictions and experimental measurements, and suggest that utilising the *interfacial*

mobility film drainage model with an m value of 49 at higher mixture velocities leads to inaccurate predictions.

4.3.2.3. Flow profiles

The semi-empirical model was solved using gPROMS ModelBuilder. The different coalescence correlations were implemented in the model and the flow profiles predicted using each parameter estimate for the cases listed in Table 4.3 are presented in this Section. The flow profiles are nondimensionalised using the internal diameter of the pipe *ID*. Dimensionless quantities are denoted with $^{+}$.

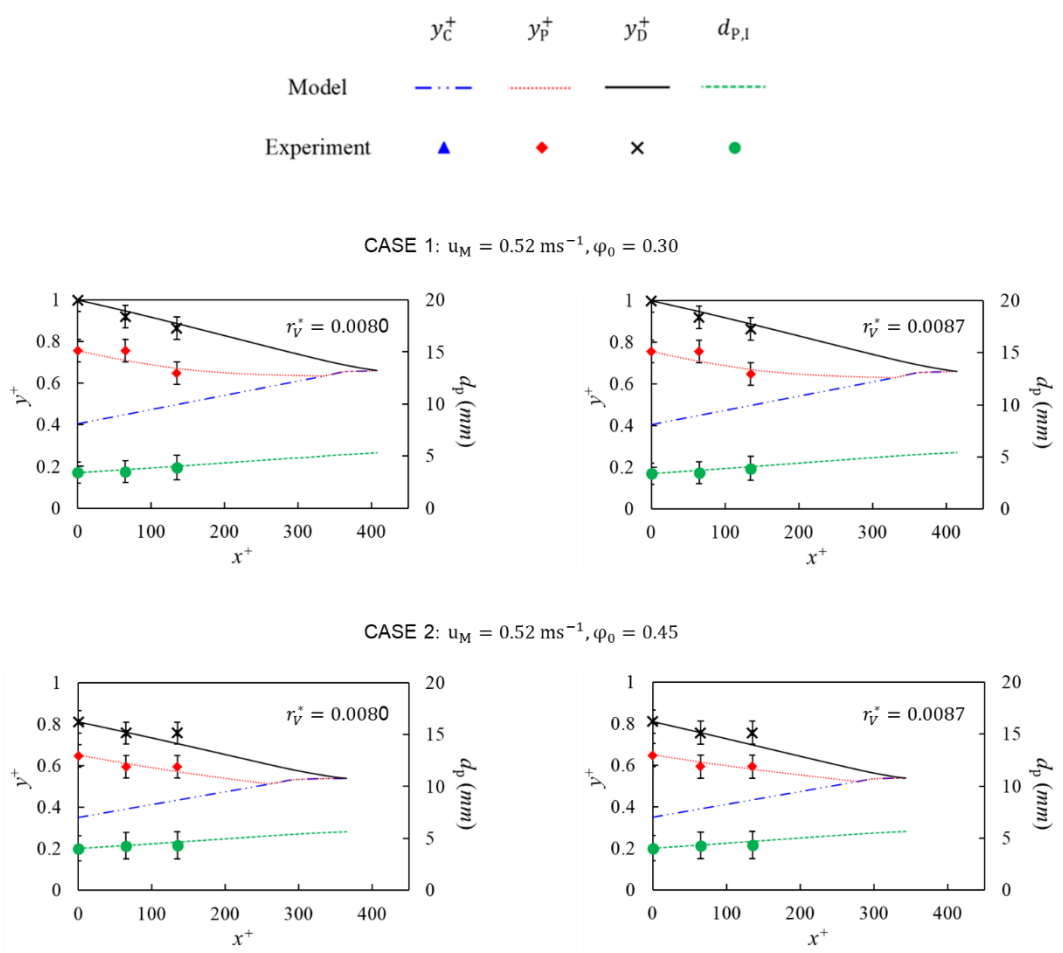

Figure 4.1. Model predictions for case studies 1 and 2 using the asymmetrical film drainage coalescence model with r_V^* values of 0.0080 (left) and 0.0087 (right), and comparison to experimental data.

An increase in the dimensionless asymmetry coefficient r_V^* from 0.0080 to 0.0087 has little effect on the predicted flow profiles, which remain nearly identical. Importantly, the model predictions consistently fall within the error bars, demonstrating good agreement between the model and experimental data.

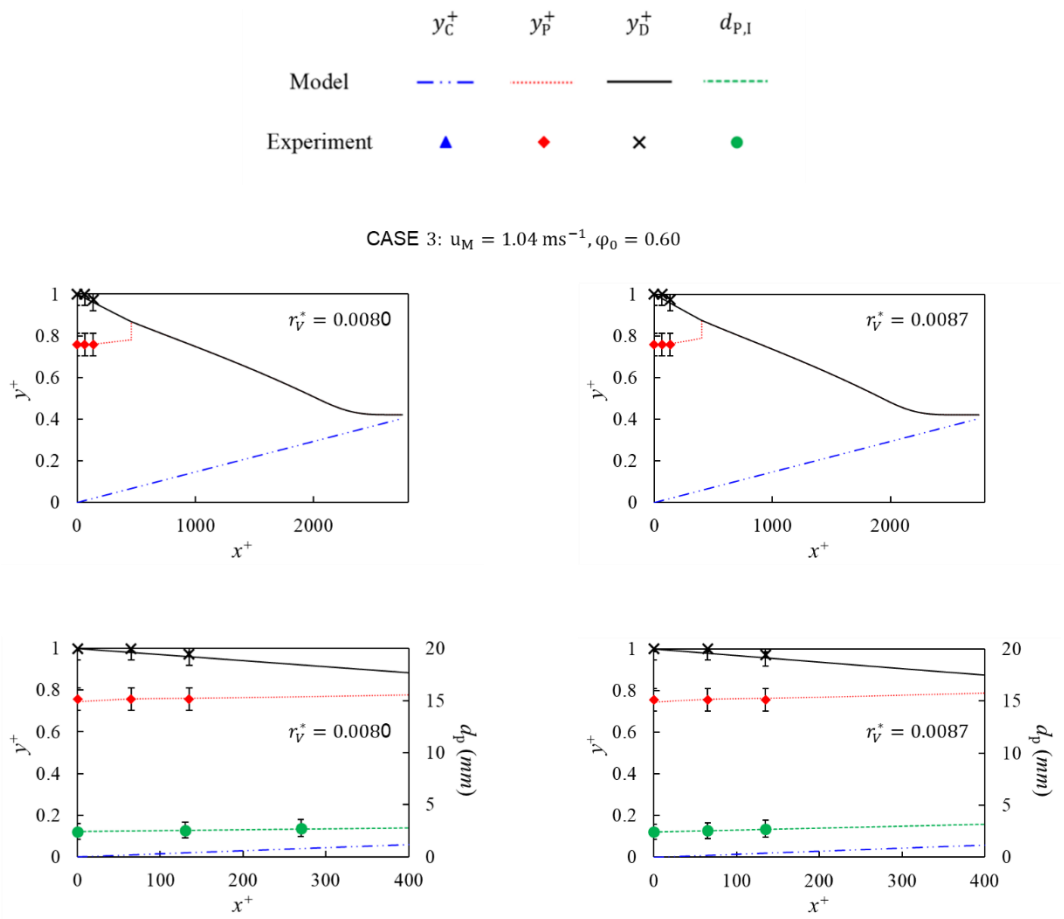

Figure 4.2. Model predictions for case study 3 using the asymmetrical film drainage coalescence model and comparison to experimental data. The figures at the top show the complete flow profiles, while the figures at the bottom focus on the region of $\mathbf{0 \leq x^+ \leq 400}$***.***

Figure 4.2 shows the predicted flow profiles of case study 3 obtained using the two parameter estimates for r_V^* in the *asymmetric film drainage coalescence model*. The top two figures show the complete flow profiles, while the bottom two figures focus on the region of $0 \leq x^+ \leq 400$, facilitating a clearer comparison between model predictions with experimental measurements. Here, the drops settle at a lower rate than the rate of

coalescence of drops with their homophase, leading in the depletion of the dense-packed layer, while the settling layer persists. Following the depletion of the dense-packed layer at $x = \bar{\bar{x}}$, drop-settling controls the rate of separation.

Although case study 3 was not used in the parameter estimation, the r_V^* estimates obtained from case studies 1 and 2, which implemented a lower mixture velocity, provide accurate predictions for the layer heights and the drop sizes that fall within the error bars. This suggests that the parameter r_V^* remains unaffected by the mixture velocity, indicating that the *asymmetric film drainage coalescence model* is a suitable choice for application to pipe flows.

Similar to case studies 1 and 2, the value of the dimensionless asymmetry coefficient r_V^* has little effect on the predicted flow profiles. The two parameter estimates result in identical separation lengths and the model predictions consistently fall within the error bars of experimental data points.

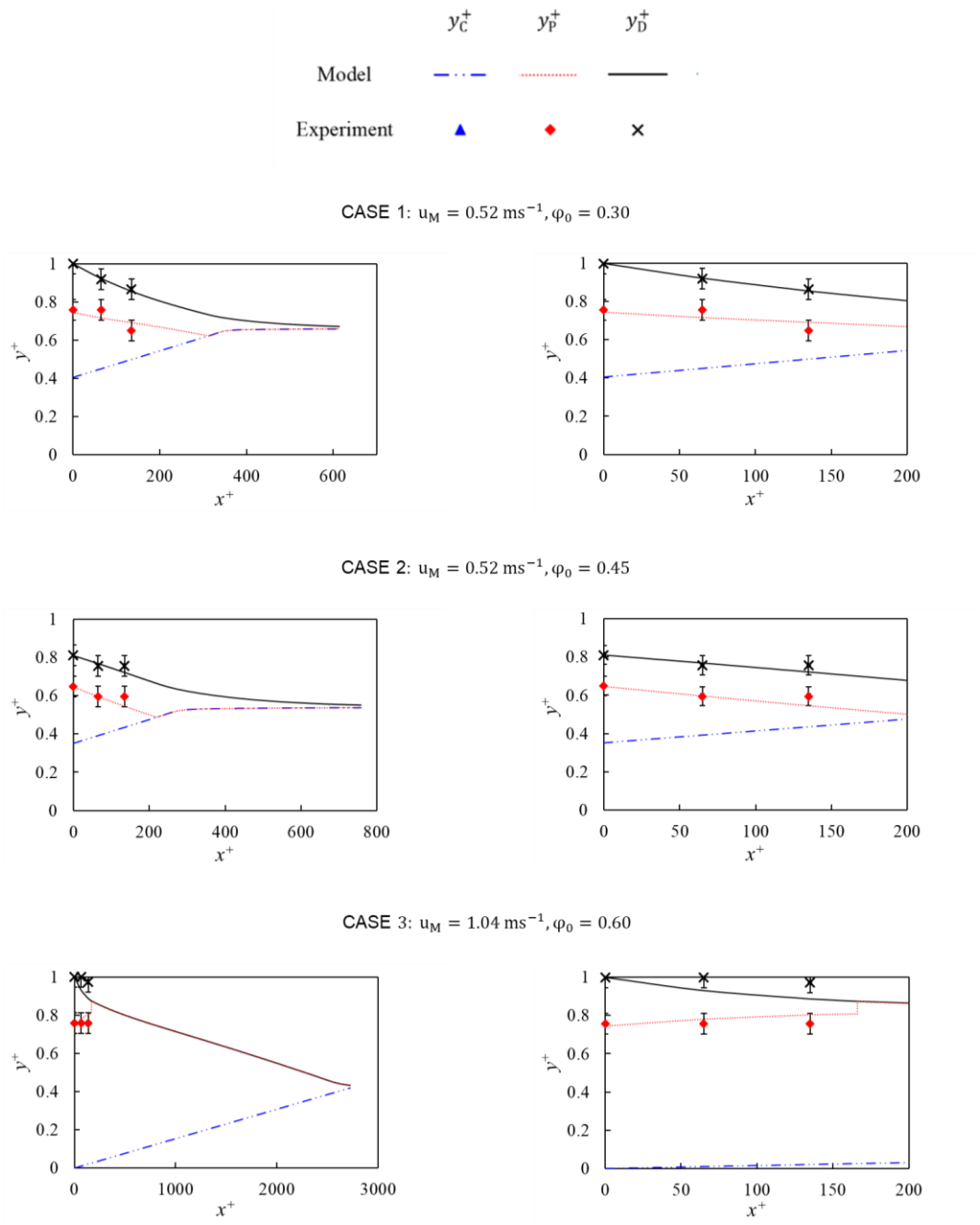

Figure 4.3. Model predictions using the interfacial mobility film drainage coalescence model and comparison to experimental data. The figures on the left show the complete flow profiles, while the figures on the right focus on the region of $0 \leq x^+ \leq 200$.

Figure 4.3 shows the flow profiles of the three case studies predicted by the *interfacial mobility film drainage coalescence model* with m value of 49. The figures on the left show the complete flow profiles, while those on the right zoom in on the region where $0 \leq x^{+} \leq 200$.

Comparing the flow profiles in Figure 4.3 to those in Figures 4.1 and 4.2, it becomes apparent that the *interfacial mobility film drainage model* predicts longer separation lengths for case studies 1 and 2 than the *asymmetric film drainage model*, suggesting smaller coalescence rates. For case study 3 the two coalescence models predict similar separation lengths. Nevertheless, the dense-packed layer depletes approximately 2.5 times faster with the *interfacial mobility film drainage model* than the *asymmetric film drainage model*, once again indicating a faster coalescence rate.

Similarly to the *asymmetric film drainage model*, predictions of this model show that the rate of drop-settling is larger than the rate of drop-interface coalescence for case studies 1 and 2. In these cases, coalescence controls the rate of separation, leading in the depletion of the settling layer first, while the dense-packed layer persists. In case study 3, the rate of drop-interface coalescence is predicted to be faster than the rate of drop-settling, hence the dense-packed layer is anticipated to deplete first. Despite the similarities in the type of separation predicted by each coalescence model, the

differences in the resulting separation profiles are large, highlighting the importance of the coalescence correlations.

In Figure 4.3 the model successfully predicts the separation of case studies 1 and 2 within the error bars, demonstrating good agreement with experimental measurements. However, the model fails to capture the behaviour of case study 3, where a larger mixture velocity was implemented. Notably, the coalescence rate is overpredicted and the model predictions for the coalescence curve y_{D} fall outside the error bars, indicating a lack of agreement with experimental measurements at the high mixture velocity. These findings are consistent with the results obtained from the χ^2 test.

4.4. Conclusions

This chapter presents a comparison of two coalescence models integral to the semi-empirical model for separating dispersed pipe flows. The coalescence models, relying on experimentally determined parameters, were assessed using data from Voulgaropoulos et al. (2016). The experimental dataset included measurements of the *dense-packed layer curve* y_{P}*, coalescence curve* y_{C}, and drop size in the dense-packed layer $d_{\mathrm{p,I}}$. Parameter estimation was carried out using cases 1 and 2, which implemented a low mixture velocity, while case study 3 with a larger mixture

velocity was used for validation and for assessing the impact of mixture velocity on coalescence parameters.

Estimation of r_V^* for the *asymmetric film drainage model* resulted in values of 0.0080 and 0.0087, which meet statistical tests that indicated sufficient precision in the parameter estimates and good agreement with experimental measurements. Estimation of m for the *interfacial mobility film drainage model* yielded a value of 49, passing statistical tests for cases 1 and 2 but failing the χ^2 test for case 3, thus suggesting a potential dependency of m on the mixture velocity. Both models predicted coalescence-controlled separation for cases 1 and 2 and settling-controlled separation for case 3; however, the *interfacial mobility film drainage model* overpredicted the coalescence rate for case 3. The *asymmetric film drainage model* exhibited strong agreement with experimental measurements, while the *interfacial mobility film drainage model* showed good agreement for cases 1 and 2 but significant discrepancies for case 3.

The *asymmetric film drainage coalescence model* emerged as the more suitable choice for separating dispersions in pipes and will be used in the next chapter. The following chapter explores model-based design of experiments techniques, aiming to optimise experiments for precise parameter estimation and further refine the efficacy of the proposed model in predicting dispersed pipe flows.

Chapter 5

5. Model-based design of experiments[3]

This chapter presents a parametric study on the semi-empirical model introduced in Chapter 3 for the separation of liquid-liquid dispersions in pipes. A combination of techniques are employed, including parameter estimation, parametric sensitivity analysis (PSA), and model-based design of experiments (MBDoE) techniques, with the aim of acquiring precise parameter estimates and propose optimal experimental conditions, thereby enhancing the accuracy of the model. Ultimately, a framework is proposed aimed at identifying the optimal experimental conditions for acquiring precise parameter estimates when employing semi-empirical models to analyse the separation of dispersed flows in pipes. The proposed approach can be employed to determine optimal experimental configurations for pre-existing setups, as well as to devise novel experimental protocols from inception, with the objective of ensuring that the measurements obtained contain sufficient information for precise estimation of the parameters. The proposed framework comprises three key components 1) the calibration of the semi-empirical model for separation of dispersed flows, 2) sensitivity analysis, and 3) model-based experimental design.

[3] The work presented in this chapter has been published in Chemical Engineering Science (Evripidou et al. 2023a).

5.1. Methodology

5.1.1. Experimental data

The experimental measurements of the *settling* and the *coalescence curves* from Pereyra et al. (2013) are used in this chapter. The experiments were conducted in a fully instrumented multiphase flow facility consisting of a transparent PVC pipe with an inner diameter (*ID*) equal to 0.1 m to allow visual observation of the distinct layers along the pipe. A static mixer was installed in series with the T-junction at the inlet of the test section to promote mixing of the two phases. Tap water and Tulco Tech 80 mineral oil were used as test fluids. The properties of the fluids are given in Table 5.1. The heights of the pure water layer y_{C} and the pure oil layer y_{D} were measured at five different locations along the pipe using measuring tapes. The readings of the measuring tapes were corrected to account for the effect of the pipe curvature. The experimental set-up and methods are described in detail in Pereyra et al. (2013).

5.1.2. Parameter estimation

Parameter estimation is the process of calculating the values of the unknown parameters of a model from physical measurements. Only two parameters are unknown here, the settling parameter C_h and the coalescence parameter r_V^*. These are specific to each system and must be determined experimentally. C_h appears in the calculation of the drop settling velocity from equation 3.2 and accounts for hindrance in drop-settling due

to the flow and droplet interactions. It also compensates for any uncertainty in the estimate of the average drop size at the inlet as shown by Evripidou et al. (2022). r_V^* is associated with coalescence and is used in equations 3.12 and 3.13 in the calculation of the drop-drop and the drop-interface coalescence times.

The two parameters were estimated using the *Model Validation* entity in gPROMS ModelBuilder as described in Section 4.2. The parameter estimates were assessed using the results of the *t*-test and the χ^2-test. The values of other parameters used in the model were obtained from Pereyra et al. (2013) and Perry et al. (1997), whenever this was possible, and are summarised in Table 5.1. The remaining parameters which appear in equation 3.2 for the calculation of the settling velocity u_S, are obtained by the correlations in Chapter 3.

Table 5.1. Model parameters

Parameter	Description	Value	Unit	Reference
ρ_{C}	Density of water	998	$\mathrm{kg\ m^{-3}}$	Perry et al. (1997)
ρ_{D}	Density of oil	857	$\mathrm{kg\ m^{-3}}$	Pereyra et al. (2013)
μ_{C}	Viscosity of water	0.00089	$\mathrm{Pa\ s}$	Perry et al. (1997)
μ_{D}	Viscosity of oil	0.027	Pa s	Pereyra et al. (2013)
γ	Interfacial tension	0.029	$\mathrm{N\ m^{-1}}$	Pereyra et al. (2013)
g	Gravitational acceleration	9.81	$\mathrm{m\ s^{-2}}$	Perry et al. (1997)
H	Hamaker coefficient	10^{-20}	$\mathrm{N\ m}$	Pereyra et al. (2013)
C_h	Settling parameter	-	Dimensionless	-
r_V^*	Coalescence parameter	-	Dimensionless	-

Table 5.2. Conditions of the experiments. (Pereyra et al. 2013)

Case	*ID* (m)	$\boldsymbol{\varphi_0}$	$\boldsymbol{u_{\mathrm{M}}}$ $(\mathbf{m\ s^{-1}})$	$\boldsymbol{y_{\mathrm{C},0}}$ $(\mathbf{m})$	$\boldsymbol{y_{\mathrm{D},0}}$ $(\mathbf{m})$
1	0.1	0.40	0.06	0.025	0.1
2	0.1	0.40	0.09	0.025	0.1
3	0.1	0.40	0.13	0.025	0.1
4	0.1	0.60	0.09	0.016	0.1

C_h and r_V^* were estimated using experimental measurements of the *settling curve* y_{C} *and the coalescence curve* y_{D}. The variance of the experimental measurements of the layer heights was assumed to be constant, with a standard deviation σ of 0.01 m. The oil fraction and/or the mixture velocity varied between cases. The conditions of the cases included in the parameter estimation are outlined in Table 5.2, together with the initial heights of the *settling curve* $y_{C,0}$ and the *coalescence curve* $y_{\mathrm{D},0}$. The average drop size at the inlet $d_{\mathrm{p},0}$ was assumed to be independent to the mixture velocity u_{M} and the oil fraction φ_0 and equal to 0.0025 m for all cases.

5.1.3. Parametric sensitivity analysis (PSA)

PSA serves as a valuable tool for identifying the pipe locations where the model outputs, such as the *settling curve* y_{C} and the *coalescence curve* y_{D}, exhibit the highest sensitivity to the uncertain parameters. This method is based on local linearization, and while more advanced methods exist in the literature (Joshi et al. 2006; Schenkendorf et al. 2018; Krausch et al. 2019), a local linearization works well in cases where there is a preliminary knowledge on the values of model parameters. By pinpointing areas of heightened sensitivity, the optimal sampling locations are determined. Measurements at these selected locations subsequently provide invaluable information for fitting the uncertain parameters with high precision.

The first-order local sensitivity $s_{\theta_i}^{y}$, or simply *local sensitivity,* of a dependent variable y with respect to the input parameter θ_i is defined as $s_{\theta_i}^{y} = \frac{\partial y}{\partial \theta_i}$, where s is also known as the *absolute sensitivity*. The absolute sensitivity can be obtained by calculating the change in output y arising from a finite small perturbation ε in parameter θ_i, i.e.:

$$\frac{\partial y}{\partial \theta_i} \approx \frac{\Delta y}{\Delta \theta_i} \approx \frac{y_i' - y_i}{(\theta_i + \varepsilon) - \theta_i}. \qquad 5.1$$

In equation 5.1, y_i' represents the predicted value of the output y after introducing a finite small perturbation ε to the parameter θ_i. Noting here that

the approximation error is of the order of ε. The accuracy of the computations can be increased further by using a second-order approximation that decreases the error to the order of ε^2.

The local sensitivities of *N* dependent variables (outputs) to *n* input model parameters can be expressed in the form of a sensitivity matrix, $\mathbf{Q}$

$$\mathbf{Q}(\boldsymbol{\phi}, \boldsymbol{\theta}) = \begin{bmatrix} \frac{\partial y_1}{\partial \theta_1} & \cdots & \frac{\partial y_1}{\partial \theta_n} \\ \vdots & \ddots & \vdots \\ \frac{\partial y_N}{\partial \theta_1} & \cdots & \frac{\partial y_N}{\partial \theta_n} \end{bmatrix} \approx \begin{bmatrix} \frac{y_1' - y_1}{(\theta_1 + \varepsilon) - \theta_1} & \cdots & \frac{y_1' - y_1}{(\theta_n + \varepsilon) - \theta_n} \\ \vdots & \ddots & \vdots \\ \frac{y_N' - y_N}{(\theta_1 + \varepsilon) - \theta_1} & \cdots & \frac{y_N' - y_N}{(\theta_n + \varepsilon) - \theta_n} \end{bmatrix}, \quad 5.2$$

where $\boldsymbol{\theta}$ is the N_θ-dimensional set of estimated model parameters, C_h and r_V^*, and $\boldsymbol{\phi} = [ID, \varphi_0, \mathrm{u}_M, \mathrm{y}_{C,0}, \mathrm{y}_{D,0}]$ is the experimental design vector. The experimental design vector $\boldsymbol{\phi}$ is defined as the vector that includes the experimental control variables that can be manipulated within a given experiment. Later in Section 5.2.3, where an optimal experiment for parameter precision is being designed using MBDoE, existing information about the model is used to determine the optimal values for the design vector with the aim of maximising the precision of the model parameters.

The Fisher Information Matrix (FIM) $\mathbf{H}_{\boldsymbol{\theta}}$ takes the form

$$\mathbf{H_\theta}(\boldsymbol{\phi}, \boldsymbol{\theta}) = \mathbf{Q^T \Sigma_y^{-1} Q}, \tag{5.3}$$

where $\mathbf{\Sigma_y^{-1}}$ is the inverse variance-covariance matrix of measurement errors.

To quantify the combined sensitivity of the model outputs to the uncertain (independent) parameters, the multidimensional nature of the FIM $\mathbf{H_\theta}$ can be summarised by a scalar measure ψ. This is essentially a single scalar quantity that combines the local sensitivities of the model responses to variations in the values of the uncertain parameters. The trace $\mathrm{Tr}(\mathbf{H_\theta})$, the determinant $\mathrm{Det}(\mathbf{H_\theta})$, and the largest eigenvalue are all popular options for ψ (Pukelsheim 1993) and are used in the alphabetic criteria discussed further in Section 5.2.3. In this work, the trace of the FIM is used for PSA, which represents the sum of squared sensitivities and exhibits a direct relationship with the sensitivities. $\mathrm{Tr}(\mathbf{H_\theta})$ is defined as

$$\psi = \mathrm{Tr}(\mathbf{H_\theta}) = \sum_i \sum_j \sigma_{jj}^{-2} \left(\frac{\partial y_j}{\partial \theta_i} \right)^2. \tag{5.4}$$

where σ_{jj} is the *j*-th diagonal element of $\mathbf{\Sigma}_y$.

In the model developed here, the trace of the FIM is a function of pipe length. The pipe profile of the sensitivity can be obtained by plotting $\mathrm{Tr}(\mathbf{H_\theta})$ against x (see Figure 5.1), enabling the identification of the pipe locations that are the most sensitive to the uncertain parameters. In the model, the uncertain parameters C_h and r_V^* affect the rates of drop settling and coalescence,

hence the heights of the layers along the pipe. A PSA was performed to determine the pipe locations where the *settling curve* y_{C} and the *coalescence curve* y_{D} (i.e. the model outputs that are measured in the relevant experimental set-up) are the most sensitive to C_h and r_V^* for the cases listed in Table 5.2. The model was executed three times, initially with the parameter estimates obtained during parameter estimation, then with a perturbation ε of 1% applied to C_h only, and finally with a perturbation ε of 1% applied to r_V^* only. The specific equations used in PSA are listed in Section A.1 of the appendix.

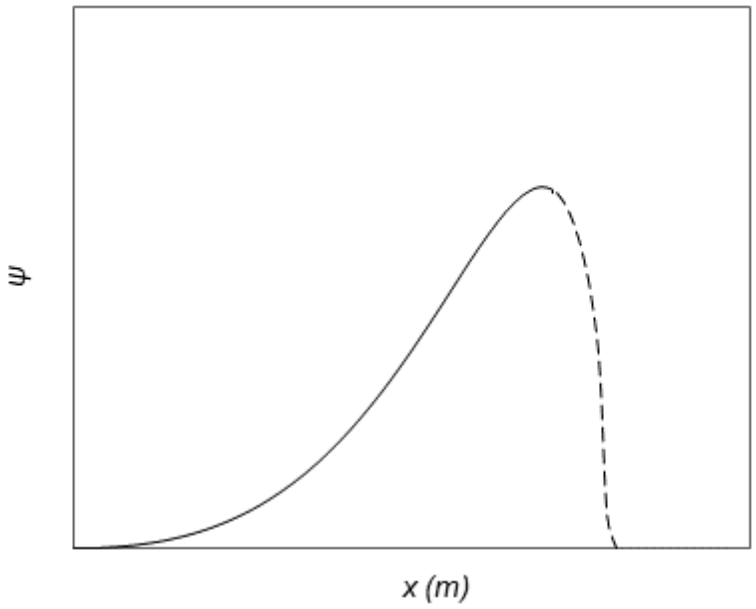

Figure 5.1: Schematic of the pipe profile of the sensitivity.

5.1.4. Experimental design for parameter precision

Physical experiments play a crucial role in enhancing the understanding of the separation mechanisms and improving the accuracy of the model.

However, the experimental conditions and the measuring locations can significantly affect the quality of the information provided by experimental measurements. MBDoE for parameter precision involves the use of current knowledge about the model, such as the model structure and preliminary parameter estimates, in order to design experiments that reduce the uncertainty in the parameter estimates. This requires to mathematically quantify the parameter estimate uncertainty in scalar form. Common approaches are the so-called alphabetic criteria described below, which are all measures of the covariance matrix $\mathbf{V}_{\boldsymbol{\theta}}(\boldsymbol{\phi}, \boldsymbol{\theta})$.

- The A-optimal criterion aims to minimise the trace of the covariance matrix, $\mathrm{Tr}(\mathbf{H}_{\boldsymbol{\theta}})$.
- The D-optimal criterion aims to minimise the determinant of the covariance matrix $\mathrm{Det}(\mathbf{H}_{\boldsymbol{\theta}})$.
- The E-optimal criterion aims to minimise the largest eigenvalue of the covariance matrix.

The alphabetic criteria can be used to optimise experimental design by determining the optimal experimental conditions and measuring locations, thereby maximizing the information held by the experimental measurements that can be used in the estimation of the model parameters. MBDoE can be performed using the *Experiment Design* module in gPROMS ModelBuilder. This is an optimisation problem that aims to find the design vector $\boldsymbol{\phi}$ values,

that minimise the chosen scalar measure of the expected variance-covariance matrix $\mathbf{V_{\theta,expected}}(\boldsymbol{\phi}, \boldsymbol{\theta})$, as shown in equation 5.10.

$$\boldsymbol{\phi}_{\mathbf{opt}} = arg\, \min_{\boldsymbol{\phi}} \psi(\mathbf{V_{\theta,expected}}(\boldsymbol{\phi}, \boldsymbol{\theta})). \qquad 5.10$$

In equation 5.10, $\boldsymbol{\phi}_{\mathrm{opt}}$ is the set of optimal experimental conditions and measuring locations and $\mathbf{V_{\theta,expected}}(\boldsymbol{\phi}, \boldsymbol{\theta})$ is the expected variance co-variance matrix, which can be approximated (using the first term Taylor expansion) by the inverse of the expected FIM, $\mathbf{H_{\theta}}$.

$$\mathbf{V_{\theta,expected}}(\boldsymbol{\phi}, \boldsymbol{\theta}) \approx \mathbf{H_{expected}}(\boldsymbol{\phi}, \boldsymbol{\theta})^{-1}. \qquad 5.11$$

To perform MBDoE for parameter precision in gPROMS ModelBuilder, initial guesses for the uncertain parameters must be provided. These guesses can be based on parameter estimates either from existing literature for similar liquid-liquid systems or from initial experiments conducted specifically for this purpose. Initial guesses, as well as lower and upper bounds are also needed for the necessary length of the test section, the initial heights of the settling curve $y_{\mathrm{C},0}$ and the coalescence curve $y_{\mathrm{D},0}$, the average drop diameter at the inlet $d_{\mathrm{p},0}$, and the controlled experimental variables (i.e. the inner diameter of the pipe ID, the oil fraction φ_0, and the mixture velocity u_{M}). gPROMS then determines the optimal values for the design variables, i.e. the length of the test section x_{pipe}, the initial conditions ($h_{\mathrm{C},0}, h_{\mathrm{D},0}, d_{\mathrm{p},0}$), and the settings of the controlled variables ($ID, \varphi_0, u_{\mathrm{M}}$) that fall between these bounds. The variables that will be measured during the experiments

must be defined under the Measurement and Sensors tab. The frequency or the location of the measurements must also be specified.

The expected improvement in the parameter estimates can be visualised through the confidence ellipses given by equations 5.12 and 5.13 for $0 \leq \vartheta \leq \pi$.

$$x = \theta_1 + \mathbf{E_{1,1}} cos\vartheta + \mathbf{E_{1,2}} sin\vartheta \qquad 5.12$$

$$y = \theta_2 + \mathbf{E_{2,1}} cos\vartheta + \mathbf{E_{2,2}} sin\vartheta \qquad 5.13$$

Here, **E** is defined as

$$\mathbf{E} = \mathbf{v} \cdot \sqrt{\mathbf{D}} \cdot sf \qquad 5.14$$

where **v** is the matrix of eigenvectors and **D** is the matrix of eigenvalues of the variance-covariance matrix, and sf denotes a scaling factor determined by the chosen confidence level.

5.2. Results

5.2.1. Parameter estimation

Parameter estimation was performed using the *Model Validation* entity in gPROMS ModelBuilder for the four cases listed in Table 5.2. Table 5.3 presents the parameter estimation results, as well as statistical measures based on the *t*-test that are used to evaluate the accuracy and reliability of the model predictions. The table encompasses the initial guesses of the

parameter values, the lower and upper bounds for each parameter which were obtained from the literature, the final parameter estimates, the distance to the bounds of the respective 95% confidence interval, the 95% *t*-value for each parameter, and a reference 95% *t*-value. A 95% *t*-value for a parameter smaller than the reference *t*-value indicates that the information in the available dataset is not sufficient to estimate this parameter precisely (Draper and Smith 1998).

Table 5.3. Parameter estimation initial guesses, results, and statistical measures based on the t-test (parameters failing the t-test are indicated in boldface).

Model parameter	**Initial guess**	**Lower & upper bounds**	**Final value**	**95% Confidence interval**	**95% *t*-value**
C_h	0.15	0.1-1	0.1982	0.1321	**1.5**
r_V^*	0.007	0.001-0.015	0.0074	0.0028	2.7
				Reference *t*-value (95%):	1.7

A weak negative correlation of -0.16 was observed between C_h and r_V^*. The 95% *t*-value for r_V^* is larger than the reference *t*-value, indicating that the coalescence parameter was estimated with sufficient precision. On the other hand, the 95% *t*-value for C_h is smaller than the reference *t*-value, suggesting that higher uncertainty is associated with the parameter estimate and that the estimate is not statistically significant. Further investigation is required to determine whether the uncertainty in C_h significantly affects the accuracy of the model. Although the model validation was repeated with different initial guesses and upper and lower bounds, they resulted in poorer fits with the experimental data.

5.2.1.1. Flow profiles

The flow profiles predicted by the model using the parameter estimates from Table 5.3 are illustrated in Figure 5.2. These profiles correspond to the four cases specified in Table 5.2. To facilitate comparison of the model predictions to experiments, the figure also includes experimental measurements along with error bars of 0.01 m.

The four distinct flow profiles in Figure 5.2 were obtained under varying operating and initial conditions. In each case, the thickness of the DPL decreases along the length of the pipe, indicating a coalescence rate that exceeds the settling rate. This observation suggests a separation process predominantly controlled by settling, ultimately leading to the depletion of the DPL. Within Cases 1-3, the flow profiles demonstrate that an increase in the mixture velocity u_{M} while maintaining other controlled variables and initial conditions constant, leads to slower separation and an increase in the separation length, x_{sep}. Moreover, the point of depletion of the DPL, $\bar{\bar{x}}$, moves further downstream from the inlet, as a response to the increase in the mixture velocity. A comparison between Cases 2 and 4 suggests that

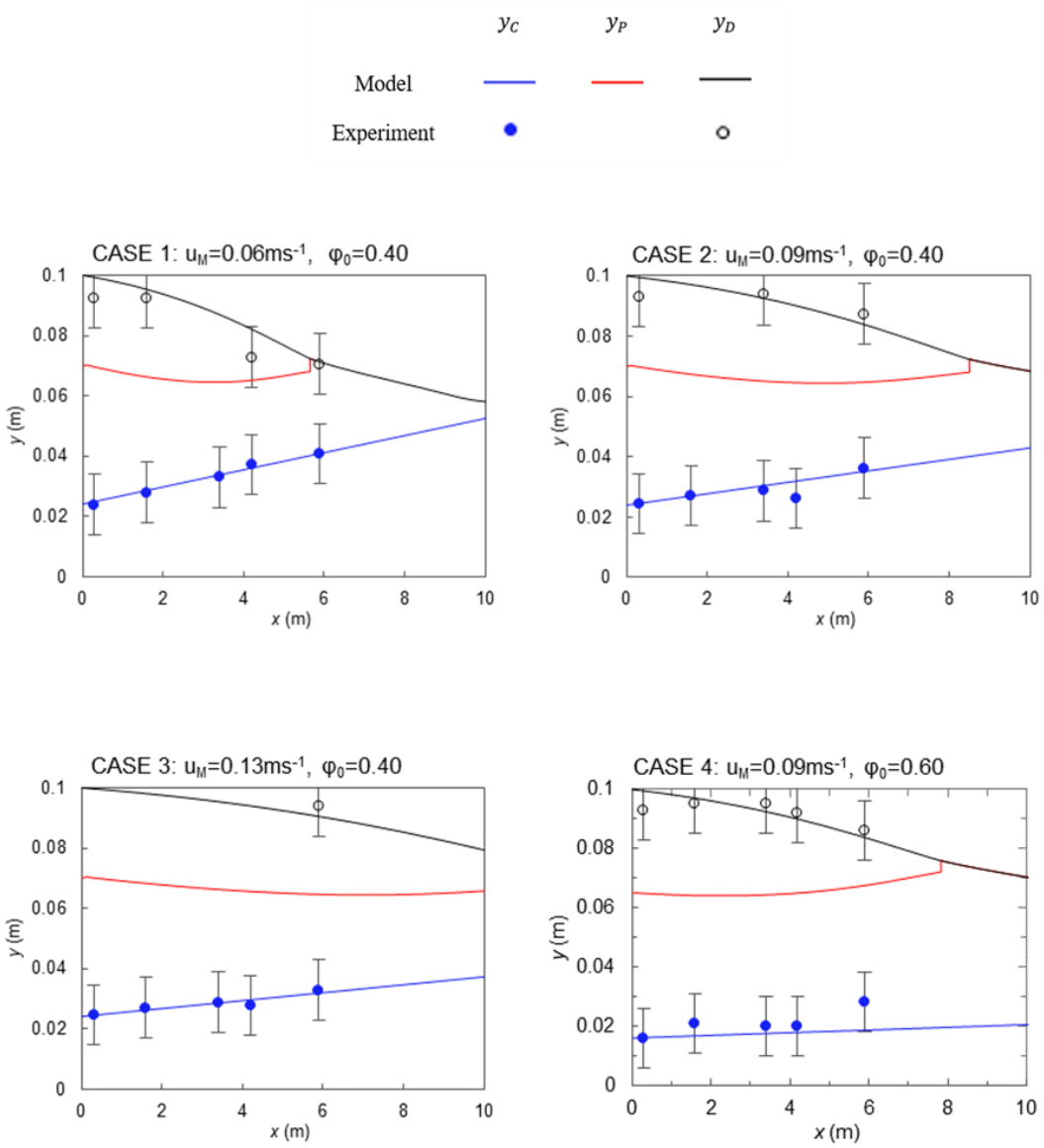

***Figure 5.2. Flow profiles obtained using the parameters estimates in Table 5.3 and experimental measurements of the coalescence and the settling curves with error bars of ±1* cm.**

the dispersed phase fraction, φ_0, has a small effect on $\bar{\bar{x}}$. Following the depletion of the DPL, slower separation is observed at the larger oil fraction.

Nevertheless, the relationship between the oil fraction and the rate of separation cannot be clearly established with the current data. This is due to the fact that in the conducted experiments, the change in the oil fraction φ_0 was accompanied by concurrent changes in the initial layer heights.

5.2.1.2. Goodness-of-fit

Table 5.4 shows the χ^2 values computed from the residuals for the settling curve, y_{C}, and the coalescence curve, y_{D}, across all cases using the model with the parameter estimates from Table 5.3, as well as the overall χ^2 values for each case and the overall χ^2 value for this model.. It is evident that all χ^2 values fall below the critical χ^2 values. The lack of a χ^2 value based on the residuals for the coalescence curve y_D for case 3 can be attributed to the fact that only a single measurement was taken at these conditions. This leads to a situation where the number of measurements (1) is lower than the number of estimated parameters (2), and the problem is underspecified. Despite this limitation, the overall χ^2 value for this model is significantly lower than the critical χ^2 value. This indicates a strong agreement between the experimental data and the model predictions obtained using the parameter estimates from Table 5.3.

Table 5.4. χ^2 values for the two measured responses obtained using the estimated parameters.

	Case 1		Case 2		Case 3		Case 4		Overall	
	X^2	X^2-crit.	X^2	X^2-crit.	X^2	X^2-crit.	X^2	X^2-crit.	X^2	X^2-crit.
y_C	0.023	6.0	0.39	6.0	0.052	7.8	1.2	7.8	1.6	26
y_D	1.4	6.0	0.55	3.8	-	-	0.61	7.8	2.6	20
Total	1.4	13	0.94	11	0.17	9.5	1.8	16	4.2	43

5.2.1.3. Effect of C_h on flow profile

As previously noted, the results in Table 5.3 reveal that the *t*-value associated with the hindered settling parameter C_h is lower than the reference *t*-value, indicating a failure of the *t*-test. This discrepancy suggests that the estimated value of C_h is characterized by higher uncertainty when compared to the coalescence parameter r_V^*. To investigate whether this uncertainty in C_h has a significant effect on the accuracy of the model, the simulations were repeated twice. In each simulation, the lower and upper bounds of the 95% confidence interval of C_h were utilised. These bounds were obtained by adding/subtracting the corresponding value for the 95%

confidence interval from Table 5.3 to the parameter estimate, resulting in $C_{h,0.05} = 0.07$ and $C_{h,0.95} = 0.33$, respectively.

The hindered settling parameter C_h plays a critical role in determining the point of depletion of the dense-packed layer. As the dense-packed layer depletes, the effect of C_h on separation becomes even more pronounced, with drop-settling in the settling layer becoming the dominant mechanism governing separation.

Figure 5.3 presents the predicted flow profiles of case 3 at the endpoints of the 95% confidence interval of C_h. This visual representation effectively captures the potential variability and the significance of parameter uncertainty, providing valuable insights into the flow behaviour and separation dynamics within the system.

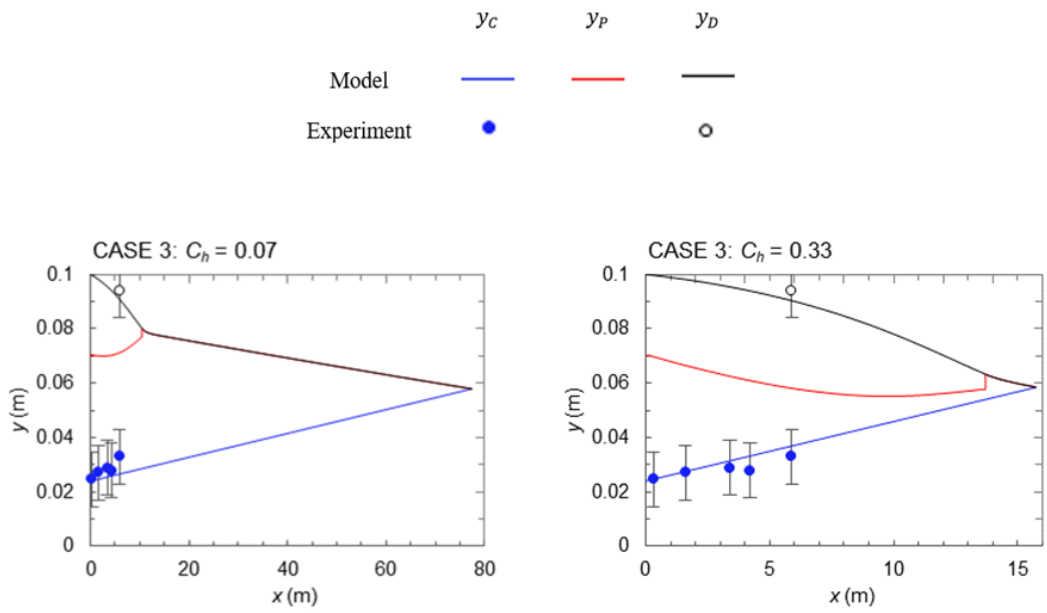

***Figure 5.3. Flow profiles of case 3 (u_M = 0.13* m s^{-1}*, φ_0 = 0.40) at the endpoints of the 95% confidence interval of C_h and experimental measurements of the coalescence and the settling curves with error bars of ±1* cm.**

The results clearly demonstrate that the hindered settling parameter C_h has a substantial impact on the expected flow profile and the separation length. Although dense-packed layer depletion occurs between 10 m and 15 m for both cases, the prediction based on $C_{h,0.05}$ indicates a separation length that is nearly five times larger compared to that projected by $C_{h,0.95}$. This significant disparity between the two flow profiles highlights the need for higher precision in the estimation of C_h to ensure reliable and accurate model predictions.

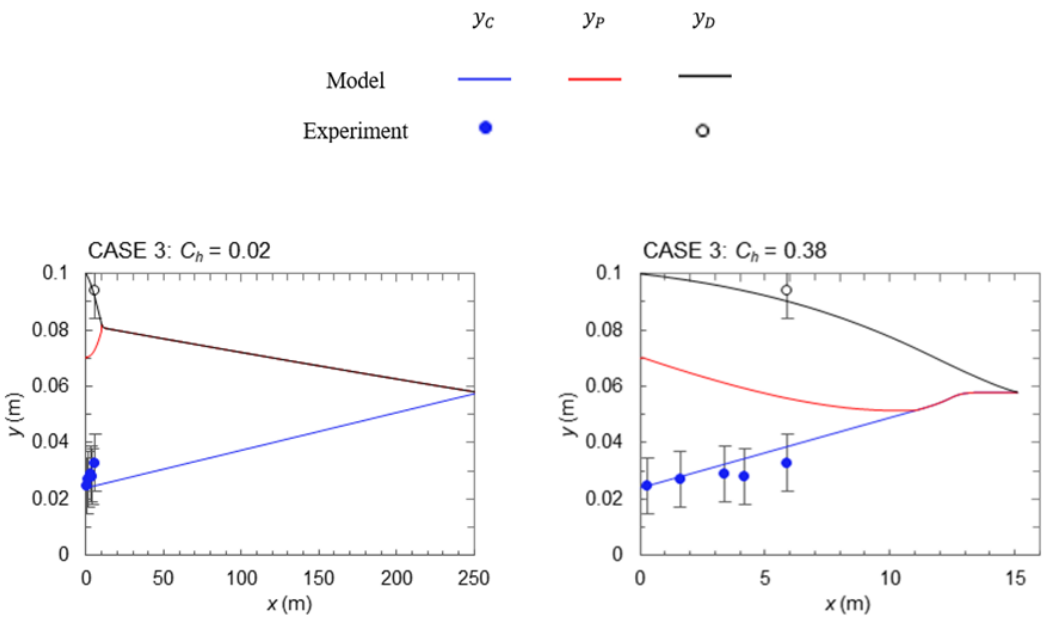

Figure 5.4. Flow profiles of case 3 (u_M = 0.13* m s^{-1}*, φ_0 = 0.40) at the endpoints of the 99% confidence interval of C_h and experimental measurements of the coalescence and the settling curves with error bars of* ±1 cm*.

The significance of the hindered settling parameter C_h becomes even more apparent when considering the wider 99% confidence interval. Figure 5.4 presents the results obtained from the boundaries of the 99% confidence interval. At the lower bound, the dense-packed layer depletes similarly to previous cases. Conversely, at the upper bound, the settling layer depletes while the dense-packed layer persists until the two phases completely separate. This observation signifies a transition in the type of separation, shifting from a settling-controlled to a coalescence-controlled separation.

Notably, the total separation length estimated using $C_{h,0.01}$ is more than 15 times greater compared to that predicted by $C_{h,0.99}$.

The influence of parameter r_V^* on model predictions has also been examined. Figure 5.5 illustrates the influence of r_V^* on the flow profiles of case 3 at the endpoints of the 95% confidence interval. The analysis led to the conclusion that the value of r_V^* is known with sufficient precision.

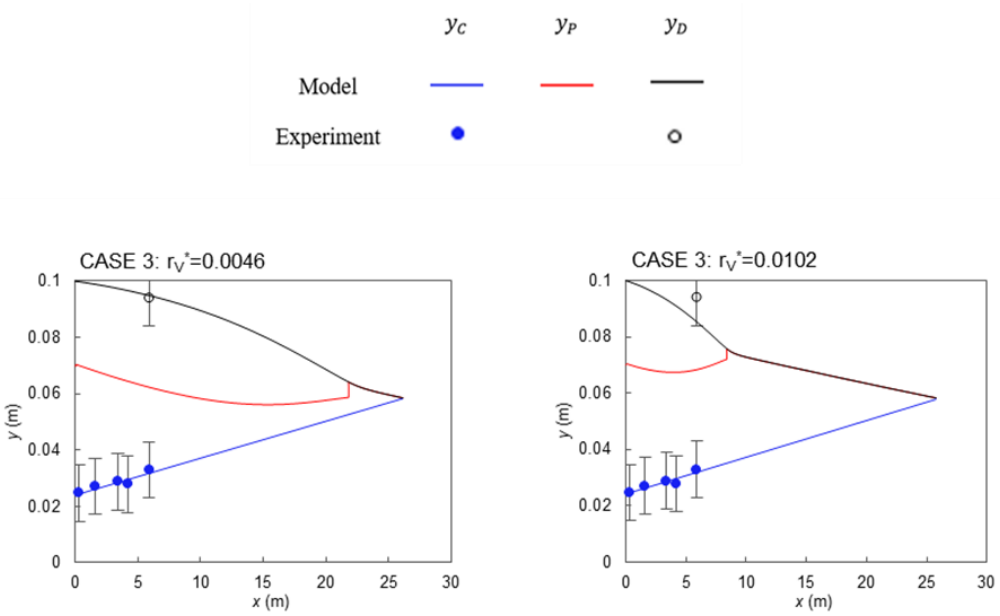

Figure 5.5: Flow profiles of case 3 (u_M = 0.13 m s^{-1}, φ_0 = 0.40) at the endpoints of the 95% confidence interval of r_V^* and experimental measurements of the coalescence and the settling curves with error bars of ±1 cm.

The findings depicted in Figures 5.3 and 5.4 emphasise the considerable impact of parameter uncertainty in the estimation of C_h. New experimental data collected at regions of high sensitivity could be useful in increasing the precision of the estimate for this parameter. By focusing on these specific areas, the uncertainty associated with C_h can be reduced, thereby improving the accuracy of the model and enhancing the reliability of its predictions.

5.2.2. Parametric sensitivity analysis (PSA)

A PSA was performed to identify the pipe lengths with the highest sensitivity of the model responses to the uncertain parameters. Measurements taken at the locations of highest sensitivity hold the most information for the estimation of the uncertain parameters. The model was solved for the parameter estimates obtained from parameter estimation θ_i and for $\theta_i + \varepsilon$, where ε is a small perturbation on the parameter of magnitude equal to 1%, to compute the absolute sensitivities for the water and the oil layer heights $s_{\theta_i}^{y_j}$ with respect to the uncertain parameters C_h and r_V^*.

Figure 5.6 plots the trace of the FIM against pipe length and shows how the combined sensitivity of the settling and the coalescence curves to both C_h and r_V^* changes along the pipe, for the four cases listed in Table 5.2. During PSA, only the 4-layer flow regime was studied to ensure that both settling and coalescence occur, thus enabling the estimation of both the settling and the coalescence parameters at the same time. The solid lines in Figure 5.6

represent the trace of the FIM in the 4-layer flow regime. The simulations were allowed to continue beyond the point of dense-packed layer depletion, and for those specific lengths, ψ is depicted in the plots using dashed lines. The plot also includes the actual measurement locations used in the experiments performed by Pereyra et al. (2013), along with the optimal measurement locations for each case that maximise the information available for parameter estimation.

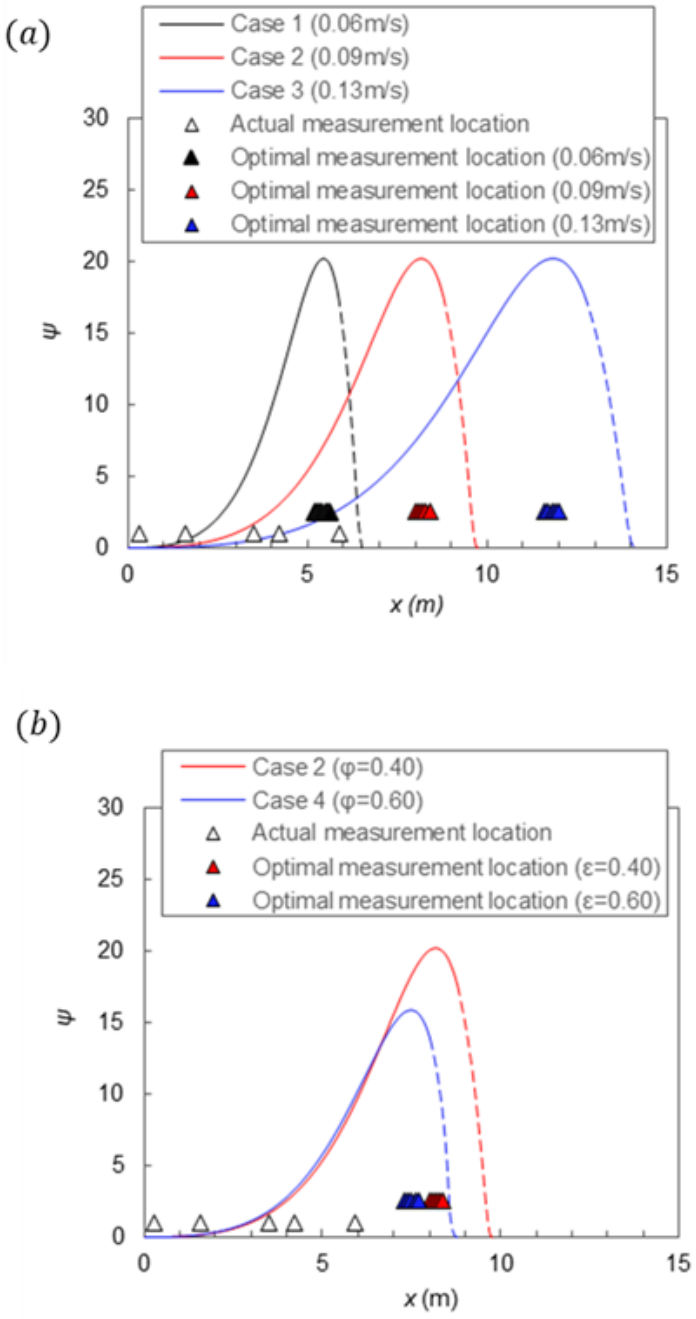

Figure 5.6. Pipe profiles of the trace of the FIM of the four cases listed in Table 5.2. Subfigure (a) demonstrates the effect of the mixture velocity at a constant oil fraction of 0.40, while subfigure (b) illustrates the effect of the oil fraction at constant mixture velocity of 0.09 **m s^{-1}.**

The plot in Figure 5.6(a) compares cases 1-3, to determine the effect of the mixture velocity on the sensitivity ψ, while other controlled variables (i.e. fluid properties, oil fraction, and pipe diameter) and initial conditions (i.e. initial layer heights and drop size at the inlet) remain unchanged. An increase in the mixture velocity from 0.06 m s^{-1} in case 1 to 0.13 m s^{-1} in case 3, moves the peak in the *sensitivity curve,* ψ_{max}, away from the inlet. Despite the shift in the location of the peak, the magnitude of ψ_{max} remains unchanged regardless of the mixture velocity. The results suggest that experiments performed at lower mixture velocities can provide the same amount of information in shorter test sections, as long as the other controlled variables and initial conditions remain unchanged.

Figure 5.6(b) aims to examine the impact of the dispersed phase fraction on the combined sensitivity of the model outputs to the two uncertain parameters by comparing cases 2 and 4. The fluid properties, the mixture velocity, the pipe diameter, and the drop size at the inlet are maintained constant between the two cases, however a variation in the layer heights at the inlet is observed. Notably, the increase in the oil fraction from 0.40 in case 2 to 0.60 in case 4 decreases the magnitude of the peak ψ_{max} but only slightly shift it towards the pipe inlet. These findings suggest that employing a lower dispersed phase fraction can enhance the available information for parameter estimation in the measurements. Nonetheless, it remains uncertain whether these observed changes resulted from the change in the oil fraction alone.

Finally, Figure 5.6 provides valuable insights into the importance of optimizing measurement locations. By strategically refining the measurement locations, specifically by taking measurements at smaller intervals around ψ_{max} , the information content of the collected data will be substantially increased. This highlights the potential of employing PSA as a means to improve the overall effectiveness of the data collection process, ultimately resulting in more precise parameter estimates.

Plots illustrating the determinant of the FIM against pipe length have also been generated and are shown in Figure 5.7. A comparison of the results in Figure 5.7 and those presented in Figure 5.6 reveals that there is less than 3% difference in peak position between the trace and the determinant.

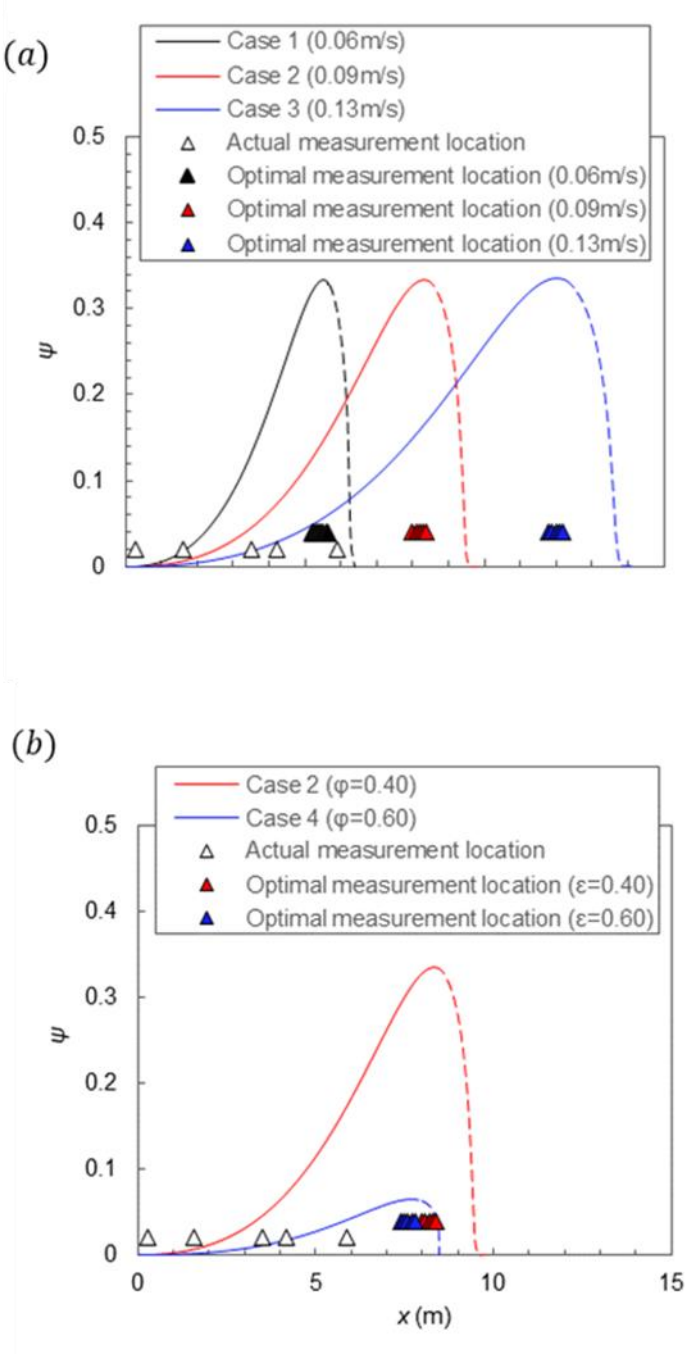

Figure 5.7: Pipe profiles of the determinant of the FIM of the four cases listed in Table 5.2. Subfigure (a) demonstrates the effect of the mixture velocity at a constant oil fraction of 0.40, while subfigure (b) illustrates the effect of the oil fraction at const

5.2.3. Experimental design for parameter precision

Model-based design of experiments in gPROMS ModelBuilder can be used to recommend experiments to improve the precision of the estimates of C_h and r_V^*. During experimental design, the internal diameter of the pipe was fixed at 0.1 m, consistent with the experimental setup described in Section 3. Additionally, the drop size in the inlet was set to 0.25 mm. The lower and upper limits for the mixture velocity u_{M} were defined as 0.03 m s^{-1} and 0.30 m s^{-1}, respectively, while the oil fraction varied between 0.1 and 0.6, to ensure that water-continuous dispersions are formed. The initial guess for u_{M} was chosen as 0.06 m s^{-1} which, out of the mixture velocities studied during PSA, this value moved the peak of the sensitivity curve closer to the inlet, as shown in Figure 5.6(a). Similarly, the initial estimate for the oil fraction was set to 0.4, since it was observed that case 2 with $\varphi_0 = 0.4$ in Figure 5.6(b) resulted to a higher peak ψ_{max} in the sensitivity. It is worth noting that sequential MBDoE was performed, hence prior experiments conducted by Pereyra et al. (2013) were taken into consideration during experiment design, and information available from those runs was incorporated into experiment design.

Optimisation of the length of the test section was performed, setting the lower and upper bounds to 4 m and 6 m respectively. An initial guess of 5.5 m was selected for the length. Consistent with experiments performed by

Pereyra et al. (2013), measurements were planned to be taken at five distinct locations. The initial guesses for the measurement locations were set as 0.3 m, 1.6 m, 3.5 m, 4.2 m, and 5.0 m, with the intention of optimising these locations. A constraint of a minimum distance of 0.1 m between the measuring locations was imposed. The optimisation process was repeated three times, using each of the A-, D-, and E-optimal criteria to enable comparison.

The initial guesses, and the lower and upper bounds of the controlled variables and the initial conditions used for model-based experiment design are outlined in Table 5.5, along with the optimal values obtained with each of the A-, D-, and E-optimal criteria. The optimal measuring locations obtained with each criterion are presented in Table 5.6. All three criteria yielded nearly identical results, which also satisfied the *t*-test. The experimental design was repeated using different initial guesses for design variables, without any improvement in the uncertainty of the model parameters.

Table 5.5. Initial guesses, and lower and upper bounds of the time-invariant controlled variables and the initial conditions used for MBDoE and optimal values obtained with each of the A-, D-, and E-optimal criteria.

Control variable	**Final value**			**Initial value**	**Variable type**	**Lower bound**	**Upper bound**
	A	**D**	**E**				
ID (m)	0.1	0.1	0.1	0.1	Fixed	-	-
φ_0	0.221	0.222	0.220	0.4	TBD*	0.1	0.6
u_{M} (m s^{-1})	0.0760	0.0759	0.0762	0.06	TBD*	0.03	0.3
Initial condition	**Final value**			**Initial value**	**Variable type**	**Lower bound**	**Upper bound**
	A	**D**	**E**				
$d_{\mathrm{p},0}$ (mm)	0.25	0.25	0.25	0.25	Fixed	-	-
$h_{\mathrm{C},0}$ (m)	0.0314	0.0314	0.0314	0.024	TBD*	0	0.1
$h_{\mathrm{D},0}$ (m)	0.0	0.0	0.0	0.0	TBD*	0	0.1

*TBD: to be determined

Table 5.6. Optimal measurement locations obtained during MBDoE using each of the A-, D-, and E-optimal experimental design criteria.

Measurement location from pipe inlet (m)			
Initial guess	**Optimal location**		
	A	**D**	**E**
0.3	5.6	5.6	5.6
1.6	5.7	5.7	5.7
3.5	5.8	5.8	5.8
4.2	5.9	5.9	5.9
5.0	6.0	6.0	6.0

The MBDoE results suggest that utilising an oil fraction of 0.22 and a mixture velocity of 0.076 m s^{-1} is recommended. The optimal measurement locations for these specific conditions, as presented in Table 5.6, are clustered around a single location. This aligns with PSA findings in Figure 5.6, where the optimal measurement locations cluster around the point of highest sensitivity. Furthermore, the measurement locations are situated near the end of the pipe, closely resembling the PSA findings for case 1 where the mixture velocity was 0.06 m s^{-1}. Similarly to PSA results, a

constant measurement interval of 0.1 m is recommended, which corresponds to the minimum allowable distance between measurements.

Table 5.7. Parameter statistics obtained during MBDoE using each of the A-, D-, and E-optimal criteria.

Para-meter	**Value**	**A-criterion**		**D-criterion**		**E-criterion**	
		95% *CI*	**95% *t*-value**	**95% *CI***	**95% *t*-value**	**95% *CI***	**95% *t*-value**
C_h	0.1982	0.0507	3.91	0.0508	3.90	0.0506	3.92
r_V^*	0.0074	0.0019	3.88	0.0019	3.89	0.0019	3.87
					Reference *t*-value (95%):		1.68

The parameter statistics can be found in Table 5.7. Notably, the 95% *t*-values are 3.9 for both C_h and r_V^* using either criterion, surpassing the reference *t*-value of 1.68. Therefore, a significant improvement in parameter precision is expected compared to their previous values listed in Table 5.3, particularly for the *t*-value of C_h, which has doubled in magnitude.

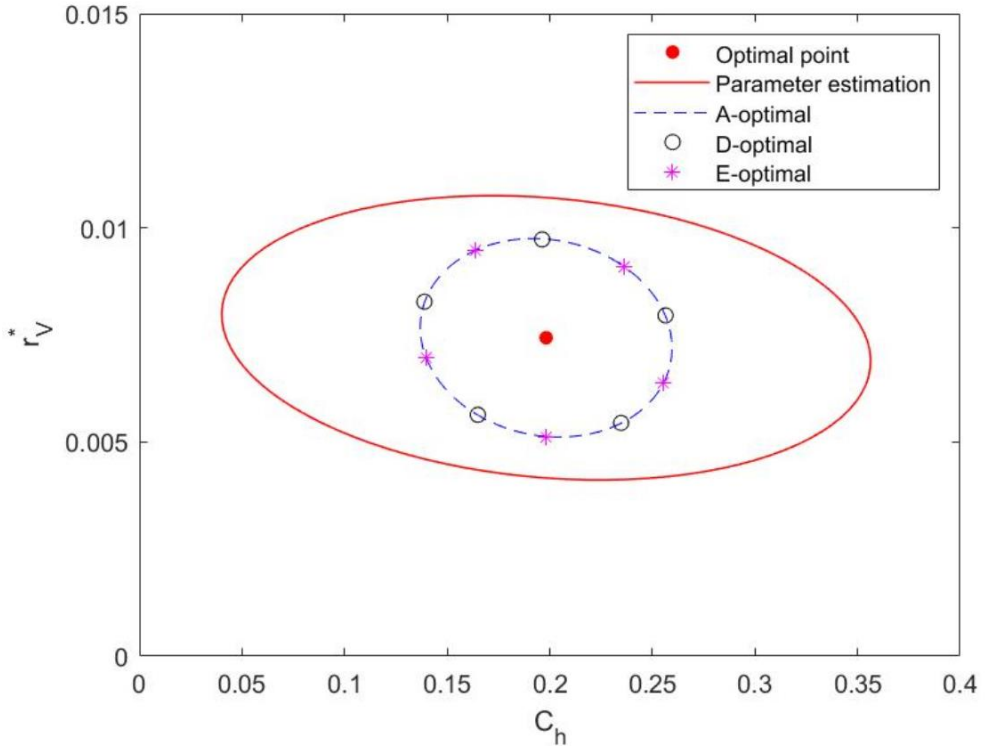

Figure 5.8. Plot illustrating the 95% confidence ellipses for C_h and r_V^* obtained from the initial parameter estimates and after MBDoE using A-, D-, and E-optimal criteria.

Figure 5.8 shows a comparison between the confidence ellipses resulting from the initial parameter estimation performed in Section 5.1 and the expected confidence ellipses obtained using the three optimisation criteria. Each confidence ellipse was plotted for the 95% confidence interval. The results demonstrate that MBDoE is expected to consistently improve parameter precision, irrespective of the chosen criterion, thus enhancing the reliability of parameter estimates.

As anticipated, the three criteria yielded similar outcomes, indicating comparable performance. The optimisation criteria exhibited substantial improvements in the expected confidence region of the parameter estimates. This enhancement is clearly demonstrated by the significant reduction in the area of the ellipse, which signifies a reduction in uncertainty and an increased level of confidence in the estimated parameters.

After conducting the newly designed experiments, it is essential to recalibrate the model. If the precision of the parameters following recalibration is still not satisfactory, the experiment design process can be repeated using the new parameter estimates. Sequential MBDoE is an iterative process that provides predictions based on the current knowledge about the system.

5.3. Conclusion

This chapter undertook a parametric study on the model introduced in Chapter 3, aiming to enhance its accuracy in predicting the separation of dispersions. Drawing on experimental data from Pereyra et al. (2013), parameter estimation, PSA, and MBDoE techniques were employed to propose an effective framework for acquiring precise parameter estimates.

Parameter estimation showed that the four experimental datasets available were sufficient for estimating the coalescence coefficient r_V^* with sufficient precision. However, it highlighted a limitation in the information content associated with the settling coefficient C_h emphasising the need for more precise parameter estimates, particularly in drop settling-controlled regions where C_h greatly influences the model predictions. PSA identified a peak in the trace of the FIM, $\psi_{max,}$ near the point of depletion of the dense-packed layer. The peak, which indicates the most parametrically sensitive pipe location, offers insights into where the information content of the measurements is maximised for parameter estimation. The study demonstrated that the location and magnitude of ψ_{max} are altered through manipulation of controlled variables and initial conditions. Finally, MBDoE using either of the A-, D-, and E- optimal criteria yielded nearly identical proposed experiments. All criteria successfully led to anticipated improvements in parameter precision, as evidenced by the substantial increase in the *t*-values.

The findings highlight the potential of both PSA and MBDoE techniques to enhance the accuracy of semi-empirical models, by enabling the precise estimation of uncertain parameters. Leveraging PSA and MBDoE optimises the experimental design process, allowing for more informed and efficient data collection, and eliminating the need for iterative trial-and-error approaches, resulting in significant savings in time and resources. This work serves as a valuable guide for future experimental work, providing a

systematic and efficient methodology for enhancing the accuracy of semi-empirical models for separating dispersions in pipes.

Chapter 6

6. Conclusions

This chapter discusses the key findings of this work and their significance. Conclusions are drawn from each chapter and suggestions for future research are provided.

6.1. Final remarks

In this work, a semi-empirical model was developed to predict the separation of liquid-liquid dispersions in pipes. The model was refined through the selection of an appropriate coalescence model. Finally, a methodology was devised for acquiring precise parameter estimates through the use of MBDoE techniques to enhance the overall accuracy of the semi-empirical model.

In Chapter 2, the main literature was summarised, illustrating the need for models predicting the separation of dispersions in pipes. Semi-empirical approaches based on drop-settling and drop-coalescence in batch vessels and horizontal pipe separators have been highlighted, and cases where these approaches fail in pipe flows have been identified.

In Chapter 3, a semi-empirical model was proposed for predicting the

separation of dispersed liquid-liquid flows in horizontal pipes. This model, based on the physical mechanisms of drop settling, drop-interface coalescence, and drop-drop coalescence, implemented the *asymmetric film drainage coalescence model* by Henschke et al. (2002), and utilised two fitted parameters, the hindered settling parameter C_h and the dimensionless asymmetry coefficient r_V^*. The proposed model was validated against available experimental data near the pipe inlet from oil-in-water dispersions. The results demonstrated good agreement between the model predictions and experimental measurements of layer heights and drop size in the dense-packed layer. The model predicted two distinct types of separation – coalescence-controlled and settling-controlled – depending on the inlet and flow conditions. Investigation of distinct case studies, revealed that smaller drop sizes were more likely to lead to settling-controlled separation, highlighting a relationship between the drop size and the rate of drop settling. Furthermore, it was demonstrated that the hindered settling parameter mitigates the impact of inaccuracies in initial drop-size estimates. As a result, the model can be applied even if accurate drop-size measurements at the inlet are not available. Finally, the model was successfully applied to water-in-oil dispersions. The results revealed that the continuous phase affects the coalescence rate, predicting lower coalescence rates and more persistent dense-packed layers for oil-continuous systems.

In Chapter 4, the *asymmetric film drainage model* was compared to the

interfacial mobility film drainage model by Jeelani and Hartland (1994). The coalescence models that rely on experimentally determined parameters were evaluated using data collected at two distinct mixture velocities by Voulgaropoulos et al. (2016). Parameter estimation utilised data from the lower mixture velocity, while validation employed data from the higher mixture velocity to assess the impact of mixture velocity on coalescence parameters. The parameter estimates for r_V^* in the *asymmetric film drainage model* demonstrated statistical significance across all cases, irrespective of whether drop-size measurements were considered in addition to layer thicknesses in the parameter estimation, indicating sufficient precision in the parameter estimates and good agreement with experimental measurements. In contrast, the parameter estimate for m in the *interfacial mobility film drainage model* met statistical criteria for cases with a lower mixture velocity but failed the χ^2 test for the high mixture velocity case, implying a possible correlation between m and the mixture velocity. The flow profiles predicted using the parameter estimates revealed that both models anticipated coalescence-controlled separation at the lower mixture velocity and settling-controlled separation at the higher mixture velocity. Nevertheless, the *interfacial mobility film drainage model* consistently predicted faster coalescence rates across all cases. While the *asymmetric film drainage model* demonstrated good agreement with experimental measurements, the *interfacial mobility film drainage model* exhibited good agreement at the lower mixture velocity but significant discrepancies at the higher mixture velocity. Upon comparing the two coalescence models, the

asymmetric film drainage model emerged as the most appropriate for the separation of dispersions in horizontal pipes and was therefore selected as the preferred coalescence model for implementation in modelling.

In Chapter 5, a parametric study was conducted on the semi-empirical model, with the aim of proposing an effective framework for acquiring precise parameter estimates and thereby enhancing the model accuracy. Experimental data from Pereyra et al. (2013) were utilised, and parameter estimation, parametric sensitivity analysis (PSA), and model-based design of experiments (MBDoE) techniques were employed. Parameter estimation revealed that the experimental dataset was sufficient for estimating the dimensionless asymmetry coefficient r_V^* with sufficient precision. However, the information content associated with the hindered settling coefficient C_h was insufficient to precisely estimate this parameter. The significant impact of C_h on model predictions, especially in regions controlled by drop settling, was demonstrated highlighting the need for a more precise parameter estimate. PSA suggested that the information content of the measurements can be increased by concentrating measurements near the point of depletion of the dense-packed layer, where a peak in the trace of the FIM, $\psi_{max,}$ was identified indicating a parametrically sensitive region. Additionally, it was demonstrated that the location and magnitude of ψ_{max} are altered through the manipulation of controlled variables and initial conditions, allowing the optimal measuring locations to be shifted. Specifically, a decrease in the mixture velocity u_{M} shifted the peak towards

the inlet without affecting its magnitude, thus allowing for shorter test sections. Finally, MBDoE for parameter precision using the A-, D-, and E-optimal criteria resulted in nearly identical optimal experiments. The three criteria substantially increased the expected *t*-values of both uncertain parameters, resulting in anticipated improvements in their precision.

6.2. Future work and perspectives

The present study has undertaken challenging tasks and has contributed to the modeling of separating liquid-liquid dispersions in pipes. Additionally, it has posed questions that currently lack answers, thereby inspiring future research in the field.

The primary contribution of this work lies in the development of a semi-empirical model for the prediction of the evolution of liquid-liquid dispersions for industrial applications. While the findings are encouraging, further experimental data is necessary to validate the model at different pipe lengths and specifically, data further downstream of the inlet and closer to the point of complete separation.

Examining different case studies with varying initial drop diameters has provided insights into the effect of drop size on the type of separation. However, considering the inherent polydispersity in most industrial applications, where distinct drops may experience different settling and

coalescence rates, incorporating various drop sizes into the model could enhance its accuracy.

Analysis of diverse datasets suggested a potential correlation between the mixture velocity and the hindered settling parameter C_h. Further experimental studies on drop-settling in dispersed pipe flows could elucidate and help establish this relationship, potentially leading to an empirical correlation between mixture velocity to C_h.

Study of the coalescence models suggested a possible relationship between the interface mobility m and the mixture velocity. Experimental investigations focusing on drop-coalescence in dispersed pipe flows could validate this relationship and offer insights into the general impact of mixture velocity on coalescence rates. Discrepancies in coalescence times predicted by the *interface mobility film drainage mode*l compared to the *asymmetric film drainage model* may be attributed to delayed coalescence of drops with the interface due to crossflow (Dong et al. 2020). Further experimental studies could clarify this matter.

Experiments designed using MBDoE techniques have yielded promising results, significantly enhancing the expected precision of the parameter estimates. However, in this work, only the design step of MBDoE was performed. It would therefore be interesting to perform the experiments

designed to assess the actual precision of the recalibrated parameter estimates.

Each of the aforementioned tasks presents a unique set of challenges and, therefore, should not be underestimated. Nevertheless, the potential outcomes hold significant promise for advancing our understanding and overcoming existing limitations in the prediction of the separation of liquid-liquid flows in horizontal pipes. This is particularly crucial in process and chemical industries employing dispersions such as continuous flow separations, where improved predictive capabilities can significantly enhance the design and operation of industrial facilities.

References

Aarts, D.G. and Lekkerkerker, H.N., 2008. Droplet coalescence: drainage, film rupture and neck growth in ultralow interfacial tension systems. *Journal of fluid mechanics*, *606*, pp.275-294.

Al-Wahaibi, T. and Angeli, P., 2007. Transition between stratified and non-stratified horizontal oil–water flows. Part I: Stability analysis. *Chemical Engineering Science*, *62*(11), pp.2915-2928.

Amundsen, L., 2011. *An experimental study of oil-water flow in horizontal and inclined pipes.* PhD thesis, Norwegian University of Science and Technology.

Angeli, P. and Hewitt, G.F., 2000a. Flow structure in horizontal oil–water flow. *International journal of multiphase flow*, *26*(7), pp.1117-1140.

Angeli, P. and Hewitt, G.F., 2000b. Drop size distributions in horizontal oil-water dispersed flows. *Chemical Engineering Science*, *55*(16), pp.3133-3143.

Asprey, S.P. and Macchietto, S., 2000. Statistical tools for optimal dynamic model building. *Computers & Chemical Engineering*, *24*(2-7), pp.1261-1267.

Balmelli, M., Steiner, L. and Hartland, S., 2000. Behaviour of turbulent dispersions in a stirred single-stage cell. *Chemical engineering science*, *55*(9), pp.1653-1660.

Xie, B., Jiang, F., Lin, H., Zhang, M., Gui, Z. and Xiang, J., 2023. Review of Core Annular Flow. *Energies*, *16*(3), p.1496.

Bard, Y., 1974. Nonlinear parameter estimation. New York, USA: Academic Press.

Barnea, E. and Mizrahi, J., 1975. Separation mechanism of liquid-liquid dispersions in deep-layer gravity settler: Part III – Hindered settling and drop-to-drop coalescence in the dispersion band. *Trans. Instn. Chem. Engrs., 53,* pp.75-82.

Barral, A.H., 2014. *Stratified wavy oil-water flows.* PhD thesis, University College London.

Bazhlekov, I.B., Chesters, A.K. and Van de Vosse, F.N., 2000. The effect of the dispersed to continuous-phase viscosity ratio on film drainage between interacting drops. *International Journal of Multiphase Flow*, *26*(3), pp.445-466.

Bernaerts, K., Servaes, R.D., Kooyman, S., Versyck, K.J. and Van Impe, J.F., 2002. Optimal temperature input design for estimation of the square root model parameters: parameter accuracy and model validity restrictions. *International Journal of Food Microbiology*, *73*(2-3), pp.145-157.

Bhardwaj, A. and Hartland, S., 1994. Kinetics of coalescence of water droplets in water-in-crude oil emulsions. J*ournal of Dispersion Science and Technology*, *15*(2), pp.133-146.

Bourdillon, A.C., Verdin, P.G. and Thompson, C.P., 2016. Numerical simulations of drop size evolution in a horizontal pipeline. *International Journal of Multiphase Flow*, *78*, pp.44-58.

Brauner, N., Moalem Maron, D. and Rovinsky, J., 1998. A two-fluid model for stratified flows with curved interfaces. *International journal of multiphase flow*, *24*(6), pp.975-1004.

Brauner, N. 2003. Liquid-liquid two-phase flow systems. In *Modelling and experimentation in two-phase flo*w, pp. 221–279. Vienna: Springer Vienna.

Charles, G.E. and Mason, S.G., 1960. The coalescence of liquid drops with flat liquid/liquid interfaces. *Journal of Colloid Science*, *15*(3), pp.236-267.

Chen, J.D., 1985. A model of coalescence between two equal-sized spherical drops or bubbles. *Journal of Colloid and Interface Science*, *107*(1), pp.209-220.

Chen, C.T., Maa, J.R., Yang, Y.M. and Chang, C.H., 1998. Effects of electrolytes and polarity of organic liquids on the coalescence of droplets at aqueous-organic interfaces. *Surface science*, *406*(1-3), pp.167-177.

Chen, J., Anastasiou, C., Cheng, S., Basha, N.M., Kahouadji, L., Arcucci, R., Angeli, P. and Matar, O.K., 2023. Computational fluid dynamics simulations of phase separation in dispersed oil-water pipe flows. *Chemical Engineering Science*, *267*, p.118310.

Chesters, A., 1991. Modelling of coalescence processes in fluid-liquid dispersions: a review of current understanding. *Chemical engineering research and design*, *69*(A4), pp.259-270.

Conan, C., Masbernat, O., Décarre, S. and Liné, A., 2007. Local hydrodynamics in a dispersed-stratified liquid–liquid pipe flow. *AIChE journal*, *53*(11), pp.2754-2768.

Coulaloglou, C.A. and Tavlarides, L.L., 1977. Description of interaction processes in agitated liquid-liquid dispersions. *Chemical Engineering Science*, *32*(11), pp.1289-1297.

Danielson, T.J., 2012. Transient multiphase flow: Past, present, and future with flow assurance perspective. *Energy & Fuels*, *26*(7), pp.4137-4144.

Danov, K.D., 2004. Effect of surfactants on drop stability and thin film drainage. In *Fluid mechanics of surfactant and polymer solutions,* pp. 1-38. Vienna: Springer Vienna.

De Malmazet, E., Risso, F., Masbernat, O. and Pauchard, V., 2015. Coalescence of contaminated water drops at an oil/water interface: Influence of micro-particles. *Colloids and Surfaces A: Physicochemical and Engineering Aspects*, *482*, pp.514-528.

DiStefano 3rd, J.J., 1981. Optimized blood sampling protocols and sequential design of kinetic experiments. *American Journal of Physiology-Regulatory, Integrative and Comparative Physiology*, *240*(5), pp.R259-R265.

Dong, T., Wang, F., Weheliye, W.H. and Angeli, P., 2020. Surfing of drops on moving liquid–liquid interfaces. *Journal of Fluid Mechanics*, *892*, p.A36.

Dörr, A., Sadiki, A. and Mehdizadeh, A., 2013. A discrete model for the apparent viscosity of polydisperse suspensions including maximum packing fraction. *Journal of Rheology*, *57*(3), pp.743-765.

Draper, N.R. and Smith, H., 1998. *Applied regression analysis* (Vol. 326). John Wiley & Sons.

Dreher, T.M., Glass, J., O'Connor, A.J. and Stevens, G.W., 1999. Effect of rheology on coalescence rates and emulsion stability. *AIChE Journal*, *45*(6), pp.1182-1190.

El-Batsh, H.M., Doheim, M.A. and Hassan, A.F., 2012. On the application of mixture model for two-phase flow induced corrosion in a complex pipeline configuration. *Applied Mathematical Modelling*, *36*(11), pp.5686-5699.

El-Hamouz, A.M. and Stewart, A.C., 1996, October. On-line drop size distribution measurement of oil-water dispersion using a Par-Tec M300 laser backscatter instrument. In *SPE Annual Technical Conference and Exhibition* (pp. SPE-36672). SPE.

Elseth, G., 2001. *An experimental study of oil/water flow in horizontal pipes.* PhD thesis, Telemark University College.

Eri, A. and Okumura, K., 2010. Bursting of a thin film in a confined geometry: Rimless and constant-velocity dewetting. *Physical Review E*, *82*(3), p.030601.

Espie, D. and Macchietto, S., 1989. The optimal design of dynamic experiments. *AIChE Journal*, *35*(2), pp.223-229.

Evripidou, N., Voulgaropoulos, V. and Angeli, P., 2019, June. Simplified mechanistic model for the separation of dispersed oil-water horizontal pipe flows. In *19th International Conference on Multiphase Production Technology*. BHR.

Evripidou, N., Avila, C. and Angeli, P., 2022. A mechanistic model for the prediction of flow pattern transitions during separation of liquid-liquid pipe flows. *International Journal of Multiphase Flow*, *155*, p.104172.

Evripidou, N., Galvanin, F. and Angeli, P., 2023a. Mechanistic modelling of separating dispersions in pipes using model-based design of experiments techniques. *Chemical Engineering Science*, p.119504.

Evripidou, N., Galvanin, F. and Angeli, P., 2023b. Effect of coalescence models on the prediction of the separation of dispersed oil-water pipe flows. In *Computer Aided Chemical Engineering* (Vol. 52, pp. 1101-1106). Elsevier.

Fang, H., Zhang, L., Luo, L., Zhao, S., An, J., Xu, Z., Yu, J., Ottova, A. and Tien, H.T., 2001. A study of thin liquid films as related to the stability of crude oil emulsions. *Journal of Colloid and Interface Science*, *238*(1), pp.177-182.

Farr, R.S. and Groot, R.D., 2009. Close packing density of polydisperse hard spheres. *The Journal of chemical physics*, *131*(24).

Ford, I., Titterington, D.M. and Wu, C.F.J., 1985. Inference and sequential design. *Biometrika*, *72*(3), pp.545-551.

Ford, I., Titterington, D.M. and Kitsos, C.P., 1989. Recent advances in nonlinear experimental design. *Technometrics*, *31*(1), pp.49-60.

Franceschini, G. and Macchietto, S., 2008. Model-based design of experiments for parameter precision: State of the art. *Chemical Engineering Science*, *63*(19), pp.4846-4872.

Frising, T., Noïk, C. and Dalmazzone, C., 2006. The liquid/liquid sedimentation process: from droplet coalescence to technologically enhanced water/oil emulsion gravity separators: a review. *Journal of dispersion science and technology*, *27*(7), pp.1035-1057.

Galvanin, F., Macchietto, S. and Bezzo, F., 2007. Model-based design of parallel experiments. *Industrial & engineering chemistry research*, *46*(3), pp.871-882.

Galvanin, F., Ballan, C.C., Barolo, M. and Bezzo, F., 2013. A general model-based design of experiments approach to achieve practical identifiability of

pharmacokinetic and pharmacodynamic models. *Journal of pharmacokinetics and pharmacodynamics*, *40*, pp.451-467.

Hartland, S. and Jeelani, S.A.K., 1988. Prediction of sedimentation and coalescence profiles in a decaying batch dispersion. *Chemical Engineering Science*, *43*(9), pp.2421-2429.

Henschke, M., Schlieper, L.H. and Pfennig, A., 2002. Determination of a coalescence parameter from batch-settling experiments. *Chemical Engineering Journal*, *85*(2-3), pp.369-378.

Hines, W.W., Montgomery, D.C. and Borror, D.M., 2008. *Probability and statistics in engineering*. John Wiley & Sons.

Hinze, J.O., 1955. Fundamentals of the hydrodynamic mechanism of splitting in dispersion processes. *AIChE journal*, *1*(3), pp.289-295.

Hodgson, T.D. and Lee, J.C., 1969. The effect of surfactants on the coalescence of a drop at an interface I. *Journal of Colloid and Interface Science*, *30*(1), pp.94-108.

Hosseinzadeh, M., Shirvani, M. and Ghaemi, A., 2018. A study on mean drop size and drop size distribution in an eductor liquid–liquid extractor. *Separation and Purification Technology*, *201*, pp.205-213.

Hosten, L.H. and Emig, G., 1975. Sequential experimental design procedures for precise parameter estimation in ordinary differential equations. *Chemical Engineering Science*, *30*(11), pp.1357-1364.

Hu, B., 2006. *Experimental and theoretical investigations of phase inversion in liquid-liquid dispersions*. PhD thesis, University of London, University College London.

Huang, C., Cattani, F. and Galvanin, F., 2023. An optimal experimental design strategy for improving parameter estimation in stochastic models. *Computers & Chemical Engineering*, *170*, p.108133.

Ibarra, R., Markides, C.N. and Matar, O.K., 2014. A review of liquid-liquid flow patterns in horizontal and slightly inclined pipes. *Multiphase Science and Technology*, *26*(3).

Ibarra-Hernandez, R.J., 2017. *Horizontal and low-inclination oil-water flow investigations using laser-based diagnostic techniques.* PhD thesis, Imperial College London.

Ioannou, K.K., 2006. *Phase Inversion Theoretical and Experimental Investigations in Oil/water Dispersed Flows in Horizontal Pipelines.* PhD thesis, University of London, University College London.

Ishii, M. and Zuber, N., 1979. Drag coefficient and relative velocity in bubbly, droplet or particulate flows. *AIChE Journal*, *25*(5), pp.843-855.

Jeelani, S.A.K. and Hartland, S., 1994. Effect of interfacial mobility on thin film drainage. *Journal of Colloid and Interface Science*, *164*(2), pp.296-308.

Jeelani, S.A.K. and Hartland, S., 1998. Effect of dispersion properties on the separation of batch liquid− liquid dispersions. *Industrial & engineering chemistry research*, *37*(2), pp.547-554.

Jeelani, S.A.K. and Hartland, S., 1986a. Prediction of dispersion height in liquid-liquid gravity settlers from batch settling data. *Chemical engineering research & design*, *64*(6), pp.450-460.

Jeelani, S.A.K. and Hartland, S., 1986b. Scale-up of industrial gravity settlers from batch settling data. In *Proceedings of the International Solved Extraction Conference ISEC* (Vol. 86, pp. 453-460).

Jeelani, S.A.K. and Hartland, S., 1988. Dynamic response of gravity settlers to changes in dispersion throughput. *AIChE journal*, *34*(2), pp.335-340.

Jeelani, S.A.K. and Hartland, S., 1993. The continuous separation of liquid/liquid dispersions. *Chemical engineering science*, *48*(2), pp.239-254.

Jeelani, S.A.K., Pandit, A. and Hartland, S., 1990. Factors affecting the decay of batch liquid-liquid dispersions. *The Canadian Journal of Chemical Engineering*, *68*(6), pp.924-931.

Jeelani, S.A.K., Benoist, G., Joshi, K.S., Gunde, R., Kellenberger, D. and Windhab, E.J., 2005a. Creaming and aggregation of particles in suspensions. *Colloids and Surfaces A: Physicochemical and Engineering Aspects*, *263*(1-3), pp.379-389.

Jeelani, S.A.K., Hosig, R. and Windhab, E.J., 2005b. Kinetics of low Reynolds number creaming and coalescence in droplet dispersions. *AIChE journal*, *51*(1), pp.149-161.

Jeelani, S.A.K., Panoussopoulos, K. and Hartland, S., 1999. Effect of Turbulence on the Separation of Liquid− Liquid Dispersions in Batch Settlers of Different Geometries. *Industrial & engineering chemistry research*, *38*(2), pp.493-501.

Joshi, M., Kremling, A. and Seidel-Morgenstern, A., 2006. Model based statistical analysis of adsorption equilibrium data. *Chemical Engineering Science*, *61*(23), pp.7805-7818.

Kalogerakis, N. and Luus, R., 1983. Improvement of Gauss-Newton method for parameter estimation through the use of information index. *Industrial & engineering chemistry fundamentals*, *22*(4), pp.436-445.

Kalogerakis, N. and Luus, R., 1984. Sequential experimental design of dynamic systems through the use of information index. *The Canadian Journal of Chemical Engineering*, *62*(6), pp.730-737.

Kavehpour, H.P., 2015. Coalescence of drops. *Annual Review of Fluid Mechanics*, *47*, pp.245-268.

Klaseboer, E., Chevaillier, J.P., Gourdon, C. and Masbernat, O., 2000. Film drainage between colliding drops at constant approach velocity: experiments and modeling. *Journal of colloid and interface science*, *229*(1), pp.274-285.

Krausch, N., Barz, T., Sawatzki, A., Gruber, M., Kamel, S., Neubauer, P. and Cruz Bournazou, M.N., 2019. Monte Carlo simulations for the analysis of non-linear parameter confidence intervals in optimal experimental design. *Frontiers in Bioengineering and Biotechnology*, *7*, p.122.

Kuboi, R., Komasawa, I., and Otake, T., 1972. Collision and coalescence of dispersed drops in turbulent liquid flow. *Journal of Chemical Engineering of Japan*, *5*(4), pp.423-424

Lavielle, M. and Aarons, L., 2016. What do we mean by identifiability in mixed effects models?. *Journal of pharmacokinetics and pharmacodynamics*, *43*, pp.111-122.

Lovick, J. and Angeli, P., 2004a. Experimental studies on the dual continuous flow pattern in oil–water flows. *International journal of multiphase flow*, *30*(2), pp.139-157.

Lovick, J. and Angeli, P., 2004b. Droplet size and velocity profiles in liquid–liquid horizontal flows. *Chemical engineering science*, *59*(15), pp.3105-3115.

Lobo, L., Ivanov, I. and Wasan, D., 1993. Dispersion coalescence: Kinetic stability of creamed dispersions. *AIChE journal*, *39*(2), pp.322-334.

Maaß, S., Wollny, S., Voigt, A. and Kraume, M., 2011. Experimental comparison of measurement techniques for drop size distributions in liquid/liquid dispersions. *Experiments in Fluids*, *50*, pp.259-269.

MacKay, G.D.M. and Mason, S.G., 1963. The gravity approach and coalescence of fluid drops at liquid interfaces. *The Canadian Journal of Chemical Engineering*, *41*(5), pp.203-212.

Mason, S.L., May, K. and Hartland, S., 1995. Drop size and concentration profile determination in petroleum emulsion separation. *Colloids and Surfaces A: Physicochemical and engineering aspects*, *96*(1-2), pp.85-92.

Mohamed-Kassim, Z. and Longmire, E.K., 2004. Drop coalescence through a liquid/liquid interface. *Physics of Fluids*, *16*(7), pp.2170-2181.

Morgan, R.G., Markides, C.N., Zadrazil, I. and Hewitt, G.F., 2013. Characteristics of horizontal liquid–liquid flows in a circular pipe using simultaneous high-speed laser-induced fluorescence and particle velocimetry. *International journal of multiphase flow*, *49*, pp.99-118.

Neitzel, G.P. and Dell'Aversana, P., 2002. Noncoalescence and nonwetting behavior of liquids. *Annual review of fluid mechanics*, *34*(1), pp.267-289.

Ng, T.S., Lawrence, C.J. and Hewitt, G.F., 2002. Laminar stratified pipe flow. *International journal of multiphase flow*, *28*(6), pp.963-996.

Ngan, K.H., 2011. *Phase inversion in dispersed liquid-liquid pipe flow* PhD thesis, University College London.

Noïk, C., Palermo, T. and Dalmazzone, C., 2013. Modeling of liquid/liquid phase separation: Application to petroleum emulsions. *Journal of Dispersion Science and Technology*, *34*(8), pp.1029-1042.

Oddie, G. and Pearson, J.A., 2004. Flow-rate measurement in two-phase flow. *Annual review of fluid mechanics*, *36*, pp.149-172.

Oliemans, R.V.A., 1986. *The lubricating-film model for core-annular flow*. PhD thesis, Delft University of Technology.

Ooms, G. and Poesio, P., 2003. Stationary core-annular flow through a horizontal pipe. *Physical Review E*, *68*(6), p.066301.

Othman, H.A., Dabirian, R., Gavrielatos, I., Mohan, R. and Shoham, O., 2018, April. Validation and improvement of the horizontal pipe separator model. In *SPE Western Regional Meeting* (p. D041S007R001). SPE.

Palermo, T., 1991. Le phénomène de coalescence. Etude bibliographique. *Revue de l'Institut français du pétrole*, *46*(3), pp.325-360.

Panoussopoulos, K., Hartland, S., Gramme, P.E. and Sontvedt, T., 1997. Drop size and hold-up profiles in the separation of crude oil-water dispersions. In *International Symposium on Multiphase Flow and Transport Phenomena*. Begel House Inc..

Pereyra, E.J., 2011. *Modeling of integrated Compact Multiphase Separation System(CMSS (c))* (Vol. 72, No. 07).

Pereyra, E., Mohan, R.S. and Shoham, O., 2013. A simplified mechanistic model for an oil/water horizontal pipe separator. *Oil and Gas Facilities*, *2*(03), pp.40-46.

Pérez, C.A., 2005. *Horizontal pipe separator (HPS) experiments and modeling*. PhD thesis, The University of Tulsa.

Perry, R.H., Green, D.W. and Maloney, J.O., 1997. Perry's handbook of chemical engineering. *Perry's Handbook of Chemical Engineering*.

Pilehvari, A., Saadevandi, B., Halvaci, M. and Clark, P.E., 1988, October. Oil/water emulsions for pipeline transport of viscous crude oils. In *SPE Annual Technical Conference and Exhibition* (pp. SPE-18218). SPE.

Pilhofer, T. and Mewes, D., 1979. *Siebboden-Extraktionskolonnen: Vorausberechnung unpulsierter Kolonnen*. Verlag Chemie.

Pinto, J.C., Lobão, M.W. and Monteiro, J.L., 1990. Sequential experimental design for parameter estimation: a different approach. *Chemical engineering science*, *45*(4), pp.883-892.

Pouraria, H., Seo, J.K. and Paik, J.K., 2016, June. CFD simulation of the effect of different oils on water wetting and internal corrosion of oil pipelines.

In *International Conference on Offshore Mechanics and Arctic Engineering* (Vol. 49965, p. V005T04A023). American Society of Mechanical Engineers.

Pukelsheim, F., 1993. *Optimal design of experiments*. New York, USA: J Wiley & Sons.

Quaglio, M., Waldron, C., Pankajakshan, A., Cao, E., Gavriilidis, A., Fraga, E.S. and Galvanin, F., 2019. An online reparametrisation approach for robust parameter estimation in automated model identification platforms. *Computers & Chemical Engineering*, *124*, pp.270-284.

Reynolds, O., 1885. On the theory of lubrication and its application to Mr. Beauchamp Tower's experiments, including an experimental determination of the viscosity of olive oil. *Phil. Trans. Roy. Soc.*, *1*, p.157.

Rodriguez, O.M.H. and Oliemans, R.V.A., 2006. Experimental study on oil–water flow in horizontal and slightly inclined pipes. *International Journal of Multiphase Flow*, *32*(3), pp.323-343.

Rommel, W., Meon, W. and Blass, E., 1992. Hydrodynamic modeling of droplet coalescence at liquid-liquid interfaces. *Separation science and technology*, *27*(2), pp.129-159.

Ryon, A.D., Daley, F.L. and Lowrie, R.S., 1960. *Design and scale-up of mixer-settlers for the DAPEX solvent extraction process* (No. ORNL-2951). Oak Ridge National Lab.(ORNL), Oak Ridge, TN, United States.

Saboni, A., Alexandrova, S., Gourdon, C. and Chesters, A.K., 2002. Interdrop coalescence with mass transfer: comparison of the approximate drainage models with numerical results. *Chemical Engineering Journal*, *88*(1-3), pp.127-139.

Saffman, P.G.F. and Turner, J.S., 1956. On the collision of drops in turbulent clouds. *Journal of Fluid Mechanics*, *1*(1), pp.16-30.

Saltelli, A, Chan, K, & Scott, EM (2009). *Sensitivity Analysis. Wiley Series in Probability and Statistics.* John Wiley & Sons.

Schenkendorf, R., Xie, X., Rehbein, M., Scholl, S. and Krewer, U., 2018. The impact of global sensitivities and design measures in model-based optimal experimental design. *Processes*, *6*(4), p.27.

Schümann, H., Tutkun, M. and Nydal, O.J., 2016. Experimental study of dispersed oil-water flow in a horizontal pipe with enhanced inlet mixing, Part 2: In-situ droplet measurements. *Journal of Petroleum Science and Engineering*, *145*, pp.753-762.

Simmons, M.J.H., Zaidi, S.H. and Azzopardi, B.J., 2000. Comparison of laser-based drop-size measurement techniques and their application to dispersed liquid-liquid pipe flow. *Optical Engineering*, *39*(2), pp.505-509.

Simmons, M.J.H. and Azzopardi, B.J., 2001. Drop size distributions in dispersed liquid–liquid pipe flow. *International journal of multiphase flow*, *27*(5), pp.843-859.

Skjefstad, H.S. and Stanko, M., 2019. Experimental performance evaluation and design optimization of a horizontal multi-pipe separator for subsea oil-water bulk separation. *Journal of Petroleum Science and Engineering*, *176*, pp.203-219.

Smoluchowski, M.V., 1917. Versuch einer mathematischen Theorie der Koagulationskinetik kolloider Lösungen. *Zeitschrift für physikalische Chemie*, *92*(1), pp.129-168.

Tobin, T., Muralidhar, R., Wright, H. and Ramkrishna, D., 1990. Determination of coalescence frequencies in liquid—liquid dispersions: effect of drop size dependence. *Chemical Engineering Science*, *45*(12), pp.3491-3504.

Trallero, J.L., Sarica, C. and Brill, J.P., 1997. A study of oil/water flow patterns in horizontal pipes. *SPE production & facilities*, *12*(03), pp.165-172.

Tsouris, C. and Tavlarides, L.L., 1994. Breakage and coalescence models for drops in turbulent dispersions. *AIChE Journal*, *40*(3), pp.395-406.

Van der Zande, M.J., 2000. *Droplet break-up in turbulent oil-in-water flow through a restriction.* PhD thesis, Delft University of Technology.

Voulgaropoulos, V. and Angeli, P., 2017. Optical measurements in evolving dispersed pipe flows. *Experiments in Fluids*, *58*, pp.1-15.

Voulgaropoulos, V., 2017. *Dynamics of spatially evolving dispersed flows.* PhD Thesis, University College London.

Voulgaropoulos, V., Zhai, L., Ioannou, K. and Angeli, P., 2016, June. Evolution of unstable liquid-liquid dispersions in horizontal pipes. In *10th North American Conference on Multiphase Production Technology*. BHR.

Voulgaropoulos, V., Jamshidi, R., Mazzei, L. and Angeli, P., 2019. Experimental and numerical studies on the flow characteristics and separation properties of dispersed liquid-liquid flows. *Physics of Fluids*, *31*(7).

Vrij, A. and Overbeek, J.T.G., 1968. Rupture of thin liquid films due to spontaneous fluctuations in thickness. *Journal of the American Chemical Society*, *90*(12), pp.3074-3078.

Walter, E., Pronzato, L. and Norton, J., 1997. *Identification of parametric models from experimental data*. Berlin: Springer.

Walvekar, R.G., Choong, T.S., Hussain, S.A., Khalid, M. and Chuah, T.G., 2009. Numerical study of dispersed oil–water turbulent flow in horizontal tube. *Journal of Petroleum Science and Engineering*, *65*(3-4), pp.123-128.

Wang, Z.M. and Zhang, J., 2016. Corrosion of multiphase flow pipelines: the impact of crude oil. *Corrosion Reviews*, *34*(1-2), pp.17-40.

Wu, C.F.J., 1985. Asymptotic inference from sequential design in a nonlinear situation. *Biometrika*, *72*(3), pp.553-558.

Yang, Z., 2014, June. A study of viscous oil and water pipe flow. In *9th North American Conference on Multiphase Production Technology*. BHR.

Yeo, L.Y., Matar, O.K., de Ortiz, E.S.P. and Hewitt, G.F., 2003. Film drainage between two surfactant-coated drops colliding at constant approach velocity. *Journal of colloid and interface science*, *257*(1), pp.93-107.

Zhong, X.F., Wu, Y.X., Li, S.M. and Wei, P.J., 2013. Investigation of pipe separation technology in the oilfield. *Advanced Materials Research*, *616*, pp.833-836.

Zullo, L., 1991. *Computer aided design of experiments. An engineering approach.* PhD thesis, University of London.

Appendix

A1. Parametric Sensitivity

The local sensitivities were calculated according to equation 5.1 and inserted in the sensitivity matrix, which becomes

$$\mathbf{Q}(C_h, r_V^*) = \begin{bmatrix} \frac{\partial y_C}{\partial C_h} & \frac{\partial y_C}{\partial r_V^*} \\ \frac{\partial y_D}{\partial C_h} & \frac{\partial y_D}{\partial r_V^*} \end{bmatrix}. \tag{A1}$$

It follows that the elements of the FIM $\mathbf{H_\theta}$ are

$$\mathbf{H_{11}}(C_h, r_V^*) = \sigma_{11}^{-2}\left(\frac{\partial y_C}{\partial C_h}\right)^2 + \sigma_{22}^{-2}\left(\frac{\partial y_D}{\partial r_V^*}\right)^2, \tag{A2}$$

$$\begin{aligned} \mathbf{H_{12}}(C_h, r_V^*) &= \mathbf{H_{21}}(C_h, r_V^*) \\ &= \sigma_{11}^{-2}\left(\frac{\partial y_C}{\partial C_h}\right)\left(\frac{\partial y_C}{\partial r_V^*}\right) + \sigma_{22}^{-2}\left(\frac{\partial y_D}{\partial C_h}\right)\left(\frac{\partial y_D}{\partial r_V^*}\right), \end{aligned} \tag{A3}$$

and

$$\mathbf{H_{22}}(C_h, r_V^*) = \sigma_{11}^{-2}\left(\frac{\partial y_C}{\partial r_V^*}\right)^2 + \sigma_{22}^{-2}\left(\frac{\partial y_D}{\partial r_V^*}\right)^2. \tag{A4}$$